Dissertation

submitted to

the Combined Faculties for the Natural Sciences and for Mathematics

of the Ruperto-Carola University of Heidelberg, Germany

for the degree of

Doctor of Natural Sciences

presented by Mariia Burdyniuk

born in Zaporizhzhia, Ukraine

Oral-examination: 24th of July 2017

Actin synchronizes chromosome capture by microtubules in starfish oocyte meiosis

Referees:

Dr. Alexander Aulehla, EMBL Heidelberg

Prof. Dr. Elmar Schibel, University of Heidelberg

Acknowledgements

First of all, I would like to thank my PhD supervisor, Péter Lénárt, for an opportunity to work on this exciting project, for directing my work, numerous hours of discussions, many comments and useful suggestions. I have gained a lot of experience.

I am equally grateful to my thesis advisory committee, Dr. Alexander Aulehla, Prof. Dr. Elmar Schiebel, Dr. Gislene Pereira, Dr. Marko Kaksonen, for great discussions and insights on my project, solid input and advice both scientific and general.

I would like to thank to François Nédélec for introducing and guiding me through the world of computational modelling in *Cytosim*.

Next, I would like to thank Darwin trust for funding my scholarship, without which it would not have been possible for me to join the EMBL PhD program.

This work would not be possible without Nilah Monnier, a former visitor at the Lénárt group, who developed a chromosome tracking script which was the key tool in my project.

Special thanks goes to Matthia Karreman - for a collaboration on a daring project and also for her support and friendship.

I am grateful to all current and former Lénárt lab members: To Kalman, for introducing me to starfish oocytes and teaching me the molecular techniques at the lab; To Andrea for his constant support and fruitful discussions; To Michal Fleszar for his input in my project in the last several months; To Natalia for constant willingness to discuss the project and a lot of support; To Philippe for teaching me the basics of Matlab and critical comments on my project; To Masashi, Joana and Johanna for all the knowledge they brought to the lab.

To my 'joint' neighboring Nédélec lab, especially to Serge and Aastha for teaching me to plot things out of Cytosim and Matlab; To Aastha for carefully reading this manuscript; To Karin Sasaki, who inspired me 'to think in the cytosim language'.

To Prof. Dr. Sylvia Erhardt, for joining the PhD defense committee at the last moment.

To many people, who made my time at EMBL brighter: Vlada, Christopher, Thoma, Martina Klünemann, who also translated my Abstract into Zusammenfassung.

Last, but most certainly not least, to Jens, for constant support during every step of this endeavor, patience and being 'extremely understanding'.

Abstract

Chromosome capture by microtubules is an early step of cell division essential for alignment and subsequent separation of sister chromatids. Failure to transmit even one chromosome results in aneuploidy, a common cause of infertility, genetic disorders or cancer.

The canonical mechanism of 'search and capture' by dynamic astral microtubules has been validated by recent studies, and additionally revealed mechanisms that facilitate microtubule search, ensuring rapid and efficient capture of chromosomes in somatic cells.

However, in specialized cell types such as oocytes with large nucleus chromosomes are located much further from microtubule asters. In these cells, the models that work in small somatic cells are insufficient to explain chromosome capture. Recently, the Lénárt group has shown that in starfish oocytes an actin-driven mechanism facilitates chromosome congression and is required to prevent chromosome loss: a contractile actin meshwork transports chromosomes to within the capture range of microtubule asters of approximately 30 μm. How these actin- and microtubule-driven mechanisms of chromosome capture are coordinated remained an open question.

Here, I investigated the cooperation between the actin meshwork transporting chromosomes and capture by microtubules in meiosis of starfish oocytes using high spatio-temporal resolution tracking of chromosome motion in 3D combined with drug-perturbation experiments. This assay allowed me to characterize chromosome capture kinetics during the two-staged chromosome congression under different conditions.

I find that the actin meshwork, while transporting the distal chromosomes to the vicinity of microtubule asters, also synchronizes their capture. I show that this synchronizing effect is due to an actin-dependent block of chromosome capture active for approx. 5 minutes after NEBD. As a result, chromosomes close to microtubule asters – that in principle could be captured immediately after NEBD – are captured simultaneously with chromosomes transported from distal nuclear locations by the actin meshwork at approx. 5-15 minutes after NEBD and independent of their distance from the asters.

I show that this delay in the capture of the proximally located chromosomes cannot be explained by altered microtubule dynamics when growing through the actin meshwork. The delay is also not the consequence of physical entrapment in the actin network 'holding back' chromosomes, because capture is not delayed in slowed or even fully stabilized actin networks.

Together, my results point to an actin-dependent mechanism, which prevents the formation of lateral kinetochore-microtubule attachments. Synchronous disassembly

of these F-actin structures exposes kinetochores and thereby synchronizes chromosome capture.

This is a first description of a mechanism by which the actin cytoskeleton directly affects spindle assembly, and which actively controls and coordinates chromosome search and capture. I show how this mechanism coordinates chromosome congression in the specialized oocyte nucleus, but it is interesting to speculate whether such mechanisms may have a broader relevance for example to synchronize mitotic events such as cell rounding mediated by the actin cytoskeleton with spindle assembly. The detailed molecular mechanism of how F-actin prevents chromosome-microtubule attachment remains an exciting open question for the future studies.

Zusammenfassung

Die Chromosomenerfassung durch Mikrotubuli ist ein früher Schritt der Zellteilung, die für die Ausrichtung und die anschließende Trennung von Schwesterchromatiden wesentlich ist. Wenn auch nur bei einem Chromosom die Übertragung versagt, führt dies zu einer Aneuploidie, einer häufigen Ursache für Unfruchtbarkeit, genetische Störungen oder Krebs.

Der kanonische Mechanismus der "Suche und Erfassung" durch dynamische Astralmikrotubuli wurde durch neuere Studien validiert und enthüllte zusätzlich Mechanismen, die die Mikrotubulumsuche erleichtern und so eine schnelle und effiziente Erfassung von Chromosomen in somatischen Zellen gewährleisten.

Allerdings sind in spezialisierten Zelltypen, wie Oozyten mit ihren großen Kernen, Chromosomen relativ weit von Mikrotubuli-Astern entfernt. In diesen Zellen sind die Modelle, die in kleinen somatischen Zellen funktionieren, nicht ausreichend, um die Chromosomenerfassung zu erklären. In jüngster Zeit hat die Lénárt-Gruppe gezeigt, dass in Seesternoozyten ein Aktin-abhängiger Mechanismus die Chromosomen-Kongression erleichtert und er außerdem notwendig ist um einen Chromosomenverlust zu verhindern: ein kontraktiles Aktinnetz transportiert Chromosomen innerhalb des etwa 30 µm großen Erfassungsbereichs von Mikrotubuliastern. Wie diese Aktin- und Mikrotubuli-abhängigen Mechanismen der Chromosomenerfassung koordiniert sind, blieb eine offene Frage.

Hier untersuchte ich die Kooperation zwischen dem Transport der Chromosomen durch das Aktinnetz und ihrer Erfassung durch Mikrotubuli in der Meiose von Seesternoozyten unter Verwendung einer zeitlich und räumlich hochauflösenden Methode zur Verfolgung der Chromosomenbewegung in 3D kombiniert mit chemischen Störungen der Zelle. Dieses Testverfahren erlaubte mir die Chromosomenerfassungskinetik während der zweistufigen Chromosomen-Kongression unter verschiedenen Bedingungen zu charakterisieren.

Ich habe herausgefunden, dass das Aktinnetz beim Transport der distalen Chromosomen in die Nähe der Mikrotubuliastern auch ihre Erfassung synchronisiert. Ich konnte zeigen, dass dieser Synchronisationseffekt auf eine aktinabhängige Verhinderung der Chromosomenerfassung zurückzuführen ist, welche für ca. 5 Minuten ab dem Zellkernhüllenabbau andauert. Dadurch werden Chromosomen in der Nähe von Mikrotubuliastern - die im Prinzip unmittelbar nach der Zellkernhüllenabbau erfasst werden könnten - gleichzeitig mit Chromosomen, die von distalen Stellen im Zellkernbereich durch das Aktinnetz transportiert wurden, ca. 5-15 Minuten nach NEBD und damit unabhängig von ihrer Entfernung von den Astern erfasst.

Eine veränderte Mikrotubulidynamik, die durch das Wachstum der Mikrotubuli durch das sich zusammenziehende Aktinnetz verursacht werden könnte, könnte die Verzögerung der proximalen Chromosomerfassung erklären. Allerdings konnte ich zeigen, dass diese Verzögerung nicht durch eine veränderte Mikrotubulidynamik erklärt werden kann. Die Verzögerung ist auch keine Konsequenz des physischen Einschlusses der Chromosomen im Aktinnetz, da die Erfassung in verlangsamten oder sogar vollständig stabilisierten Aktinnetzen nicht verhindert ist.

Zusammen zeigen meine Ergebnisse auf einen Aktin-abhängigen Mechanismus hin, der die Bildung von lateralen Kinetochor-Mikrotubuli-Befestigungen verhindert. Der synchrone Abbau dieser F-Aktin-Strukturen legt die Kinetochore frei und synchronisiert damit die Chromosomenerfassung.

Dies ist die erste Beschreibung eines Mechanismus, durch den das Aktin-Zytoskelett direkt den Spindelaufbau beeinflusst, und welcher die Chromosomensuche und -erfassung aktiv steuert und koordiniert. Ich zeige, wie dieser Mechanismus die Chromosomenkongression im spezialisierten Oozytenkern koordiniert. Solche Mechanismen könnten eine breitere Relevanz haben, wie beispielsweise um mitotische Ereignisse wie Zellrundung, die durch das Aktin-Zytoskelett mit Spindelanordnung vermittelt wird, zu synchronisieren. Der detaillierte molekulare Mechanismus, wie F-actin die Chromosomen-Mikrotubulus-Befestigung verhindert, bleibt eine aufregende offene Frage für zukünftige Studien.

Table of content:

Acknowledgements	i
Abstract	ii
Zusammenfassung	iv
Table of content	vi
List of figures	ix
List of abbreviations	xii
1. Introduction	**1**
1.1. Cell division and essential components of the spindle	1
1.1.1. Kinetochores: the microtubule binding platforms on the chromosomes	2
1.1.2. Microtubules: the dynamic polymers building up the spindle	3
1.2. Chromosome congression: lateral transport of chromosomes and end-on kinetochore – microtubule attachments	5
1.2.1. Initial lateral kinetochore-microtubule attachments	5
1.2.2. Stable end-on kinetochore-microtubule attachments	7
1.2.3. Mechanisms of the chromosome congression	7
1.3. Microtubules “search and capture”	9
1.3.1. Origin of the “search and capture” model	9
1.3.2. Mechanisms that facilitate chromosome search by microtubules	10
1.3.3. Exception to the rule: acentrosomal spindle assembly	13
1.4. Actin in cell division	15
1.4.1. Possible roles of actin in spindle assembly	15
1.4.2. Cooperation between actin and microtubules: focus on spindle formation	17
1.5. Chromosome congression in starfish oocyte	21
1.5.1. Starfish as a model system to study cell division	21
1.5.2. Several actin structures are formed during oocyte meiosis	22
1.5.3. Overview of chromosome congression in starfish oocytes	24
2. Aims	**27**
3. Materials and methods	**28**
3.1. Starfish and oocyte handling	28

3.2. Cloning of the fluorescent markers 28
3.3. RNA synthesis 29
3.4. Oocyte microinjection 29
3.4.1. Protein injection 31
3.4.2. Phalloidin injection 32
3.5. Chemical and inhibitor treatments 33
3.6. Confocal microscopy 33
3.7. Basic image processing 35
3.8. Chromosome tracking in 3D 38
3.9. Oocyte chemical fixation and immunostaining 39
3.10. Computational modelling in *Cytosim* 40
3.11. Correlative light-electron microscopy of starfish oocytes 41
3.11.1. Sample preparation 41
3.11.2. Oocyte chemical fixation 41
3.11.3. Sample processing and resin infiltration 41
3.11.4. MicroCT imaging 42
3.11.5. Image registration with Amira software 42
3.11.6. Sample trimming, serial sectioning and EM imaging 43
Acknowledgements 44
4. Results **45**
4.1. Phases of chromosome congression in starfish oocytes 45
4.1.1. Initial chromosome-microtubule attachment is lateral 49
4.1.2. Dynein transports laterally attached chromosomes along the microtubules 51
4.1.3. No chromosome - mediated microtubule nucleation detected in early prometaphase 52
4.2. Cooperation between actin and microtubules during chromosome congression 54
4.2.1. Actin synchronizes chromosome capture by microtubules 54
4.2.2. Microtubule dynamics is not affected by the actin meshwork 59
4.2.3. Chromatin is not directly interacting with the actin meshwork 60
4.2.4. Chromosomes can be captured and transported through the stabilized actin meshwork 62

4.2.5. Actin meshwork contraction speed does not affect chromosome capture kinetics 63

4.3. Computational model of the two-staged chromosome congression 68

4.3.1. Establishment of a mathematical model of chromosome congression and capture 68

4.3.2. Modelling predicts delay in chromosome capture caused by blocking the kinetochores 71

Summary of the results 73

5. Discussion **74**

5.1. A coordinated action of actin and microtubules is required to prevent aneuploidy during chromosome congression in starfish oocytes 74

5.2. Chromosome capture by microtubules during the two-staged chromosome congression 75

5.3. Formins, possible molecular player coordinating actin and microtubules during the chromosome congression 76

5.4. Depolymerization of the 'actin patches' correlates with the chromosome capture 77

5.5. Suggested mechanism: F-actin structures shield kinetochores delaying microtubule attachments 79

5.6. Future directions: how to address role of actin in the chromosome capture 80

6. Appendix **83**

6.1. Visualization of chromosomes with correlative light - electron microscopy 83

6.2. Microtubule spatial search is quite robust 87

6.3. *Cytosim* script for the chromosome congression modelling 89

6.4. Chromosome capture events for individual oocytes in control, upon actin meshwork disruption or stabilization 92

7. References **94**

List of figures

Figure 1.1. Stages of mitosis in the somatic cells 1

Figure 1.2. Scheme and ultrastructure of the vertebrate kinetochores 2

Figure 1.3. Kinetochore structure 3

Figure 1.4. Microtubule structure and dynamics 5

Figure 1.5. Molecular mechanisms underlying kinetochore-microtubule interactions 6

Figure 1.6. Immunostaining of the early prometaphase in newt cells containing mono-oriented and unattached chromosomes 8

Figure 1.7. Chromosome congression model in cells with the centrosomal spindle assembly mechanism 9

Figure 1.8. Models of microtubule - kinetochore capture 11

Figure 1.9. Acentrosomal spindle assembly in mouse oocyte 14

Figure 1.10. Mitotic spindle in plant cells contains F-actin filaments 16

Figure 1.11. Nabkin, a kinesin associating with actin and microtubules that is essential for spindle positioning in *Xenopus* oocytes 19

Figure 1.12. A model of kinetochore – microtubule attachments containing formin mDia3 20

Figure 1.13. Immature oocyte from starfish *Patiria miniata* 21

Figure 1.14. Steps in starfish oocyte meiosis 22

Figure 1.15. F-actin shell and actin spikes facilitating nuclear membrane fragmentation 23

Figure 1.16. Actin patches, formed simultaneously with the actin shell around the chromosomes, incorporate into the actin meshwork 23

Figure 1.17. Model of contractile actin meshwork transporting chromosomes 24

Figure 1.18. Actin meshwork and microtubules during chromosome congression 25

Figure 1.19. Chromosome congression by actin meshwork is independent of microtubules 25

Figure 1.20. Overview of the chromosome congression by actin and microtubule driven mechanisms 26

Figure 3.1. Principle of the oocyte microinjection 31

Figure 3.2. The basic principle of Airyscan detection 35

Figure 3.3. The principle of the 3D chromosome tracking algorithm 37

Figure 3.4. Defining the chromosome capture events as a transition point between actin- and microtubule-driven chromosome transport 39

Figure 4.1. Overview of the chromosome congression process from NEBD until spindle formation 46

Figure 4.2. Microtubule asters morphology during actin meshwork contraction 48

Figure 4.3. Microtubules attach laterally to the chromosomes and immediately transport them to the animal pole 50

Figure 4.4. Dynein transports chromosomes along the microtubules 51

Figure 4.5. Microtubule nucleation from chromatin 53

Figure 4.6. Chromosome capture kinetics in the starfish oocyte 55

Figure 4.7. Chromosome capture kinetics upon actin disruption 56

Figure 4.8. Scheme of chromosome gravity settlement in the oocyte 56

Figure 4.9. Actin synchronizes chromosome capture 57

Figure 4.10. Chromosome capture time and capture distance are independent from the chromosome initial position 58

Figure 4.11. Microtubule behavior is not affected by actin meshwork 59

Figure 4.12. Comparison of the microtubule tips lengths with and without the functional actin meshwork 60

Figure 4.13. Chromatin is not directly interacting with the actin meshwork 61

Figure 4.14. Chromosomes can be congressed through the completely stabilized actin meshwork 63

Figure 4.15. Decreasing actin meshwork contraction rate through the F-actin stabilization 65

Figure 4.16. Chromosome capture through the stabilized actin meshwork 65

Figure 4.17. Simulation of the two-staged chromosome congression process in starfish oocyte 67

Figure 4.18. Chromosomes and kinetochores morphology in the experiment versus simulation 68

Figure 4.19. Comparison of the microtubule lengths in simulation and experimental data 70

Figure 4.20. Modelling of the two-staged chromosome congression process 71

Figure 4.21. Modelling predicts, blocked kinetochores cause a delay of the chromosome capture in the control oocytes 72

Figure 22. Graphical summary of the results 73

Figure 5.1. F-actin patch depolymerization is synchronized with the chromosome capture 77

Figure 5.2. Structure and temporal dynamics of the actin patches around the chromosomes 78

Figure 5.3. Hypothetical F-actin structure, shielding kinetochores from the microtubules attachment 79

Figure 5.4. Scheme of the experiment addressing actin role in chromosome capture 82

Figure 6.1. CLEM imaging allows to target individual chromosomes in the starfish oocyte 86

Figure 6.2. Ultrastructure of a chromosome with a kinetochore plate 87

Figure 6.3. Long astral microtubules stabilized with Paclitaxel capture all the chromosomes without actin meshwork 88

Figure 6.4. Actin synchronizes chromosome capture by microtubules 92

Figure 6.5. Actin meshwork stabilization with the Utrophin-CH protein 93

List of abbreviations:

NEBD – nuclear envelope breakdown

Chr. – chromosome

MT(s) – microtubule(s)

CLEM – correlative light-electron microscopy

EM - electron microscopy

microCT - microscopic X-ray computed tomography

TEM – transmission electron microscopy

ROI – region of interest

3D – three-dimensional

TMA – transient microtubule array

1-MA – 1-methyladenine

bp - nucleotide base pairs

1. Introduction

1.1. Cell division and the essential components of the spindle

During the cell division process, the whole genome has to be correctly segregated between the two daughter cells. In most cell types, chromosome capture is mediated by centrosome nucleated astral microtubules, which grow and shrink in search of chromosomes. During prophase, chromosomes, each consisting of duplicated sister chromatids, get fully condensed. This is followed by nuclear envelope breakdown (NEBD), during which the nuclear membranes are disassembled (fig. 1.1). Consequently, all chromosomes are distributed within the volume of the whole cell, and cytoplasmic microtubules can access chromosomes. In the prometaphase, centrosomes begin to nucleate dynamic microtubules, searching for specialized chromosomal regions called the kinetochores. When all chromosomes are captured by microtubules, the cell transits to the metaphase: microtubules form stable end-on attachments on both sister kinetochores, one on each of the chromatids. At the end of this phase, chromosomes are aligned into the metaphase plate: sister kinetochores of each chromatid are attached to the microtubules from the opposite spindle poles (bi-orientation), creating tension. Correct attachment of all kinetochores to the spindle microtubules silences the spindle assembly checkpoint, allowing the cell to transit to anaphase: sister chromatids lose cohesion and are pulled to the opposite poles of the spindle. At telophase, which is the final stage of the cell division, the nuclear envelope is re-assembled and the chromosomes are de-condensed. Simultaneously, cytokinesis occurs (Alberts et al., 2007).

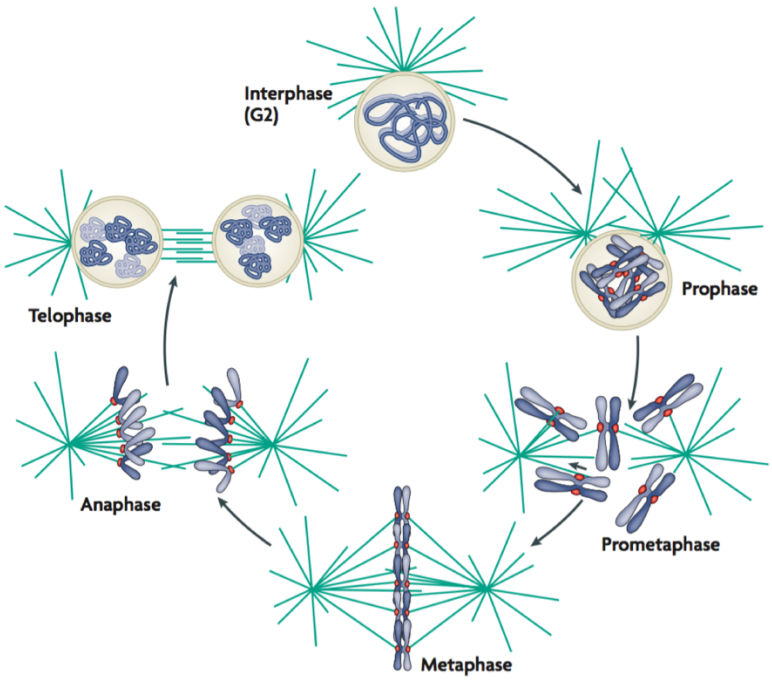

Figure 1.1. Stages of mitosis in the somatic cells. Schematic overview. Figure and legend adapted from (Cheeseman and Dessai, 2008).

1.1.1. Kinetochores: the microtubule binding platforms on the chromosomes

Kinetochores are multi-protein assemblies on the centromeric regions of chromosomes, which form right after the nuclear envelope breakdown (NEBD) (reviewed by Musacchio and Dessai, 2017). Centromere length varies in different species: from a point centromere in yeast, which consists of only one nucleosome (125 bp), to expanded chromosome regions in higher eukaryotes (Clarke and Carbon, 1980). In humans, centromere regions are organized from 171 bp long α–satellite repeats that can span over 4 million bp in size (Aldrup-Macdonald et al., 2014). However, centromeres are defined not only by the DNA sequence, but rather by the chromatin signature: centromere repeats are always flanked by heterochromatin regions (Murphy and Karpen, 1998; Karpen and Allshire, 1997). Their key molecular features, conserved among all animals (and fungi) are the canonical histone H3, replaced with its homolog, CENP-A (also known as CenH3) (Earnshaw et al., 1985). Unlike canonical histones, CENP-A is loaded into the nucleosomes already in the anaphase right after the sister chromatids separation, ensuring centromere maintenance through the cell cycle (Jansen et al., 2007; Schuh et al., 2007). CENP-A containing nucleosomes are more open, which leads to lower chromatin compaction and, consequently, looping out of the centromere DNA to form a kinetochore (Warburton at al., 1997). Other kinetochore proteins bind to CENP-A and create a functional kinetochore (Sullivan et al., 1994). Based on EM observations, kinetochores of higher eukaryotes are 250 nm wide and 80 nm deep three-layered structures, consisting of the inner and outer kinetochores, and a *fibrous corona*, which provides an interface for microtubule binding (Cheeseman and Dessai, 2008) (fig. 1.2).

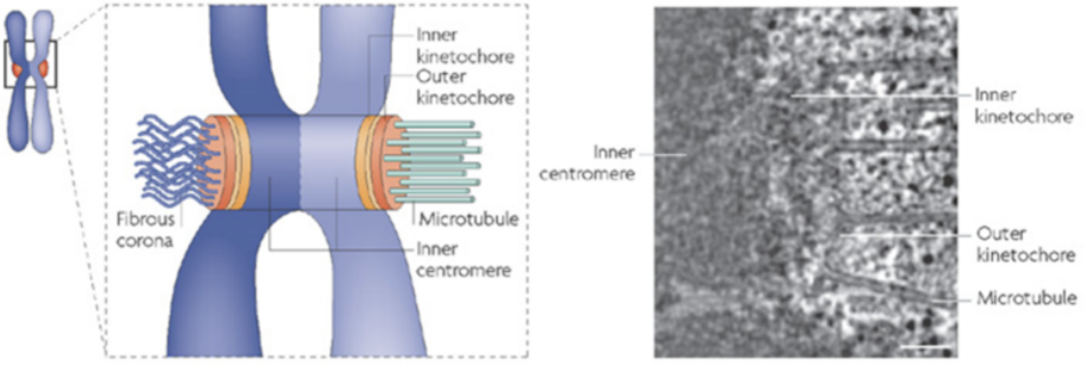

Figure 1.2. Scheme and ultrastructure of the vertebrate kinetochores. Figure and legend adapted from (Cheeseman and Dessai, 2008), scale bar 100 nm.

The inner kinetochore CCAN complex (Constitutive Centromere Associated Network) consists of 14 CENP proteins assembled in a hierarchical order (reviewed in Musacchio and Dessai, 2017) (fig. 1.3.). One of the central CCAN components, CENP-C, further stabilizes the centromeric nucleosomes (Klare at al., 2015) and connects them with the outer kinetochore protein Mis12 (Cheeseman and Dessai, 2008). Ndc80, the main microtubule capturing protein in the outer kinetochore, which from one end interacts with the inner kinetochore proteins and from the other with the microtubules

(Cheeseman et al., 2004; DeLuca et al., 2006). Ndc80 forms a high-density array, which is required for efficient microtubule binding (Alushin et al., 2010). Apart from Ndc80, a robust interaction with the microtubules is mediated by the Ska complex, or the Dam1 protein in yeast (Abad et al., 2016). Through oligomerization, Dam1 creates a ring-like structure that holds the microtubule tip and additionally stabilizes Ndc80 binding to microtubules (Ramey et al., 2011). Another component of the outer kinetochore, the RZZ complex, recruits motor protein dynein and its activator dynactin to the kinetochore (Karess, 2005). Dynein, as well as CENP-E, which is a kinesin-like motor protein, mediate the initial lateral kinetochore-microtubule attachment and transport the chromosomes along the microtubule walls (Martin-Lluesma et al., 2002; Tanudji et al, 2004; Maia et al., 2010).

Kinetochore functions not only include the initial microtubule attachment, but also corrections of the existing erroneous attachments, and spindle assembly checkpoint regulation. Several checkpoint proteins associate with the kinetochore *fibrous corona* and ensure correct chromosome segregation (reviewed in Lampson and Grishchuk, 2017).

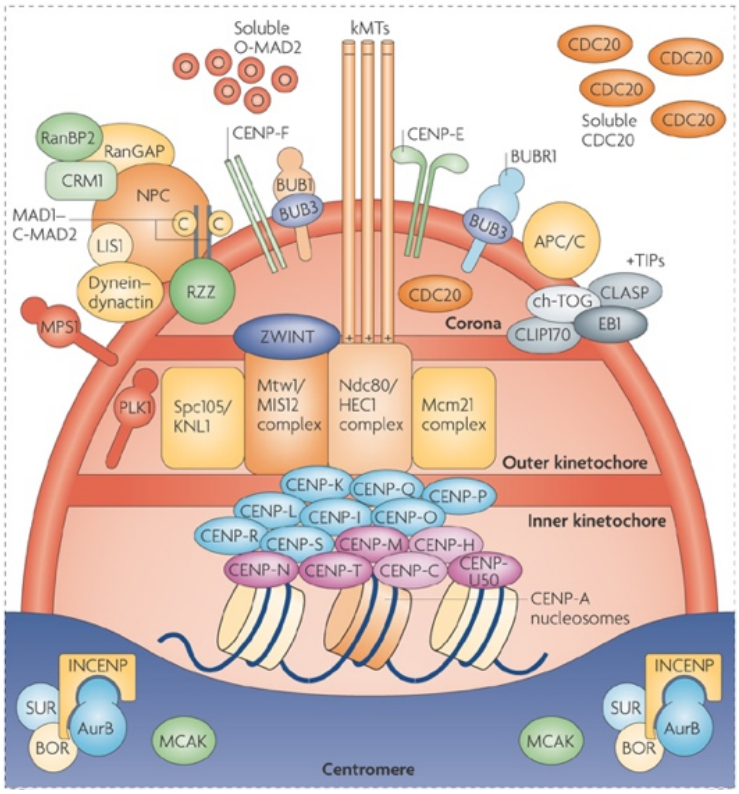

Figure 1.3. Kinetochore structure. In the centromere region, a specialized nucleosome containing CENP-A histone H3 homolog is defining the kinetochore position. Several inner kinetochore proteins associate with CENP-A through the cell cycle (CCAN complex in cyan and purple). Several other proteins associate with the CCAN during the cell division and form an outer kinetochore. They recruit the spindle assembly checkpoint (SAC) proteins. Furthermore, Ndc80 is directly binding microtubules. Several other proteins, like dynein and CENP-E, are important for the establishment of the lateral attachment. Figure and legend modified from (Musacchio et al., 2007).

1.1.2. Microtubules: the dynamic polymers building up the spindle

Microtubules are polymer filaments built from dimers of two proteins: α- tubulin and β- tubulin. Tubulin α/β- dimers polymerize into protofilaments, creating a hollow cylinder which is 24 nm thick on the outer diameter. In the protofilament, dimers interact in the head-to tail fashion. As a result, each protofilament as well as the whole microtubule has an intrinsic polarity: the end exposing α-tubulin is called the minus-end and the one opposite to it with β-tubulin as a plus-end (fig. 1.4.) (Mitchison, 1993). Microtubule minus–ends are much more stable than the plus-ends and have lower probability of depolymerization (Walker et al., 1988). Plus–ends, in contrast, are very dynamic with the beta tubulin protein exposed at the microtubule tip.

A tubulin dimer, containing GTP can bind to the growing microtubule end. Interaction of the α-tubulin from the new dimer with the β-tubulin exposed on the tip of the filament causes GTP hydrolysis. Once the GTP molecule is hydrolyzed to GDP, β-tubulin changes conformation causing α/β-dimer dissociation from the microtubule (Nogales, 2015). However, if a new α/β-dimer binds to the attached tubulin dimer containing GTP, such a filament will form a GTP cap. As a result, the microtubule becomes stabilized and can undergo polymerization (Carlier, 1988). Next, GTP is hydrolyzed to GDP along the microtubule lattice, thereby, promoting microtubule depolymerization, or catastrophe. GDP is exchanged to GTP when tubulin monomer is in the free unpolymerized state. These rounds of polymerization/depolymerization are reversible. Altogether, GTP hydrolysis drives this intermittent growth regime of microtubules called dynamic instability.

During mitosis or meiosis microtubules are in the dynamic instability mode (Mitchison and Kirschner, 1884): the plus-end is always polymerizing/depolymerizing, while the minus-end is stabilized with the γ-tubulin ring complex. Depending on the tubulin concentration, as well as on the microtubule binding proteins regulating the polymerization and depolymerization rates, dynamic instability can be modulated in different ways. Either the plus-end can be oscillating between growing and shrinking states, like in mitosis, or the microtubule length may be maintained stable, like during the interphase. Dynamic instability is crucial for chromosome search and capture, spindle maintenance and chromosome segregation (reviewed in Akhmanova and Steinmetz, 2008).

Microtubules serve as tracks for the cellular transport, guiding the motion of the chromosomes during the cell division. Due to the intrinsic polarity of the microtubules, the transport is directed and mediated by the microtubule molecular motors dependent on ATP. The two main classes are kinesins, which are mainly plus-end directed motors, and dyneins, minus-directed motors (Alberts et al., 2007). In most cell types, spindle microtubules are nucleated at the MTOCs (Microtubule Organizing Centers) or the centrosomes (Schuh and Ellenberg, 2007). In the MTOCs, a γ-tubulin

ring complex (γ-TURC) creates the seed for α/β-tubulin dimer polymerization (reviewed in Lin et al., 2015). Thus, microtubules are protected at the minus-end, and the dynamic plus-ends are growing in all directions, while searching the chromosomes.

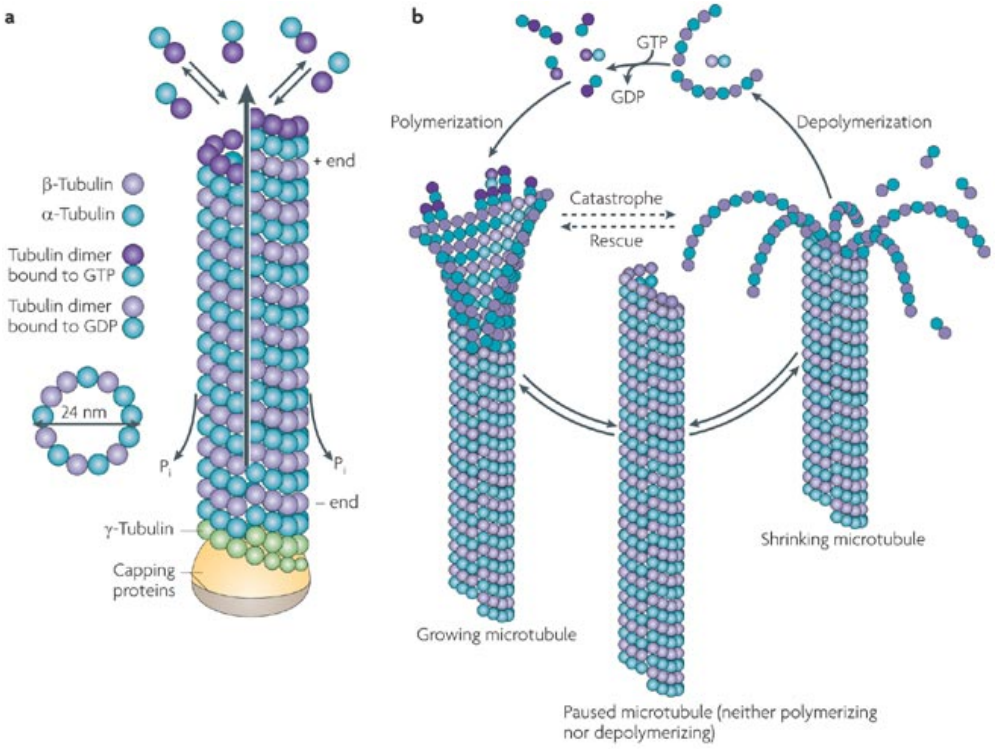

Figure 1.4. Microtubule structure and dynamics. Microtubules are polymers of α- and β-tubulin heterodimers, which align into a ring of 13 protofilaments, building the hollow microtubules of typically 24 μm in diameter. The alignment of protofilaments ensures distinct intrinsic polarity: α-tubulin defines a stable minus-end and β-tubulin, the plus-end. A cap of GTP at the plus-end follows microtubule polymerization at the plus-end. Depolymerization results from microtubule destabilization due to the GTP hydrolysis. As a result, the microtubule undergoes catastrophe and shrinks, though reversibly. The minus-end is often stabilized by capping proteins. Figure and legend from (Conde and Caceres, 2009).

1.2. Chromosome congression: lateral transport of chromosomes and end-on kinetochore – microtubule attachment

1.2.1. Initial lateral kinetochore-microtubule attachments

The initial attachment between the microtubule and the kinetochore can occur almost immediately after the nuclear envelope breakdown (NEBD), and is called *lateral attachment*. At this stage, kinetochore is binding to the wall of a single microtubule, while the microtubule end remains free and can grow further. The lateral type of attachment is a weak attachment, but sufficient to ensure chromosome movement to one of the spindle poles (fig. 1.5.). At this stage, transport is realized either by the dynein, or CENP-E molecular motors (Barisic et al., 2014). Chromosomes are typically transported with the speed of 25-55 μm/min (Rieder and Alexander, 1990). Notably, during the chromosome segregation in the anaphase, chromosomes are transported with similar velocity. While establishing the lateral attachment, kinetochore tethering to the microtubule walls provides a larger contact area for the stochastic microtubule-

kinetochore capture and, thus, increases the efficiency of the search (Alexander and Rieder., 1991; Magidson et al., 2011).

As soon as the chromosomes attach to the microtubules, they start moving to achieve bi-orientation. If the chromosome at the NEBD is favorably located between the microtubule asters, it will be directly transported to the metaphase plate via *direct congression*. However, if the chromosome is initially located at the periphery of the cell, it will be first transported to the aster center and then to the spindle equator. This mechanism is called *peripheral congression* (reviewed in Maiato et al., 2017). Such polar chromosomes are first transported by dynein to the pole, and only later with CENP-E to the middle of the spindle (Barisic et al., 2014). Thereby, an interesting question arises: how is the position of the chromosomes distinguished in the cell and how is the work of different molecular motors coordinated? The 'spindle navigation system' is based on tubulin post-translational modifications. In the spindle, several microtubule populations co-exist simultaneously, differing in tubulin post-translational modifications, such as tyrosination levels (so called, tubulin-code) (Gundersen et al., 1984; Barisic et al., 2015). Using these differences, dynein mediated transport of polar chromosomes can be overtaken by CENP-E to drive the congression of the chromosomes to the mitotic plate (Janke, 2014).

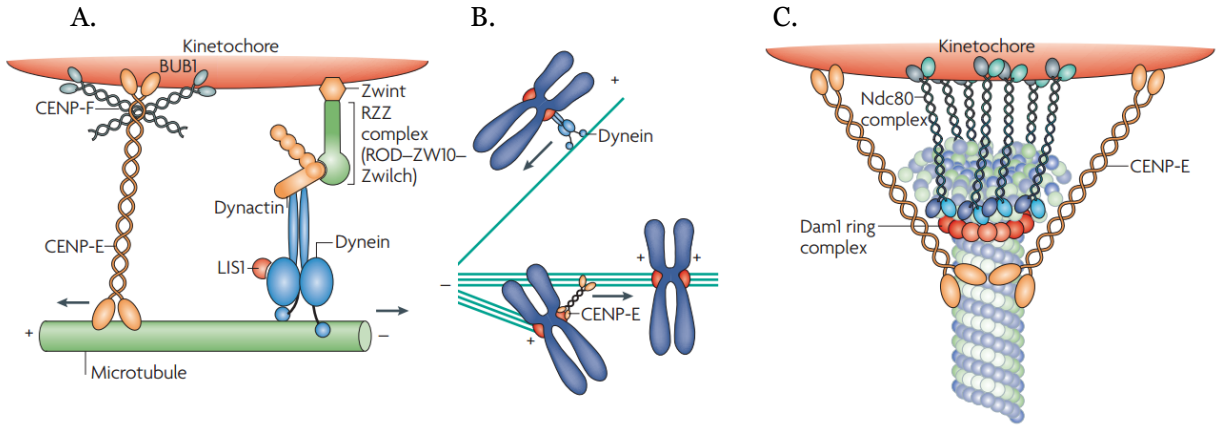

Figure 1.5. Molecular mechanisms underlying kinetochore-microtubule interactions. **A.** Chromosome lateral transport. The two motor proteins transporting the kinetochores on the microtubules are CENP-E and dynein. Dynein is associated to the ROD-ZW10-Zwilch (RZZ) protein complex, part of the outer kinetochore protein ensemble. **B.** Overview of the chromosome motion on the microtubules. Different attachment states are shown, as well as molecular motors contributing to lateral chromosome transport. **C.** Mature kinetochore-end-on attachment. Microtubule depolymerization is coupled to the chromosome movement. Several Ndc80 complexes interact with the single microtubule. This interaction is further stabilized by the Ska complex (Dam1 in yeast), which oligomerizes and additionally stabilizes the dynamic attachment. Figure and legend adapted from (Cheeseman and Dessai, 2008).

1.2.2. Stable end-on kinetochore-microtubule attachments

During lateral chromosome movement, the chromosome has a chance to interact with other microtubules, including those from the opposite spindle pole. Subsequently, lateral chromosome attachment to the microtubule wall needs to be converted into the

stable end-on attachment (Drpic et al., 2015), where the kinetochore plate is oriented perpendicularly to the microtubule plus-end (Tanaka et al., 2005). End-on attachment is arranged such that microtubule plus-end remains free for the microtubule growth and shrinkage (Gandhi et al., 2011). This type of attachment is realized primarily through the Ndc80 protein (fig 1.5.C) (Maure et al., 2011). The interaction between Mis12 and Ndc80 proteins provides a binding surface for the microtubules (Kline et al., 2006; Cheeseman et al., 2006). The end-on attachment is further stabilized by the Ska complex (Dam1 protein in yeast) (Legal et al., 2016), as well as CENP-E (Kim et al., 2008). Using the electron tomography, McIntosh lab revealed a ring-independent mechanism coupling microtubule dynamics to the kinetochore motion, based on the direct interactions between individual curved protofilaments at the microtubule plus-tip and kinetochore fibrils, presumably via CENP-E and Ndc80 (McIntosh et al., 2008).

Conversion of the lateral to end-on microtubule attachment was recently described by the Draviam lab using high resolution imaging assay (Shrestha et al., 2013). Authors demonstrated that laterally attached kinetochores seldom detach from the microtubule walls. The two intermediate stages of the lateral to end-on conversion were imaged live. The first step was CENP-E tethering to the microtubule wall that was required for the establishment of the partial end-on attachment. In the second step, microtubule plus-end depolymerization by the MCAK was required to get a final end-on attachment. Altogether, lateral to end-on conversion is a sequence of pre-determined events, rather than stochastic direct plus-end microtubule capture (Shrestha et al., 2013).

1.2.3. Mechanisms of the chromosome congression

Once the chromosomes are attached to the microtubules, they start to move to achieve bi-orientation (reviewed in Maiato et al., 2017). A microtubule attached to the kinetochore is called a *k-fiber* (kinetochore fiber) (fig. 1.6). Over the course of k-fiber maturation and stabilization of the kinetochore attachment, several microtubules align parallel and attach to the same kinetochore (McEwen et al., 1997). Typically, at the anaphase onset mature k-fiber consists of 20-30 single microtubules anchored with their plus ends on the kinetochore plate (Dong et al., 2007). K-fibers generate pulling forces on the kinetochores, which drives chromosome oscillation around the spindle equator (Rieder and Alexander, 1990).

Microtubule dynamic instability generates a force from the spindle poles to the equator: polar ejection forces, which are also known as polar wind. The nature of the polar ejection forces was studied by C. Reader using laser microsurgery (Rieder et al., 1986). The authors generated acentric chromosome fragments (i.e. without the kinetochores). Kinetochore-less chromatin fragments were immediately ejected from the spindle area, while the kinetochore-containing fragments were transported to the spindle pole. Thus, polar ejection forces are generated by the astral microtubules acting

on the chromosome arms and counterbalancing the kinetochore pulling forces (Rieder and Salmon, 1994). This force-balancing mechanism is hypothesized to be the main driver of the chromosome oscillations starting after their bi-orientation. According to this hypothesis, chromosome alignment into the metaphase plate can be explained as a result of a force balance of the kinetochore-pulling forces towards each of the spindle poles and opposing polar ejection forces (Maiato et al, 2017).

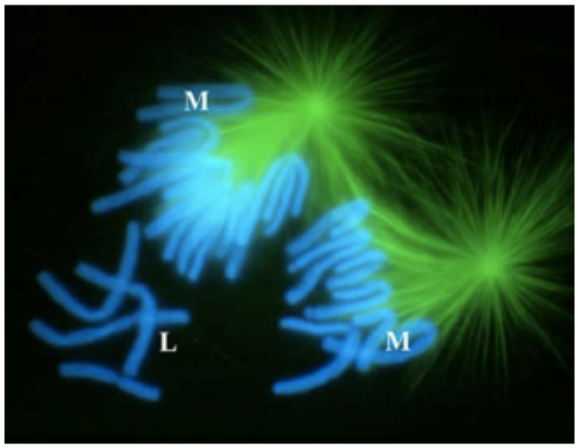

Figure 1.6. Immunostaining of the early prometaphase in newt cells containing mono-oriented and unattached chromosomes. Several chromosomes incorporated into the spindle (M) seem to possess only a single K-fiber. No microtubules are detected in the vicinity of the lost chromosomes (L). Figure and legend adapted from (Rieder, 2005).

Chromokinesins, which are plus-end directed microtubule motors, possess DNA-binding properties and associate with the chromosome arms during cell division (Wang and Adler, 1995; Vernos et al., 1995). Given such activity, chromokinesins could contribute to the polar ejection forces in the spindle. However, it was demonstrated that the processivity of these motors is low. They are not the main contributors of chromosome movement to the equator, although, chromokinesins push the chromosome arms out of the spindle body towards the cell periphery (Wandke et al., 2012; Yajima et al., 2003; Cane et al., 2013).

In summary, chromosome congression and alignment into the metaphase plate is a result of coordinated activity of the kinetochore and chromosome arm associated microtubule motors, as well as polar ejection forces and k-fiber polymerization-depolymerization activity. Altogether it is formalized as the 'push-pull hypothesis' (Rieder and Salmon, 1994; Skibbens et al., 1993; Barisic and Maiato, 2015). The integrated model is schematically represented in fig. 1.7.

Another function of the chromosome congression process is preventing erroneous kinetochore-microtubule attachments. In the vicinity of the spindle poles, kinetochores-microtubules attachments are destabilized by high Aurora A kinase activity causing Ndc80 phosphorylation, among other proteins. This leads to lower Ndc80 affinity to the microtubules (Ye et al., 2015; Chmátal et al., 2015). Moreover, tension generated after the chromosome bi-orientation is requited for the stabilization

of the correct attachments (King and Nicklas, 2000). Once all the chromosomes achieve amphitelic bipolar attachment, the cell is ready for the anaphase onset (Lara-Gonzalez et. al., 2012). However, the main player establishing correct kinetochore-microtubules attachments is Aurora B kinase, which is a component of the Chromosome Passenger Complex (CPC) complex localized between the sister chromatids. Lack of tension between sister chromatids upon a syntelic or merotelic attachment is sensed through the Aurora B, which phosphorylates several proteins, including Ndc80. This results in microtubule detachment from the kinetochore, and, thereby, ensures accurate chromosome segregation (Tanaka et al., 2002; Hauf et al., 2003; Cheeseman et al., 2006).

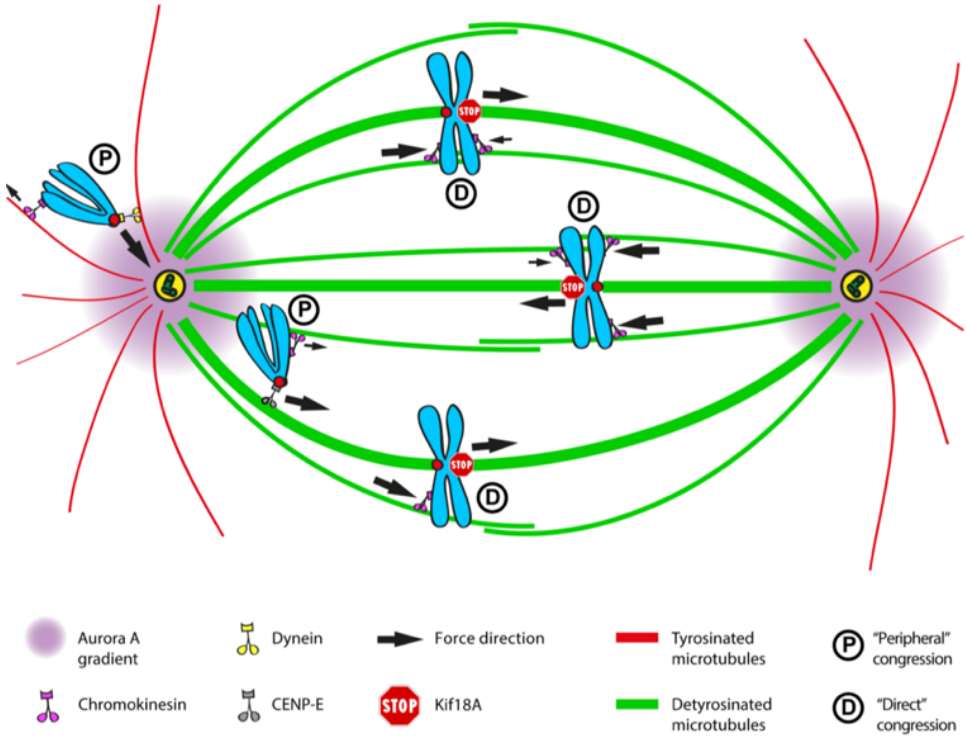

Figure 1.7. Chromosome congression model in cells with the centrosomal spindle assembly mechanism. Kif18A regulates the microtubule length and dynamics at the metaphase plate (Stumpff et al., 2008). Other molecular players in the model are discussed in the text. Figure and legend adopted from (Maiato et al., 2017).

1.3. Microtubule "search and capture"

1.3.1. Origin of the "search and capture" model

As mentioned previously, microtubule dynamic instability was first described by Mitchison and Kirschner (Mitchison and Kirschner, 1984). Based on these observations, two years later the same authors suggested the "chromosome search and capture" hypothesis (Kirschner and Mitchison, 1986). In contrast to other cytoskeletal elements, microtubule plus-end tips are able to quickly oscillate between growing and shrinking regimes in a highly regulated manner. Upon entry into mitosis or meiosis, microtubules change their behavior from long stable interphase microtubules to short dynamic polymers, alternating their length over several micrometers. Such behavior suggests that microtubules could "search" for the chromosomes. When such a

microtubule binds to its target (kinetochore), the microtubule tip is stabilized: a "capture" event occurs. Given that the dynamic microtubules are long enough to span the volume of the whole cell during the prometaphase, the "search and capture" mechanism incorporates all chromosomes into the spindle.

Subsequently, direct kinetochore-microtubule capture was visualized in the living cells (Hayden et al, 1990; Rieder and Alexander, 1990), which confirmed the hypothesis. However, the question remained whether such a "search and capture" mechanism is efficient enough to capture all 46 chromosomes in the human somatic cell. Computer modelling predicts that unbiased "search and capture" would take unrealistically long time: incorporation of all the chromosomes in the cell through the unbiased search would take almost 20 hours, while in cells all the chromosomes are captured within 15-20 minutes (Wollman et al., 2005). Furthermore, not all the chromosomes are located in a favorable orientation to the centrosomes, thus, hindering the capture process. Altogether, these calculations imply existence of the facilitation mechanism(s) increasing the "search and capture" efficiency. In recent years, several of them were discovered.

1.3.2. Mechanisms that facilitate chromosome search by microtubules

The probability to capture the chromosomes through the unbiased stochastic microtubule polymerization is directly linked to the volume of the cell (Wollman et al., 2005). Thereby, the probability to capture a 200 nm large kinetochore at the distance of 15 -20 μm is extremely low. Nevertheless, in most cell types "search and capture" is the predominant mechanism for chromosome incorporation into the spindle (McIntosh et al., 2002) (summarized on fig. 1.8). One reason is that, kinetochores and chromatin actively facilitate this process by nucleating microtubules. Similarly, viral DNA or plasmid DNA-coated beads, injected into the cytoplasm or in cell extract, nucleate microtubules (Heald et al., 1996; Karsenti et al., 1984). Chromosomes stabilize the microtubule plus-ends in their direct proximity and facilitate *de novo* microtubule nucleation (reviewed in Heald and Khodjakov, 2015). Small GTPase Ran is one of the key regulators of this process (Dasso, 2002; Hetzer et al., 2002). Several other players required for the bipolar spindle assembly include γ-tubulin, TPX2, augmin, etc. (Wilde et al., 2001; Gruss et al., 2002; Uehara et al., 2009; Petry and Vale, 2015).

Adding RanGTP to the *Xenopus* egg extracts causes assembly of the spindle-like structures (Kalab et al., 1999; Carazo-Salas et al., 1999; Wilde and Zheng, 1999). RanGTP gradient in generated around the chromosomes via the following mechanism: guanine exchange factor RCC1 associates with the chromatin and promotes the formation of GTP-bound Ran close to the chromosomes. While diffusing away from the chromosomes, RanGTP is hydrolyzed to RanGDP by RanGAP, which is free in the cytoplasm, thereby, creating a molecular gradient. RanGTP gradient was first

demonstrated in *Xenopus* egg extracts (Caudron et al., 2005; Kalab et al., 2002), and later directly visualized in the living cells (Kalab et al., 2006). Blocking the RanGTP has severe consequences for the acentrosomal spindle assembly. However, somatic cells with the centrosomal microtubule nucleation are less dependent on RanGTP gradient perturbation (Kalab et al., 2006). RanGTP not only stabilizes microtubule plus-ends, but also indirectly controls the microtubule assembly by the microtubule-associated protein TPX2 (Gruss et al., 2002; Gruss et al., 2004). Not only chromosome arms, but also kinetochores are nucleating microtubules. RanGTP localization on the kinetochores depends on the RCC1 activity. Kinetochore-nucleated microtubules, as well as those nucleated around the chromosomes speed up the kinetochore capture and spindle assembly (Maiato et al. 2004; Khodjakov et al., 2003).

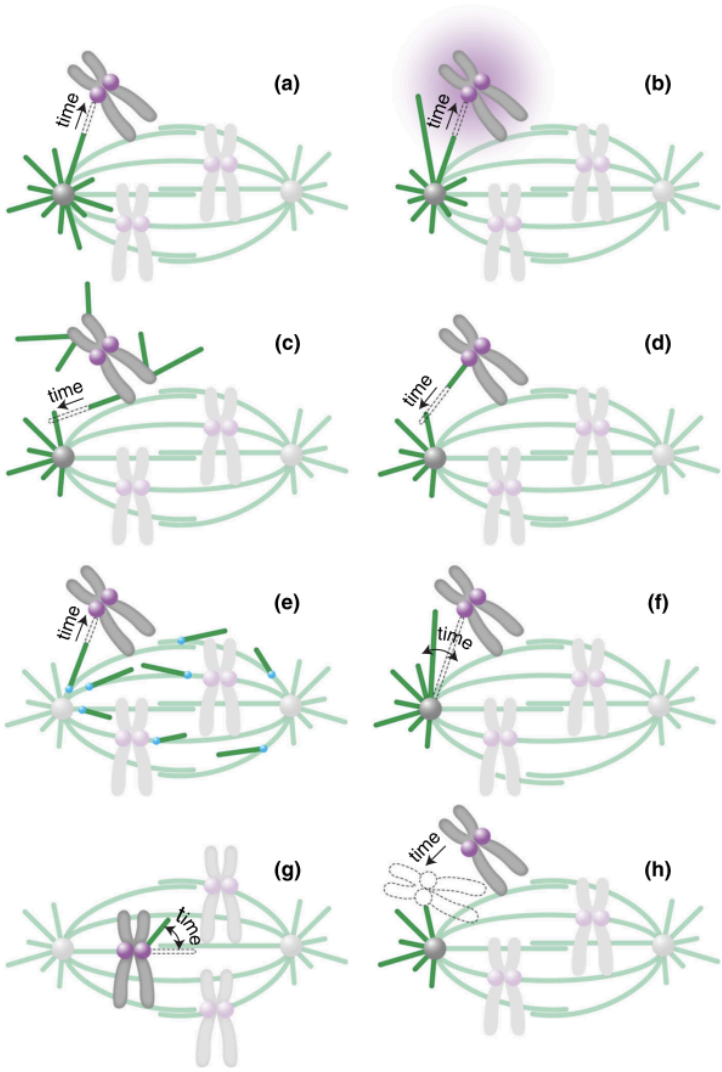

Figure 1.8. Models of microtubule- kinetochore capture. a. Classical search and capture. **b**. Biased microtubule nucleation towards the chromosome. **c**. Microtubule outgrowth from the chromosomes. **d**. Microtubule outgrowth from the kinetochores. **e**. Branched microtubule nucleation. **f**. Microtubule pivoting. **g**. Pivoting of the kinetochore-nucleated microtubule. **h**. Chromosome motion. Figure and legend adapted from (Pavin and Tolić-Nørrelykke, 2014).

An interesting question arises about the polarity of the microtubules nucleated from the kinetochores and chromosome arms. Microtubules nucleated from the chromatin

are polymerized from the plus-end (Kitamura et al. 2010), thus, are growing in the opposite orientation to the spindle microtubules. Once such chromosomal microtubule is attached to the existing spindle microtubules, and a new kinetochore lateral attachment is formed, this microtubule is disassembled (Kitamura et al. 2010).

Microtubules are known to be nucleated not only from the centrosomes and chromosomes, but also from the existing microtubules (Mahoney et al., 2006; Brugues et al., 2012). *Branched microtubule nucleation* depends on the γ-tubulin complexes (Goshima et al., 2007), which are specifically targeted to the spindle microtubules by augmin (Uehara et al., 2009, Petry et al., 2011). Branched microtubules grow parallel to the template microtubule, thus preserving the microtubule polarity in the spindle (Petry et al., 2013).

The branched microtubule nucleation model explains the assembly of extremely large asters in *Xenopus* eggs, which are more than 1 mm large and divide every 30 min (Ishihara et al., 2014). In this model, microtubules are initially nucleated at the centrosomes, while later aster growth is sustained by the branched microtubule nucleation away from the centrosomes from the already existing microtubules. This hypothesis explains how asters can span the volume of such large cells in a short time.

In small cells like fission yeast, chromosomes can be captured by *microtubules pivoting*, i.e., by planar exploration of space as they search for the kinetochores (Kalinina et al., 2013). The direction of the pivoting is random and does not require ATP energy or additional microtubule polymerization. The model predicts that this type of interaction is efficient for the capture of all chromosomes, however only in extremely small cells like fission yeast (Cojoc et al., 2016).

Computer modeling predicts that if all 46 chromosomes were randomly positioned in human cells, only approximately 3% of them would be sterically accessible for the spindle microtubules (Paul et al., 2009). In this model, once one of the kinetochores is captured by the microtubule, the whole chromosome rotates, positioning the second lagging kinetochore favorably for the microtubule capture. Special mechanisms drive the predominant positioning of unattached (or laterally attached) chromosomes into certain spatial patterns. Thus, kinetochores are being actively presented to the searching microtubules (Magidson et al., 2011; Kitajima et al., 2011), and arranged into the toroid- or belt-like shape at the cell equator. Chromokinesins generate forces on the chromosome arms, predominantly pushing them outside of the spindle (Rieder and Salmon., 1994; Vanneste et al., 2011). Consistently with this, depletion of the chromokinesins increases the spindle assembly time and chromosome segregation errors during the anaphase (Magidson et al., 2011).

Several modelling and experimental studies suggest that the capture efficiency of small kinetochores is quite low, thus increasing the search time (Wollman et al., 2005;

McEwen et al., 1998). Indeed, kinetochore enlargement has been observed in several cell types (Hoffman et al., 2001; Thrower et al., 1996; Wynne and Funabiki, 2015). Recently, with the advances in correlative light and electron microscopy, yet another facilitation mechanism was revealed: during prophase, unattached kinetochores are enlarged, thereby accelerating the spindle assembly. Once the end-on kinetochore attachment is formed, the chromosome aligns and the kinetochore plate compacts under the tension. Modelling of the described process confirmed that such kinetochore expansion-contraction facilitates spindle assembly by reducing the chromosome search time, as well as the number of the erroneous kinetochore-microtubule attachments (Magidson et al., 2015).

Moreover, recent studies by Tsai and Ma (Tsai et al, 2006; Ma et al., 2011) suggest that the area around the spindle can be partially shielded by nuclear envelope remnants from the rest of the cell. Such compartmentalization keeps all the components of the spindle apparatus in a confined space, and creates a barrier for tubulin monomer diffusion, as well as other proteins regulating mitosis. In somatic cells, the above-mentioned cage-like structure can be composed of intermediate filaments that surround the nucleus in the interphase (Mandeville and Rieder, 1990). On the other hand, this barrier also prevents other cellular organelles from entering the spindle area and sterically hindering the microtubule search.

1.3.3. Exception to the rule: acentrosomal spindle assembly

Oocytes are specialized cells that undergo two steps of meiotic (reductional) division in order to become a fertile egg. These cells grow extremely large in order to store nutrients (proteins, RNA, and lipids) needed to support embryonic development. To maintain the enormous cell size, meiotic division has to be highly asymmetric, producing a small polar body and a large gamete cell that retains nutrients for a single egg. Constrained by this high asymmetry of division, the meiotic spindle needs to be very small as well, while the chromosomes are scattered in a large nuclear volume of the cell (Alberts et al., 2007).

In most of the species, oocytes eliminate their centrioles before meiotic division (Szollosi et al., 1972; Manandhar et al., 2005), for reasons still speculated. Presumably, removing centrosomes and astral microtubules could serve as a mechanism to form a small spindle for the asymmetric meiotic division. Furthermore, in this way, oocytes avoid premature parthenogenetic division and/or multipolar spindle formation upon fertilization (Bennabi et al., 2016). Interestingly, in somatic cells, which normally assemble spindles from the centrosomes, if the centrioles are laser-ablated, these cells are still able to divide (Khodjakov et al., 2000; Debec et al., 2010). Moreover, all plant cells undergo acentrosomal spindle assembly, with actin involved in this process (see chapter 1.4) (Czaban and Forer, 1992).

In *Drosophila* oocytes, microtubule nucleation starts directly from the chromatin (Matthies et al., 1996). A similar mechanism of spindle formation is also observed in *Xenopus* egg extracts, when the spindle assembles on the DNA-coated beads or sperm DNA (Karsenti et al., 1984). However, *in vivo Xenopus* oocyte spindle assembly is understood much less (see below). In mouse oocytes, the spindle is organized from several aMTOCs (acentrosomal microtubule organizing centers), which localize at the nuclear membranes before NEBD and capture chromosomes in prometaphase (Schuh and Ellenberg, 2007) (fig. 1.9). Notably, in mice centrioles are assembled *de novo* in the early embryogenesis, however during the course of the first few embryonic divisions, the spindle assembly gradually switches from aMTOCs to the canonical centrosomal pathway (Clift and Schuh, 2013). In human oocytes, as was described recently, the mechanism is yet different: Spindle assembly starts from the chromosomes and takes a very long time (16 hours). At certain stages, the spindle is intrinsically instable and possesses abnormal microtubule-kinetochore attachments (Holubcova et al., 2015). Acentrosomal spindle assembly is believed to be very erroneous, often causing the formation of aneuploid female gametes (reviewed in Webster and Schuh, 2017). The following steps of spindle assembly are conserved in all the species: after/during the chromosome capture, microtubules align into parallel arrays. Several kinesin types are required for 'closing' the spindle poles and forming a bi-polar spindle. This mechanism allows the formation of a very small spindle compared to oocyte size (Bennabi et al., 2016).

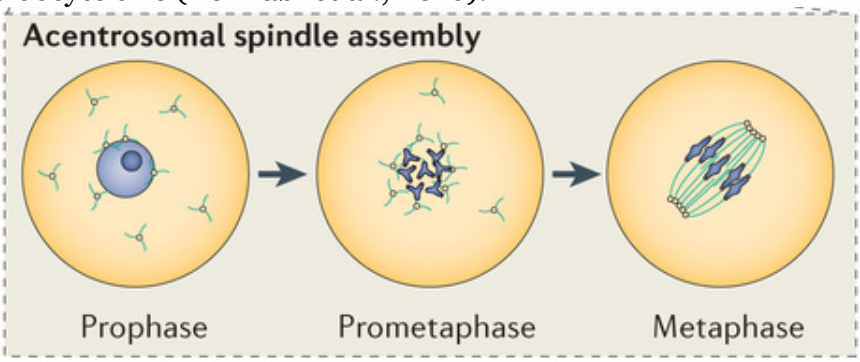

Figure 1.9. Acentrosomal spindle assembly in mouse oocyte. Acentrosomal MTOCs surround the nucleus at NEBD and capture the chromosomes. During the spindle pole formation aMTOCs cluster together. Figure and legend adapted from (Clift and Schuh, 2013).

Given the small size of the nucleus and asymmetry of the meiotic division, the spindle itself is positioned asymmetrically in the oocyte. Both in somatic cells and oocytes, spindle positioning is an actin-dependent process. Mouse oocytes form a low-density actin meshwork in the cytoplasm. Pulling forces of the meshwork are generated by non-muscle myosin Vb (Schuh and Ellenberg, 2008) and are translated into the spindle migration to the cell cortex, while the actin filaments are nucleated by formin 2 (Schuh and Ellenberg, 2008; Azoury et al., 2008). Rab11a positive vesicles drive actin meshwork contraction (Holubcova et al., 2013).

1.4. Actin in cell division

1.4.1. Possible roles of actin in spindle assembly

Actin is a small globular protein forming microfilaments in the cell. Actin cytoskeleton is involved in cell shape maintenance and locomotion, as well as establishment and maintenance of the cellular junctions. During cell division, a contractile acto-myosin ring is required for successful cytokinesis. Furthermore, actin is involved in spindle positioning in somatic cells and oocytes. These processes have a long history of research and are extensively reviewed in the literature (Pollard and Cooper, 2009; Field and Lénárt, 2011; Almonacid et al., 2014). In the following chapter I will review what is known about roles of actin in spindle assembly and chromosome congression.

Research on actin functions in cell division was hindered for decades by the unavailability of a reliable live-cell actin marker. Since actin is one of the most abundant proteins in the cell (Koestler et al., 2009), probes that bind to the whole actin pool provide very poor signal-to-noise ratio, since most of the protein is in the soluble monomeric pool (G-actin). Several recently developed probes labeling polymerized F-actin (LifeAct, Utrophin CH-domain) provide better spatial resolution for live-imaging. However, they are prone to additionally stabilizing the F-actin structures in the cell (Burkel et al., 2007; Riedl et al., 2008). To some extent, this issue can be solved by titrating down the concentration of the probe (Ballestrem et al., 1998). Furthermore, due to the extreme conservation of the amino-acid sequence across animal species, actin has very low antigenicity, therefore immunostaining of the chemically fixed samples or immuno-EM becomes challenging (Barak et al., 1981). During sample preparation for EM, due to the small size of the protein, actin filaments provide poor signal-to-noise ratio on the background of the cytoplasmic proteins (reviewed in Small et al., 1999; Wesolowska and Lénárt, 2015), which prevents studying the structure within the cell. Another considerable issue in imaging cytoplasmic actin elements is that the cellular cortex has higher actin abundance, sequestering most of the fluorescent marker to the periphery of the cell (Wu and Pollard, 2005).

The first evidence for actin filaments localizing in the spindle was demonstrated in plant cells by electron microscopy (Forer and Jackson, 1979). Subsequently, this observation was confirmed in chemically fixed phalloidin-stained samples (Traas et al, 1987), as well as by immunostaining (Yasuda et al., 2005). Unlike animal somatic cells, all plants cells have acentrosomal spindle assembly: microtubules form arrays around the nucleus before the NEBD and very quickly capture chromosomes upon prometaphase onset. Following this, several groups confirmed presence of filamentous actin in the spindle, using different methods. During cell division, actin is also localized in the cell cortex, where it forms a highly dynamic pool. In the spindle, actin fibers are aligned in parallel to the microtubule arrays (fig. 1.10). During metaphase, F-actin extends from the spindle margins and forms poles of the spindle. Later in anaphase,

actin forms the fragmoplast (cytokinesis plate), which separates the chromosomes into the daughter cells.

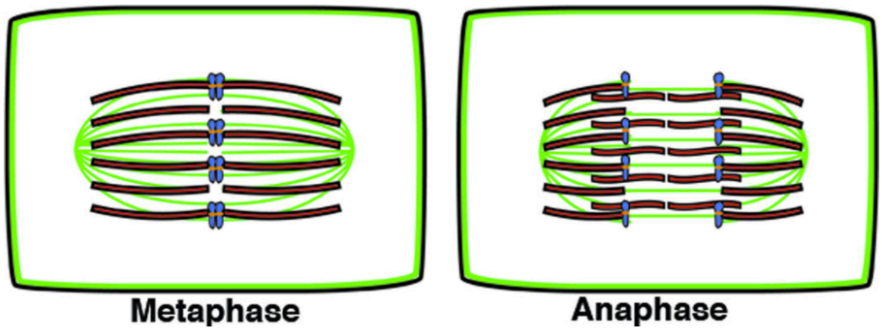

Figure 1.10. Mitotic spindle in plant cells contains F-actin filaments. Microtubules assemble the spindle acentrosomally (red) around the chromosomes (blue). Cortical F-actin and spindle F-actin in green. Figure and legend adapter from (Sandquist et al., 2011).

In animal cells, F-actin in the spindle was visualized in a few model systems: crane-fly spermatocytes (Silverman-Gavrila and Forer, 2000), *Xenopus* oocytes (Weber et al., 2004) and mouse oocytes (Schuh and Ellenberg., 2008; Azoury et al., 2008), where it was imaged live for the first time using Utrophin-CH probe. In addition to being required for spindle positioning, actin meshwork in mouse oocytes also forms a cage-like structure around the nucleus and extends individual F-actin cables in the body of the spindle. Consistently, actin was reported to be required for spindle mid-zone stabilization at the anaphase (Landino and Ohi, 2016). In addition to actin filaments, myosins, actin-dependent molecular motors, were localized in the meiotic spindle: myosin 2 and myosin 5b in mouse oocytes (Schuh and Ellenberg, 2008; Holubcova et al., 2013), and myosin 10 in *Xenopus* oocytes (Weber et al., 2004). Remarkably, in all these cell types, spindles assemble without centrosomes, reminiscent of plant cells. Thus, actin may be particularly involved in the mechanisms of acentrosomal spindle assembly, providing additional mechanical support to the spindle, as well as maintaining spindle pole integrity (reviewed in Sandquist et al., 2011).

The question arises whether and to which extent actin is involved in the spindle assembly in somatic cells. An argument against this hypothesis is that a decade of research on the *Xenopus* cell-free extract on the spindle assembly mechanisms (reviewed in chapter 1.3.2.) was performed after actin depolymerization with Cytochalasin D. This was dome to decrease the viscosity of the extract, and, thereby, allow easy handling. Also, in somatic cells actin depolymerization does not block mitosis until cytokinesis stage. This strongly suggests that actin is not involved in somatic, centrosomal spindle assembly. However, acto-myosin is required at the earlier steps of cell division, namely for centrosome separation and positioning (Rosenblatt et al., 2004). Furthermore, actin can be nucleated from the centrosomes both *in vitro* and *in vivo* (Farina et al., 2016). These studies suggest that F-actin is not directly requited, but may facilitate spindle assembly.

Indeed, localization of F-actin and several types of myosin was reported in the spindles of somatic cells. In *Xenopus* embryonic epithelial cells, actin filaments form bundles around the spindle and seem to anchor it to the cell cortex (Weber et al., 2004). Furthermore, in these cells myosin 10 directly interacts with actin and microtubules, maintaining spindle length. Depletion of myosin 10 causes fragmentation of the spindle poles (Woolner et al., 2008). Similarly, in *Dictyostelium*, myosin-1 is required for the spindle stability (Itoh et al., 2007; Rump et al., 2011). Several actin and actin associated protein drug-perturbation experiments (eg: actin depolymerization with Cytochalasin D and Latrunculin (Forer and Pickett-Heaps, 1998), formin inhibition by SMIFH2 (Kim et al., 2015), myosin inhibition (Forer et al., 2007), etc.) report some spindle assembly defects.

Quite exceptionally, in *Xenopus* oocytes, F-actin is involved in the prophase of the meiosis I. These oocytes are up to 1.3 mm in diameter, with the nucleus 400 μm in diameter, which is up to 100000 times larger than in the somatic cells. During the interphase oocyte maturation, a dense actin meshwork is formed in the nucleus. Normally, during the interphase actin is present in the cytoplasm of a cell; localization controlled by exportin 6 (Stüven et al., 2003). However, in the *Xenopus laevis* oocytes exportin 6 is down-regulated. Thus, actin is not exported into the cytoplasm, unless exportin 6 is microinjected exogenously. If exportin 6 is ectopically expressed in the cells, the intranuclear meshwork is not formed and the egg nuclei become extremely fragile, suggesting that actin meshwork provides the mechanical support in the nucleus (Bohnsack et al., 2006). Additionally, as proposed by a recent study, actin meshwork might serve as a scaffold preventing aggregation of the multiple nucleoli in the nucleus (Brangwynne et al., 2011).

In conclusion, the possible roles of filamentous actin during mitosis or meiosis are keeping the integrity of the spindle, maintaining spindle length and pole integrity, and producing forces for the chromosome segregation (reviewed in Sandquist et al., 2011). Overall, in somatic cell mitosis actin is not essential, but may help to facilitate cell division, while in the highly - specialized cells, like oocytes, it may have as well essential functions.

1.4.2. Cooperation between actin and microtubules: focus on spindle formation

Cross-talk between microtubules and the actin cytoskeleton is well described in several cellular processes, such as cell growth, filopodia and lamellpodia formation, cell shape maintenance and cytokinesis (Akhshi et al., 2014). However, the proven molecular players directly linking these two cytoskeletal systems in spindle formation process remain scarce. In the following chapter I have summarized three examples on direct actin-microtubule cooperation during the process of cell division: (1) actin - binding

kinesin; (2) microtubule binding myosin; (3) formin, stabilizing end-on kinetochore - microtubule attachment.

1. During oocyte maturation in *Xenopus*, several meiosis specific cytoskeletal structures are formed: actin meshwork, as mentioned above, serving as an inner nuclear scaffold, and also a *transient microtubule array* (TMA). The TMA is formed before the prophase onset at the perinuclear cytoplasm from the vegetal side of the nucleus (Gard, 1992). During chromosome congression, the TMA shrinks and elongates, moves to the animal pole and subsequently forms the meiotic spindle (fig. 1.11 A-C). Notably, actin colocalizes with the TMA during chromosome congression, as well as with the assembled spindle (Gard et al., 1995).

Recently performed F-actin interactome screen in the *Xenopus* oocyte nuclei revealed a new kinesin NabKin (Nuclear actin-bundling Kinesin), which directly binds both F-actin and microtubules and is essential for cytokinesis (Samwer et al., 2013). NabKin colocalizes with filaments of the actin meshwork and the TMA in prophase, and later at the spindle attachment site and in the first polar body. Upon NabKin disruption, spindle anchoring is disturbed and cytokinesis fails yielding polyploid eggs. During chromosome congression, NabKin is colocalized with the actin meshwork and the TMA. Thus, a deficiency of this kinesin could lead to chromosome loss. Thus, NabKin is one of the few proteins connecting two different cytoskeletal systems during the spindle assembly process (Samwer et al., 2013).

2. Myosin 10 is one of the few examples of direct *in vivo* interaction of actin and microtubules in cell division process. During *Xenopus laevis* meiosis, myosin 10 is crucial for spindle anchoring to the cell cortex, as well as spindle assembly (Weber et al., 2004). Furthermore, it localizes actin to the spindle. During mitotic division of the *Xenopus laevis* embryonic epithelial cells, myosin 10 localizes to the spindle poles and directly interacts with the microtubules (Woolner et al., 2008). Additionally, actin filaments are formed from the spindle poles to the periphery of the cell (Woolner et al., 2008). Dominant-negative myosin 10 causes the formation of multipolar spindles in the somatic cells. Altogether, myosin 10 is required for spindle length and spindle pole integrity maintenance during the somatic cell division (Woolner et al., 2008).

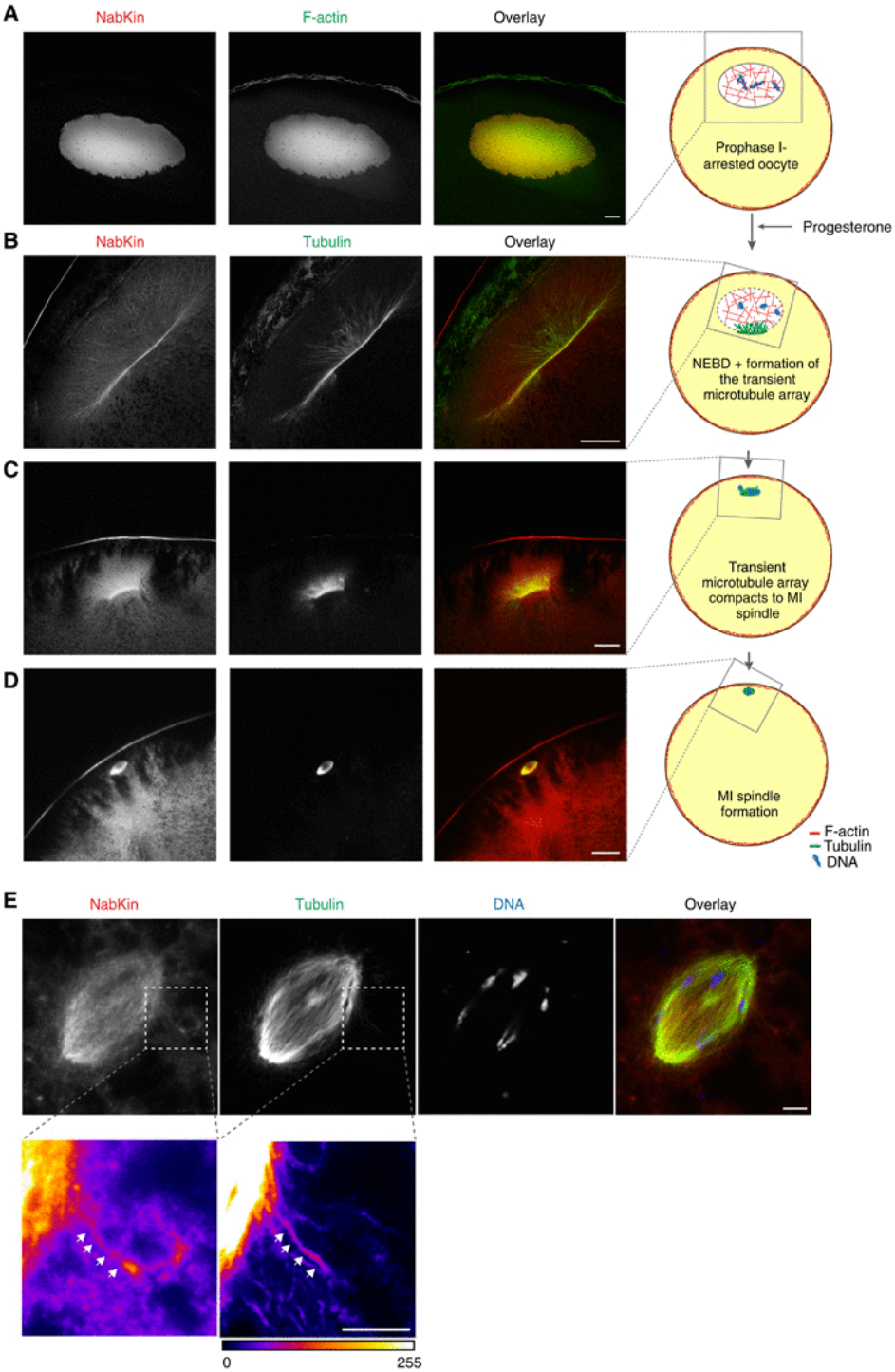

Figure 1.11. Nabkin, a kinesin associating with actin and microtubules, that is essential for spindle positioning in *Xenopus* oocytes. A. stage VI oocyte arrested in the prophase. **B.** Formation of the TMA on the vegetal side of the nucleus. **C.** Compaction of the TMA and its movement towards the animal pole. **D.** Meiotic spindle formation. **E.** Magnified image of a meiotic spindle: NabKin colocalizes with the spindle microtubules and with the individual microtubule extending from the spindle body. A-D: scale bar 50 μm. E: scale bar 5 μm. Figure and legend adapted from (Samwer et al., 2013).

3. Formins are actin nucleating factors that assemble long unbranched actin filaments. Members of this protein family can directly bind to microtubules and stabilize their dynamics. For example, at the leading edge of the migrating cell, formins stabilize growing microtubule plus-ends and cause actin polymerization. Furthermore, the

formin mDia3 contributes to chromosome congression: depletion of mDia3 in somatic cells causes chromosome misalignment, similar to Ndc80 depletion phenotype (Yasuda et al., 2004). Recently, mDia3 was reported as a novel kinetochore tracking protein (Cheng et al., 2011). In the end-on conformation, microtubules are oscillating between growing and shrinking states. The main plus-end stabilizing proteins in end-on attachments are Ndc80, as well as the Ska (Dam1) complex. mDia3 is suggested to additionally stabilize microtubule plus-ends via the interaction with Ndc80 and/or EB1-APC plus-end tracking proteins (fig. 1.12).

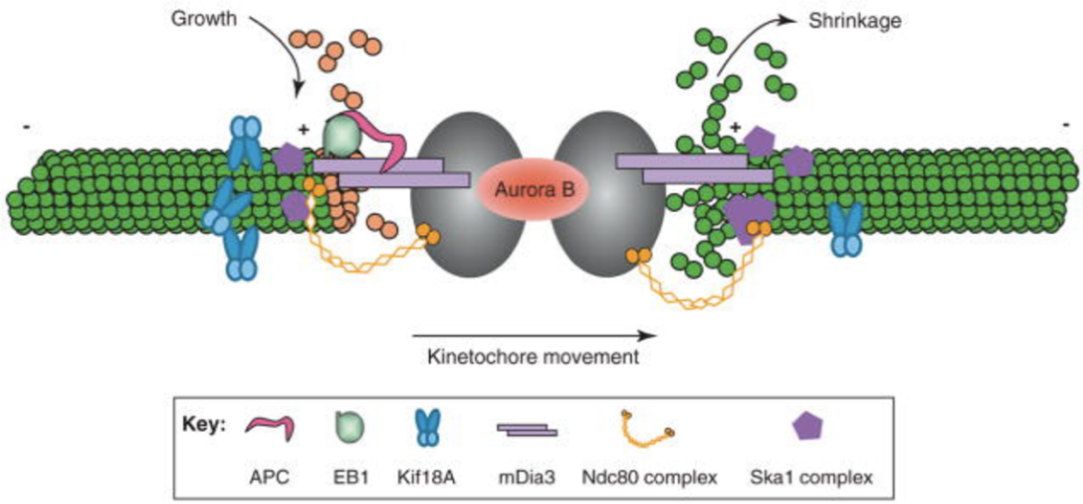

Figure 1.12. A model of kinetochore – microtubule attachments containing formin mDia3. Ndc80 is the main complex stabilizing microtubule plus-end. In addition, plus-end tracking proteins (EB1 and APC) localize on the kinetochore. Kinetochore tracking protein mDia3 could possible link Ndc80 and APC-EB1 complex additionally stabilizing the microtubule growing tip. Figure and legend modified from (Mao, 2011).

1.5. Chromosome congression in starfish oocyte

1.5.1. Starfish as a model system to study cell division

Oocytes from the starfish *Patiria miniata* are among the biggest cells with 180 µm diameter. A fully-grown oocyte has a large nucleus of 70 µm diameter. The nucleus is anchored to the cell cortex, off-center, defining an intrinsic polarity in the oocyte (Terasaki et al., 2001). The animal pole contains the pair of centrosomes nucleating long interphase microtubules to anchor the nucleus (Miyazaki et al. 2000) (fig. 1.13).

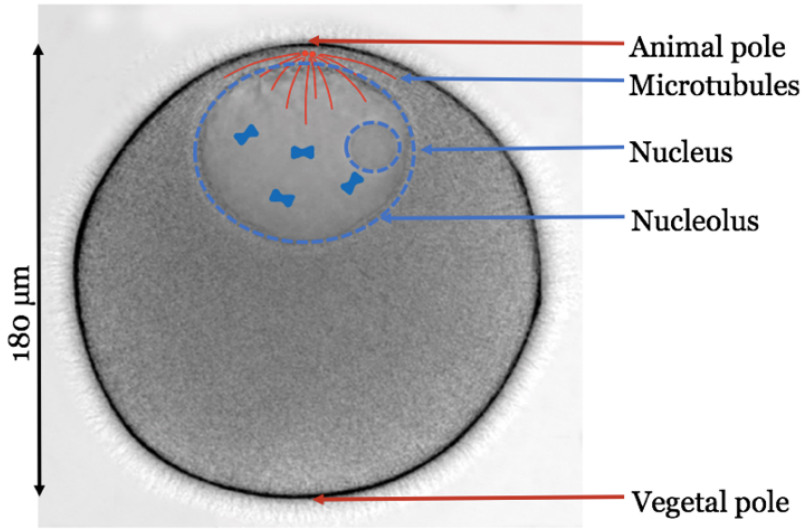

Figure 1.13. Immature oocyte from starfish *Patiria miniata*.

While the oocyte grows to its final size, nutrients required for the embryo development are deposited in the form of yolk vesicles typically 1-2 µm in diameter (Terasaki et al., 2006). Pre-synthesized nuclear proteins are stored in the large nucleus. Starfish oocytes are easy-to-handle, highly transparent, and extremely large cells that are not very light sensitive. Hence, they are well suited for fluorescence microscopy studies.

Oocytes, arrested in prophase of the first meiotic division, are densely packed in the ovaries present in the starfish arms. These oocytes can be easily isolated by biopsy. In the isolated oocytes, treatment with maturation hormone 1-methyladenine (1-MA) induces their re-entry into meiosis (Kanatani et al., 1969). After 1-MA addition, the oocytes start NEBD in approximately 20 minutes and extrude the first polar body in 1 hour. Meiosis is completed in 1.5 hours (fig. 1.14).

At the meiosis onset, each chromosome consists of two bivalents, or four chromatids (*4n*). During the first meiotic division, the whole chromosomes are segregated, reducing the oocyte ploidy to *2n*. During the second meiotic division, the sister chromatids get separated, yielding a *1n* mature oocyte and a *1n* polar body. Fully condensed chromosomes are only 1-2 µm in size. In the following sections, I will refer to the *4n* paired chromosomes as chromosomes (see fig. 1.14).

1.5.2. Several actin structures are formed during oocyte meiosis

Due to the very large size of the oocyte and its nucleus, several mechanisms have evolved in starfish oocytes to facilitate these specialized divisions. An *f-actin shell* promotes nuclear envelope disassembly at NEBD (Mori et al., 2014). After disassembling the nucleus, an *actin meshwork* transports the chromosomes into microtubule capture range (Mori et al., 2011). The role of the *actin patches*, which are formed around the chromosomes at the nuclear rim, remains unknown (fig. 1.14) (Lénárt et al., 2005). Here I will introduce these three structures in detail.

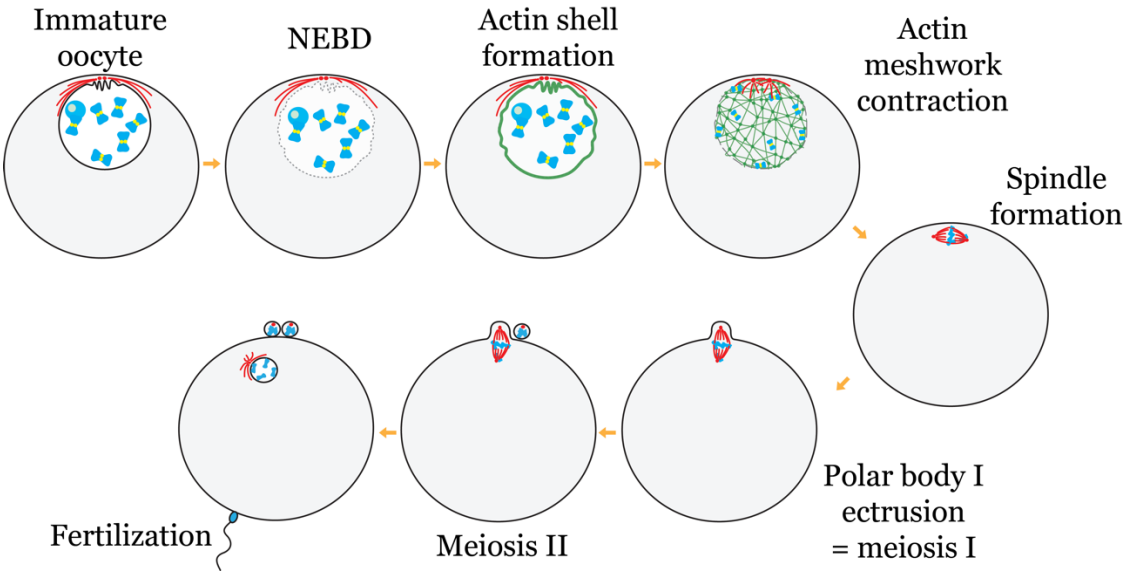

Figure 1.14. Steps in starfish oocyte meiosis. Actin structures in green, microtubules in red, chromosomes in blue. Starfish oocytes are arrested in prophase of the first meiotic division. 20 minutes after the maturation hormone addition, oocytes resume meiosis: NEBD occurs, followed by formation of the actin shell and actin patches. Chromosome meshwork transports the chromosomes into microtubule capture range, where the spindle is eventually assembled. The first meiotic division is characterized by the segregation of whole chromosomes. Thus, anaphase I results in the formation of (*2n*) polar body and (*2n*) oocyte. The oocyte immediately divides again, producing a mature (*1n*) egg and a second polar body (*1n*). This egg is ready for fertilization. The entire oocyte meiotic division in starfish takes 1,5 hours.

The *actin shell* is a transient thick layer of Arp2/3 polymerized actin nucleated under the inner nuclear membrane simultaneously with the NEBD, and is involved in the rapid fragmentation of the nuclear membranes (Mori et al., 2014). In contrast to somatic cells, where nuclear envelope fragmentation is mostly done by astral microtubules (Beaudouin et al., 2002), large cells like starfish oocytes require a facilitation mechanisms to achieve rapid permeabilization of the nuclear envelope at the NEBD onset. Based on electron microscopy images, spike-like protrusions, extending from the actin shell, appear to 'pierce' the bi-layered nuclear membrane. Depletion of the actin shell with the Arp2/3 inhibitor CK-666 prevents membrane rupture, as well as causes chromosome loss in the following steps leading to the formation of aneuploid eggs.

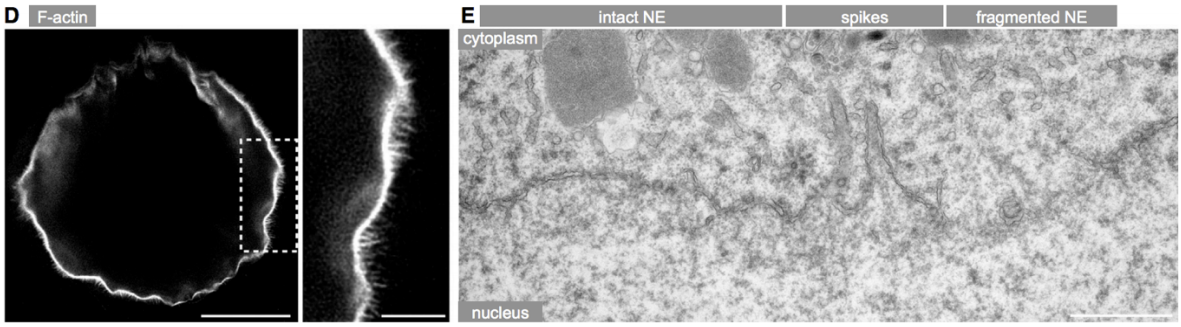

Figure 1.15. Actin shell and actin spikes facilitating nuclear membrane fragmentation. A. Actin shell with actin spikes in fluorescent microscopy. **B.** Electron microphotograph of the nuclear membranes and actin spikes protruding into the cytoplasm. Figure and legend adapted from (Mori et al., 2014).

Actin patches are nucleated simultaneously with the actin shell around the chromosomes located in direct proximity of the nuclear membranes (fig. 1.16). Like the actin shell, actin patches are also nucleated by Arp2/3 complex. Chromosomes, located in the interior of the nucleus, not direct contact of the nuclear envelope, do not possess actin patches. Formation of these patches requires the presence of RanGTP generated on chromatin, and proximity to the nuclear membranes. Unlike actin shell, which is quickly depolymerized, actin patches get incorporated into the actin meshwork and are transported along with the chromosomes. The function of the actin patches remains unknown. Possibly, they could facilitate chromosome detachment from the nuclear envelope (unpublished data from P. Lénárt and M. Mori).

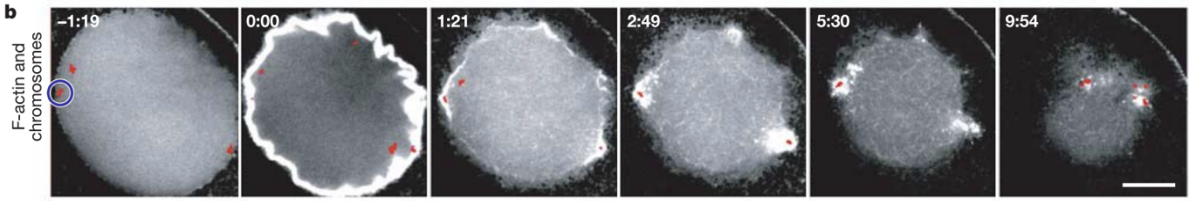

Figure 1.16. Actin patches, formed simultaneously with the actin shell around the chromosomes, incorporate into the actin meshwork. Figure and legend adapted from (Lénárt et al., 2005).

The *actin meshwork* is made of short actin filament bundles interconnected together into a mesh. It spans the volume of the whole nucleus and is concomitant with the actin shell. The actin meshwork sterically traps the chromosomes and transports them into microtubule capture range. Inert beads, comparable to chromosome size, injected into the nuclear area are transported by the actin meshwork just like the chromosomes. Chromosome trajectories suggest that meshwork contraction is homogenous in time and isotropic in space. The actin meshwork is anchored to the cell cortex at the animal pole, thereby providing the directionality of the contraction (Mori et al., 2011).

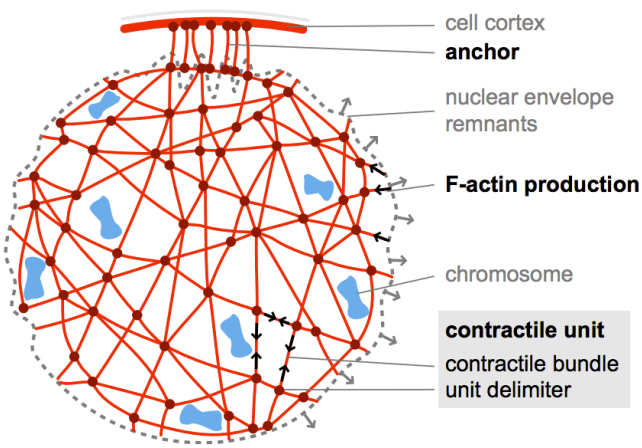

Figure 1.17. Model of contractile actin meshwork transporting chromosomes. Figure and legend adapted from (Mori et al., 2011).

Actin meshwork contraction is independent of non-muscle myosin 2. Instead, F-actin depolymerization is suggested as the main driving force of meshwork contraction. Treatment with F-actin depolymerizing drug Latrunculin B causes rapid actin meshwork collapse. Presumably, under these conditions, the actin meshwork loses its connections anchoring it to the nuclear envelope remnants, which causes it to rapidly shrink. Laser-cutting experiments further necessitate the requirement of connection to the nuclear boundaries for the homogenous contraction. Computer modelling predicts that steady F-actin depolymerization coupled to reversible actin-meshwork cross-linking could be the mechanism driving meshwork contraction (Philippe Bun, Lénárt lab, manuscript in preparation). F-actin nucleating factor remains unknown.

1.5.3. Overview of chromosome congression in starfish oocytes

Unlike most other species, starfish oocytes do not eliminate centrioles until later stages (Borrego-Pinto et al., 2016). Thereby, the meiotic spindle is assembled by two microtubule asters, like in somatic cells (see chapter 1.2). In starfish oocyte, astral microtubules connect off-center, at the animal pole. Due to this geometry, initial chromosome capture is separated from the chromosome bi-orientation both spatially and temporally. This provides a unique opportunity to study initial chromosome capture by microtubules separately from the following process of bi-orientation, which in somatic cells occur simultaneously.

During prometaphase, spindle microtubules grow up to 20 μm in length both in somatic cells and starfish oocytes (Lénárt et al., 2005). Since microtubule asters are located asymmetrically at the animal pole of the oocytes, the actual microtubule capture range is up to 30 μm from the animal pole of the oocyte. Nevertheless, chromosomes are scattered in the area of 70 μm in diameter, and are first congressed by the contractile actin meshwork towards the animal pole, followed by the chromosome capture by spindle microtubules (see fig. 1.18).

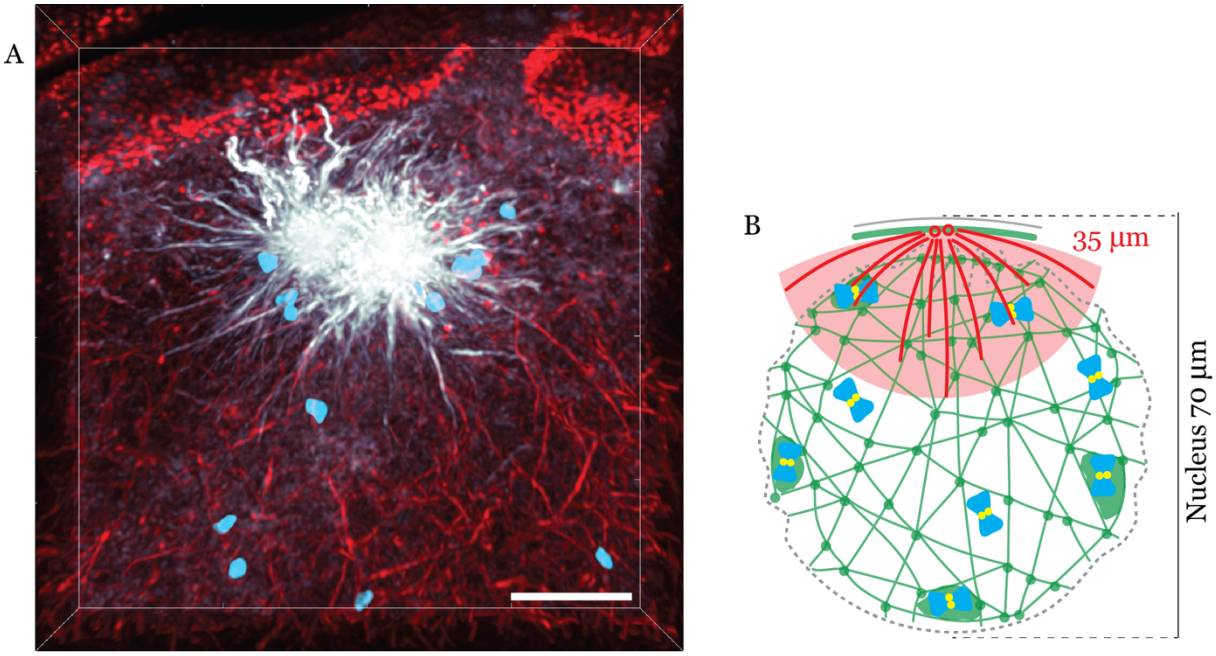

Figure 1.18. Actin meshwork and microtubules during chromosome congression. A. Immunostaining of a mature oocyte fixed at 5 min after NEBD. Microtubules (α-tubulin antibody) in gray; Actin meshwork (Phalloidin A561) in red; Chromosomes (Draq5 staining) in cyan. Scale bar, 10 µm. Z step = 130 nm. Pixel size = 38 nm. 3D rendered confocal stack, deconvolved. **B.** Scheme: microtubule capture range covers only part of the nucleus. Chromosomes are congressed there by the actin meshwork.

Although actin meshwork and microtubules perform similar functions during the chromosome congression, from first insight, they work independently. Upon actin drug-depolymerization, chromosomes located within the microtubule capture range (30 µm) get incorporated into the spindle. Distally located chromosomes remain lost in the nucleoplasm. On the other hand, microtubule depolymerization with nocodazole does not affect actin meshwork function. Chromosomes are transported with typical temporal dynamics and congress to a region of approximately 20 µm diameter around the animal pole (fig. 1.19) (Lénárt et al., 2005).

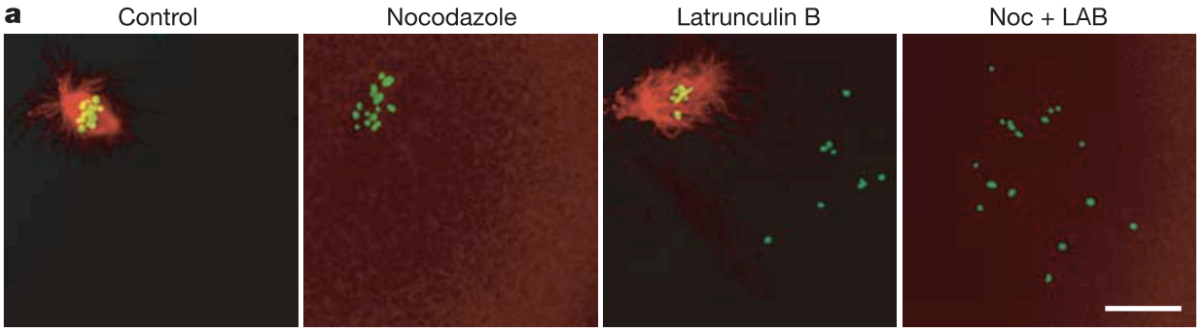

Figure 1.19. Chromosome congression by actin meshwork is independent of microtubules. Immunostaining of the oocytes threated with Nocodazole (3.3 µM), Latrunculin B (250 nM) or both. Oocytes were fixed 30 minutes after NEBD. Microtubules shown in green, chromosomes in red. Scale bar 20 µm. Figure and legend adopted from (Lénárt et al., 2005).

In interphase, chromosomes are scattered in the volume of the nucleus. During contraction, actin meshwork transports chromosomes towards the animal pole and into microtubule capture range. Actin-driven chromosome congression begins

approximately 1 minute after NEBD, when the actin meshwork is polymerized. Thereafter, microtubules capture the chromosomes and a spindle is formed. Chromosome motion within the actin meshwork is slow and jiggling, while upon microtubule capture chromosome transport turns faster and directed (Mori et al., 2011). Based on the chromosome trajectories in 3D and their pole-ward velocities, the transition between these two modes of chromosome transport can be distinguished on the level of individual chromosomes. The suggested mechanism of the two-staged chromosome congression is represented on fig. 1.20.

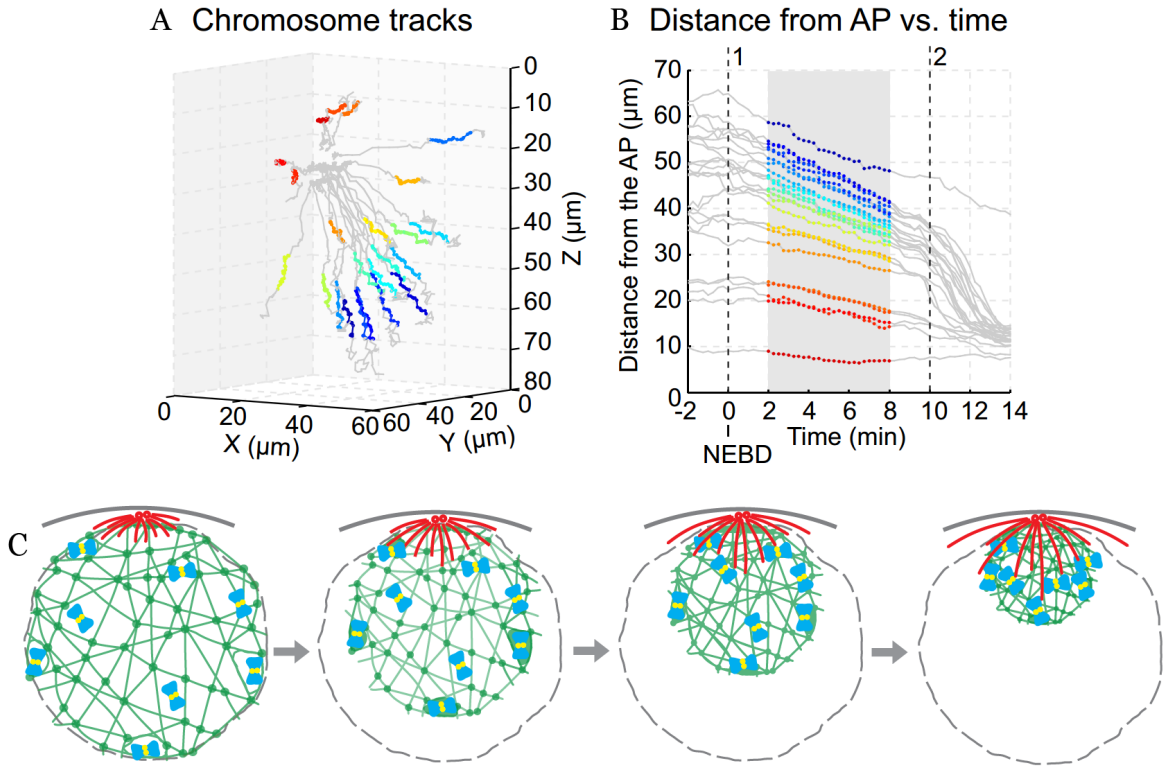

Figure 1.20. Overview of chromosome congression by actin and microtubule driven mechanisms. A. Chromosome trajectories tracked in a 3D dataset. **B.** Chromosome pole-ward velocities calculated as a distance between a chromosome and animal pole at each moment of time. Actin-driven phase of chromosome congression is plotted in color, conserved in A and B for each chromosome. Figure and legend adapted from (Mori et al., 2011). **C.** Scheme of actin-driven chromosome congression. Due to homogenous isotropic contraction of the actin meshwork, nuclear space occupied by chromosomes shrinks to approximately one half of the original diameter. The newly synthesized actin filaments at the nuclear periphery are not shown. Following this, chromosomes will be captured by microtubules and incorporated into the spindle.

2. Aims

In order to become a fertile egg, the immature oocyte has to undergo two sequential reductional divisions. Multiplication or a failure to transmit even a single chromatid in these divisions will lead to the formation of the aneuploid egg and, hence, infertility and unviable or defective progeny (reviewed in Webster and Schuh, 2017). Therefore, faithful capture, alignment and segregation of chromosomes in oocyte meiosis is essential for sexual reproduction of animal species.

The canonical mechanism of chromosome search and capture by astral microtubules was described decades ago and explains this process for small somatic cells (Kirschner and Mitchison, 1986). By contrast, how chromosomes are captured in the orders of magnitude larger volume of oocytes and transported to the small meiotic spindle is much less well understood.

The Lénárt lab recently discovered in starfish oocytes that the actin cytoskeleton facilitates chromosome congression in the exceptionally large oocyte nucleus: during prometaphase I, a contractile actin meshwork collects chromosomes to the range from which centrosomal microtubules are able to capture them and assemble the meiotic spindle (Lénárt et. al., 2005, Mori et. al., 2011). Importantly, despite a good understanding of actin- and microtubule-driven mechanisms of chromosome congression separately, very little is known about how these mechanisms are coordinated with one another.

The overall aim of my PhD project was to understand how actin and microtubule driven mechanisms of chromosome transport and capture are coordinated to prevent chromosome loss in starfish oocytes. Specifically, I first aimed to provide a *detailed characterization of chromosome capture* by astral microtubules in starfish oocytes. In starfish, the meiotic spindle assembles from the centrosomes, providing a unique opportunity to study the process of chromosome search and capture in the geometry of a large cell. Secondly, I aimed to characterize the transition from actin-driven transport to capture by microtubules to understand the *cooperation between actin and microtubules* in the process of two-staged chromosome congression. To achieve these goals, I analyzed the kinetics of chromosome capture by tracking chromosome motion in 3D at high-resolution in the presence and absence of the actin meshwork, and combined this with computational modeling.

In summary, the overall goal of my PhD project was to reveal the *interaction between the actin meshwork transporting chromosomes and capture by microtubules* in meiosis of starfish oocytes, as an example of interplay between these two major cytoskeletal systems in the early stages of cell division.

3. Materials and methods

3.1. Starfish and oocyte handling

Starfish *Patiria miniata* were collected from several locations at the Pacific coast of North America (Southern California Sea Urchin Co., Corona del Mar, CA; Marinus Scientific LLC, Newport Beach, CA; Monterey Abalone Company, Monterey, CA) and transported to EMBL. The starfish were kept in the EMBL animal facility in sea water aquariums at 16°C through the whole year. They were fed with half a shrimp twice a week.

Oocytes were collected as described in (Terasaki et al., 1994). Female starfish were punctured with a small biopsy puncher (Miltex) from the dorsal side at the base of an arm. A small piece of the ovaries was collected from the wound with the forceps and kept in calcium-free artificial sea water supplemented with 50 μM L-phenylalanine for 15-20 minutes, which prevents spontaneous oocyte maturation. Treatment with Ca-free sea water is required for the removal of the follicle cells, which nourish the oocytes. In the following, oocytes in the ovaries ware transferred into another Petri dish with filtered sea water containing 100 μM acetylcholine. Under this treatment, ovaries contract and release oocytes, which are subsequently transferred into fresh filtered sea water and kept in a 14°C incubator for up to three days and used for experiments.

Oocyte maturation was induced with the maturation hormone 10 μm 1-methyladenine (1-MA) (Kanatani et al., 1969). Nuclear envelope breakdown (NEBD), which indicates entry into prometaphase of the first meiotic division, occurs on average 20 min after adding the hormone.

3.2. Cloning of the fluorescent markers

Constructs for the fluorescent markers used in this work are listed in the table 3.1. In my project, I used several constructs previously developed by other Lénárt lab members. H2B-mEGFP3, the most-used chromosome marker in this project, was cloned using the 'copy-paste' strategy.

Briefly, the human H2B sequence was cut out of PGEM-HE-H2B-mRFP construct with restriction enzymes and a mEGFP triple-tandem sequence was taken from the pmEGFP3-N1 vector. The acceptor vector pGEM-HE contains an Ampicilin-resistance site and a T7 promoter, which is required for mRNA synthesis. The two inserted fragments, as well as the linearized acceptor vector, were purified using a Qiagen gel-extraction kit. In the next step, I performed a three-piece ligation reaction with T4 ligase, transformation into the bacterial cells, and a search of the ampicilin-resistant colonies. The obtained H2B-mEGFP3 construct was verified via sequencing (GATC Biotech AG, Constance). The plasmid was amplified via midi-prep Qiagen kit. All the restriction enzymes used in the cloning were purchased either from NEB (New

England Biolabs) or Thermo-Fisher (Thermo-Fisher Scientific).

Name of the construct	Vector	Generated by
H2B-mEGFP3	pGEM-HE	Mariia Burdyniuk
H2B-mCherry	pGEM-HE	Masashi Mori
EB3-mCherry3	pGEM-HE	Natalie Daigle, Ellenberg lab
Utrophin-CH-mCherry3	pGEM-HE	Masashi Mori

Table 3.1. List of the fluorescent marker constructs. All fluorescent markers in these constructs are tagged in the C-terminal position.

3.3. RNA synthesis

In order to perform live imaging, I injected oocytes with mRNA of the gene of interest, coupled with a fluorescent tag. All the mRNAs used in the project were synthesized *in vitro*. For this, pGEM-HE plasmid constructs were linearized with SgrAI, AscI, or AflIII enzymes. Linearized DNA was additionally purified with phenol-chloroform extraction. Next, mRNA was transcribed using AmpliCap-Max™ T7 High Yield Message Maker kit (Cellscript) and 5'- capping following the manufacturer instructions. After the polyA tail synthesis with the A-Plus™ Poly(A) Polymerase Tailing Kit (Cellscript), mRNA was purified via phenol/chloroform extraction followed by isopropanol precipitation, and dissolved in RNase-free water. The concentration of the synthesized mRNA was estimated on NanoDrop and on the agarose gel in 1:10 dilution. Moreover, the quality of the synthesized mRNA was directly tested by the probe expression levels in the oocyte. For that, the synthesized mRNA was injected the day before imaging in order to allow for the protein synthesis overnight.

3.4. Oocyte microinjection

Microinjections into the oocyte were performed as described in (Borrego-Pinto et.al., 2016) and previously at (http://mterasaki.us/panda/injection/). For starfish single oocyte injections, a syringe method is used, where a microneedle containing small amounts of mercury is tip-loaded with the solution of interest. Pressure-induced small changes in the mercury position translate into picolitres of the injected solution. Altogether, this yields high precision in terms of the volume of injection and of temporal control.

Oocytes are sensitive to contaminations, including those from glass cover slips (Menzel Glaeser #1) and chambers. Therefore, prior to use, the cover slips were washed in a detergent solution, followed by overnight incubation in 1M HCl solution while stirring. Afterwards the cover slips were thoroughly rinsed with distilled water and kept in ethanol until use.

To allow injection and imaging, the oocytes were transferred into U-shaped plastic chambers specifically designed for starfish oocytes (fig. 3.1.). A chamber contains a shelf-like structure made of a larger and a small piece of glass, glued together by two

layers of sticky tape. The small cover slip creates an edge wide enough to host exactly one layer of oocytes (approx. 300 μm). The oocytes are loaded onto the shelf with a small pipet, and the chamber is then assembled with a standard cover slip from the bottom and the cover slip containing 'shelf' with the oocytes from the top and sealed with silicone grease (GE Bayer Silicones). Then the chamber is filled with normal sea water by a small glass pipet avoiding the dislocation of the oocytes from the 'shelf'. Injection chambers also have one or two ridges parallel to the entry to position the loading capillaries with mRNA.

Oocytes can be injected with various substances (RNA, proteins, Phalloidin solution, small inert beads, marker molecules) following this protocol:

1. The solution for injection is loaded into the injection capillary (Drummond) between two layers of dimethylpolysiloxane silicone oil (20 cts viscosity, Sigma), as shown on fig. 3.1.
2. Needles for microinjection are prepared from glass capillaries (Drummond) on a needle puller (Narishige PN-3 Glass Microelectrode Horizontal Needle Pipette Puller). In the next step, the needle is filled with small amounts of mercury (Sigma) from the back. It is then mounted onto a CellTram Oil manual injector, which is attached to a wide-field microscope (Nikon Eclipse Ti). The manual injector is filled with mineral oil (Sigma) to transmit its manipulation into pressure.
3. Once loaded, the tip of the needle has to be broken by gently tapping it against the wall of the injection chamber, aiming for a tip opening as small as possible.
4. Once the needle is open, the pressure in the injection system is increased and the mercury is pushed gently to fill the entire volume of the needle tip, aiming to push all the air out of the tip. This is done in order to achieve maximum responsiveness from the pressure changes to the picolitres injected into the oocyte.
5. Next, the needle is filled with 100 units of silicone oil. This is done to create a buffering zone in order to prevent mercury contamination of the injection set-up, as well as the oocytes and the chamber.
6. The RNA or other solution of interest is tip-loaded into the capillary, usually between 20 to 60 units. This volume of solution for injection is then 'sealed' with a final loading of approximately 20 units of silicone oil. In the following step, when the needle is submerged into the sea water on the line to the oocyte line-up, the silicone oil cap prevents mixing of the RNA or other injection solution with water. This is crucial not only to prevent the dilution of the solution of interest, but also to avoid injecting calcium ions from the sea water into the cytoplasm. Injection of silicone oil is not harmful to the oocyte and is actually helpful for keeping track of injected oocytes. Moreover, inert oil droplets of different size were used as landmarks for the CLEM (see chapter 6.1)

7. The loaded microneedle tip needs to be submerged into the chamber and positioned pointing at the oocyte, specifically the middle plane of an oocyte. The injection is made by gently inserting the needle tip into the oocyte and quickly increasing the pressure in the set-up, releasing the silicone cap and the solution of interest into the cytoplasm. This sequence is repeated for all oocytes in the chamber, which are in the orientation favorable for imaging.

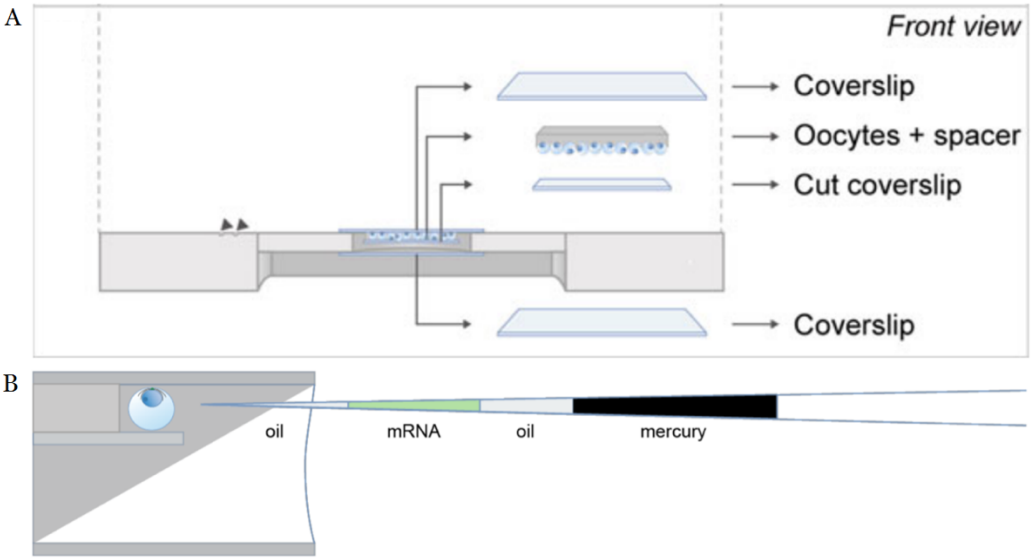

Figure 3.1. Principle of the oocyte microinjection. **A**. Scheme of the injection chamber. **B.** Scheme: microinjection needle loaded with mRNA oriented in front of the oocyte in the chamber. Figure and legend adopted from (Borrego-Pinto et al., 2016).

When performing drug-perturbation experiments, in order to avoid contamination, oocytes on the cover slip with a 'shelf' were transferred onto small Petri dishes (Ibidi µ-Dish, diameter 35 mm) with plastic bottoms. A window to fit the shelf is cut with a scalpel into the bottom of the dish and the cover slip is sealed onto it with grease. For chemical fixation and single oocyte imaging, the injected oocytes were sorted and transferred individually into the µ slide well (Ibidi µ-slide for angiogenesis, volume 100 µl).

3.4.1. Protein injection

The proteins injected into the oocytes must be concentrated. A typical protein solution for injection is between 5 and 50 µM, which dramatically increases the viscosity of the solution. Thus, microinjection becomes problematic, as the needle often gets clogged and the pressure responsiveness is altered. To overcome this, protein solutions were supplemented with NP-40 to a final concentration of 0.05%. Small amounts of NP-40 detergent greatly reduce the viscosity of protein solutions, thus facilitating the microinjection. Meanwhile, 0.05% of NP-40 in the injection mix does not affect oocyte viability and maturation. This protocol was optimized by Masashi Mori in the Lénárt lab, EMBL.

In my project, I used:

- H1 protein (from calf thymus Meck), labeled previously with Alexa-568 or Alexa-647 fluorescent dies;
- Cy3-tubulin, purified from pig brain, labeled by Katarzyna Tarnawska (Nedelec lab, EMBL), and kindly gifted. Cy3-tubulin was dissolved in BRB80 buffer (80 mM PIPES, 1 mM MgCl2, 1mM EGTA, pH = 6.8).
- recombinant Utrophin-CH domain protein (human sequence), synthesized at the EMBL protein expression and purification core facility. Subsequently, Utrophin-CH domain was chemically labeled with Alexa488 or Alexa568 fluorescent dies by Philippe Bun (Lénárt lab, EMBL) using Alexa Fluor® 488 Protein Labeling Kit or Alexa Fluor® 568 Protein Labeling Kit accordingly.
- GFP-Ndc80 protein was a gift from Stefano Maffini (Musacchio lab, MPI Dortmund). The protein was dissolved in a buffer containing 25 mM Hepes and 150 mM NaCl, pH=7.5. For the injection, it was supplemented with 0.05% NP-40.

3.4.2. Phalloidin injection

Phalloidin is an extremely potent F-actin stabilizing compound, which immediately and irreversibly binds to and 'freezes' all actin filaments in the cell.

Phalloidin-A568 stock is dissolved in methanol. For injection into oocytes, an aliquot of the stock solution (usually 20 to 40 µl) is completely dried in a SpeedVac centrifuge and reconstituted in PBS buffer. Next, the Phalloidin-A568 solution is loaded into the injection capillary, as described above.

When loading the needle for microinjection, some traces of the drug are prone to adhere to the inner walls of the needle, therefore, decreasing the concentration of the drug. For Phalloidin, the adhesion effect is quite pronounced. In order to prevent alternations of the drug concentration, the injection needle was loaded with 100 units of the drug and kept for at least 15 minutes. Thus, in the following experiments, the Phalloidin concentration was kept at the same level, allowing cross-comparing the results.

For the complete actin meshwork stabilization experiment, Phalloidin-A568 was injected into the cytoplasm of the oocyte 1.5 minutes after the first signs of NEBD were detected. While injecting, I aimed to deliver the drug as close to the nucleus as possible. This method allows to greatly slow down the meshwork contraction up to its complete inhibition. Meanwhile, the delay allows for complete assembly of the shell, the actin shell had assembled fully, thus safeguarding that all nuclear envelope membranes are disassembled.

3.5. Chemical and inhibitor treatments

Inhibitors and chemicals used in this project, their solvents, stock and final concentrations, are listed in table 3.2. Drug aliquots were kept at -20°C. Proteins in small aliquots (usually 2 µl) were stored at -80°C after flash-freezing in liquid nitrogen. All aliquots were thawed immediately before use.

3.6. Confocal microscopy

Most of the imaging was performed with a Leica SP5 microscope equipped with SuperZ Galvo stage and three Hybrid detectors (Leica HyD). For life imaging, I used a 1.1 NA HC PL APO 40x water immersion objective (Leica).

For the quantitative chromosome tracking, I imaged the whole nuclear volume in 3D in 5 sec time steps (xyzt mode). Fully-condensed chromosomes in starfish oocytes are bright 1-2 µm round-shaped structures. To increase speed of imaging, I used a large pinhole diameter and increased Z-steps (sub-optical sampling). Specifically, the following setting were used:

- acquisition with 700 Hz speed
- one-directional z- stage motion
- bi-directional line imaging
- no line averaging
- confocal pin-hole opened for 3 Airy units
- Z step – 2.2 µm, usually 29 Z slices covering up to 65 µm
- zoom 4, image size 200x200 pixels, thus voxel = 0.5 x 0.5 x 2.2 µm
- minimum laser power to avoid sample bleaching

I performed immunostaining of oocytes, aiming to resolve individual spindle microtubules and to reconstitute the microtubule search and capture of the chromosomes. Imaging of the immunostained oocytes was performed with a Leica SP8 microscope with an HC PL APO 1.40 NA 100x oil immersion objective (Leica), white-light laser (470-670 nm), and two Hybrid detectors (Leica HyD). In order to achieve the highest possible spatial resolution, the imaging was performed with relatively slow speed (400 Hz); pinhole diameter 0.7 Airy units; very dense sampling in Z (voxel size 0.038 x 0.038 x 0.125 µm). To prevent cross-talk between the channels, green and red channels were imaged sequentially line by line. The far-red channel was imaged simultaneously with the green one.

The highest temporal resolution for chromosome tracking was achieved on a Zeiss LSM 880 microscope equipped with Airyscan fast module and 40x 1.1 NA or 1.2 NA water immersion. The basic principle of the Airyscan detector is shown on fig. 3.2. Due to the cell-like detector shape, the out-of-focus light, which is discarded by the canonical confocal microscope, is collected by the Airyscan detector, yielding higher detection efficiency.

Name	Function	Supplier	Stock concentration	Final concentration	Solvent	Time of action
Cytochalasin D	Actin capping	Sigma-Aldrich	10 mM	40 µM	DMSO	40 min
Ciliobrevin D	Dynein inhibitor	Calbiochem	25 mM	100 µM	DMSO	10 min
Latrunculin B	Actin depolymerization	EMD Biosciences	1 mM	7 µM	DMSO	2 min
Phalloidin	F-actin stabilization	Invitrogen	10 mg/ml	250 pg	PBS	immediately
Paclitaxel	Microtubules stabilization	Sigma	10 mM	55 nM	DMSO	5 min
Nocodazole	Microtubules depolymerization	EMD Biosciences	10 mM	3.3 µM	DMSO	2 min
Combrestatin A4	Microtubules depolymerization	Sigma-Aldrich	50 mM	100 µM	DMSO	20 min
RO-3306	Cdk1 inhibitor	Santa Cruz	10 mM	100 µM	DMSO	5 min
Flavopiridol	Cdk1 inhibitor	Sigma-Aldrich	10 mM	10 µM	DMSO	5 min
Roscovitine	Cdk1 inhibitor	Merk Millipore	10 mM	10 µM	DMSO	5 min
Zeocin	DNA damage agent	Invitrogen	100 mg/ml	1:10	water	1 h
10 kDa Dextran	Inert fluorescently labeled marker	Invitrogen	20 mg/ml	2 ng	water	immediately
Ampicillin	Antibiotic	Sigma	100 mg/ml	1:1000	water	immediately
Paraformaldehyde	fixative	EMS	16%	1%	water	immediately
Glytaraldehyde	fixative	EMS	25%	0.1%	water	immediately

Table 3.2. List of the drug and chemical compounds

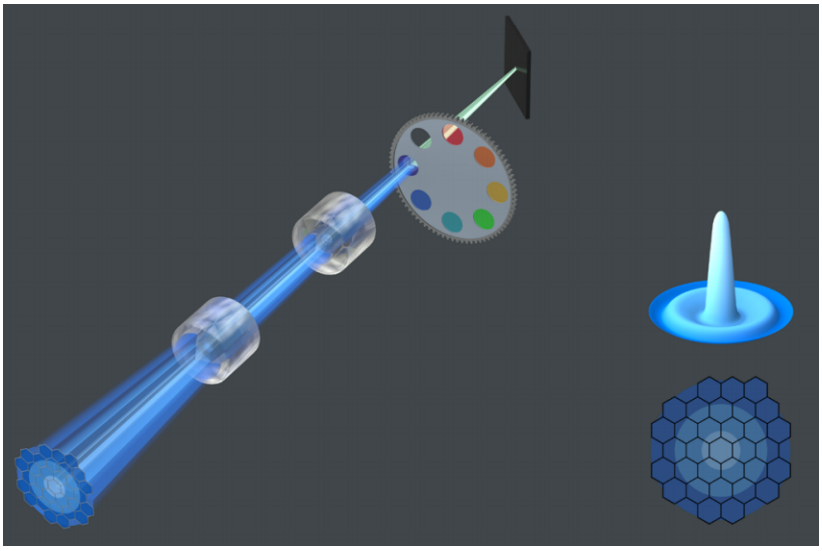

Figure 3.2. The basic principle of Airyscan detection. The Airyscan detector is arranged from 32 GaAsP detector elements. The central detector is located on the optical axis of the microscope. Other detectors are grouped around it in increasing circles. The highest resolution can be achieved with 1.25 Airy units. The light intensity distribution coming from the sample is plotted above. Figure and legend adopted from (Weisshart, 2014).

The Zeiss LSM 880 microscope is equipped with an AiryFAST module, where the same Airyscan detector is tuned to collect light from four lines simultaneously. In this mode, only 16 GaAsP elements are active, creating the oval shaped detector. 4 central elements of the AiryFAST detector are detecting light from four pixel-lines at the same time. In the AiryFAST set-up, image acquisition is performed 4 times faster, although sacrificing some spatial resolution.

Using the AiryFAST detection, I was able to acquire 65 µm Z stacks of the nuclear area in only 3 seconds (Voxel size = 0.13 x 0.13 x 1.2 µm with 41 Z step). Furthermore, in 2D mode I was able to visualize live microtubule-chromosome attachments. For this, two channels were imaged sequentially (chromosomes labeled with H2B-mEGFP3, and dynamic microtubule tips labeled with EB3-mCherry3), providing good spatial resolution and 0.7 second time steps (see fig. 4.1. and 4.2.).

Post-acquisition, all the images were processed with an Airyscan deconvolution algorithm to reconstitute the images after mosaic detection.

3.7. Basic image processing

For the general data processing and visualization, I used Fiji/ImageJ (https://fiji.sc). I commonly used the following functions: adjusting 'Brightness and Contrast' of the images; 'Channel tool' for the colocalization analysis; different look-up tables (LUTs) for better data visualization; Maximal intensity projection, as well as sum of slices for visualizing 3D datasets.

A Gaussian blur filter or Gaussian filter 3D with the middle sigma value (between 1 and

2) was commonly used to remove the low frequency noise before chromosome tracking with a Matlab algorithm (MathWorks® Inc). For the visualization of the chromosome tracking results, I used the MtrackJ plug-in. The chromosome tracking tool is described below. To open data files in other formats than .tiff, I used the 'Bio-formats importer' plug-in.

Deconvolution was performed with the Huygens Remote Manager (http://hrm.svi.nl/) with manual threshold selection. Processed images were exported with the .ometif extension and with 32-bit depth.

For the rendering of 3D data sets I used Imaris (http://www.bitplane.com/imaris).

3.8. Chromosome tracking in 3D

In order to study chromosome kinetics, I performed live-imaging of the oocytes starting from the NEBD until full chromosome congression, aiming for the highest possible temporal resolution, while still collecting a stack covering the entire 3D volume (see chapter 3.6.). For the quantitative analysis, I used a three-dimensional particle-tracking algorithm specifically developed for tracking chromosomes in starfish oocytes by Nilah Moonier (currently, Stanford University). The algorithm was described in (Mori et al., 2011; Monnier et al., 2012).

This algorithm, developed in Matlab (MathWorks® Inc), is adapted for processing both 2D and 3D time-lapse images. As input, the script requires a .tiff file, and is fully automated. The key feature of this algorithm is an advanced statistics-based prediction tool for assembling trajectories from the data points, under-sampled both in 3D and time. Furthermore, the algorithm employs a water-shedding function, which is absolutely required at the late stages of the chromosome congression, as they approach each other and often merge on the images, while they still need to be treated as separate objects for analysis.

An example of a typical dataset with 5 seconds time resolution step is shown in fig. 3.3. as selected still images. Once the script is running, the following steps are performed for each time-point of the time-lapse:

1. Gaussian blur filtering to remove high-frequency noise. This step is required to reduce the number of identified false-positive particles, thereby facilitating further analysis steps. This step is one of the longest in the terms of computational time, and therefore was often performed externally in Fiji/ImageJ prior to the automated analysis.

2. Water-shedding was performed automatically on every Z slice and time-frame of the file, although required only at the later time-points, when the chromosomes had congressed.

3. A morphological opening filter, targeted to identify bulky features on images, was used for nucleolus identification and mathematical removal. The nucleolus was discarded from the tracking analysis, as it gets disassembled soon after NEBD. Additionally, the bulky structure of the nucleolus may prevent identification of the real chromosome signals.

4. Next, the masks of the nucleolus, identified previously, was subtracted from the Gaussian filtered and water-shed filtered image. The previous three steps were performed on each of the Z slices. Thresholding for the chromosome identification was performed in 3D. Each chromosome was identified as a small 3D object with a calculated center of mass.

5. These objects were assigned to individual chromosome trajectories based on the probabilistic function. Chromosome trajectories were exported as 3D coordinates in a .mat file. Furthermore, a .mdf file was generated visualizing the trajectories in Fiji/ImageJ with the MtrackJ plug-in.

The tracking results were then rigorously checked in 2D and 3D and false-positive trajectories were discarded manually.

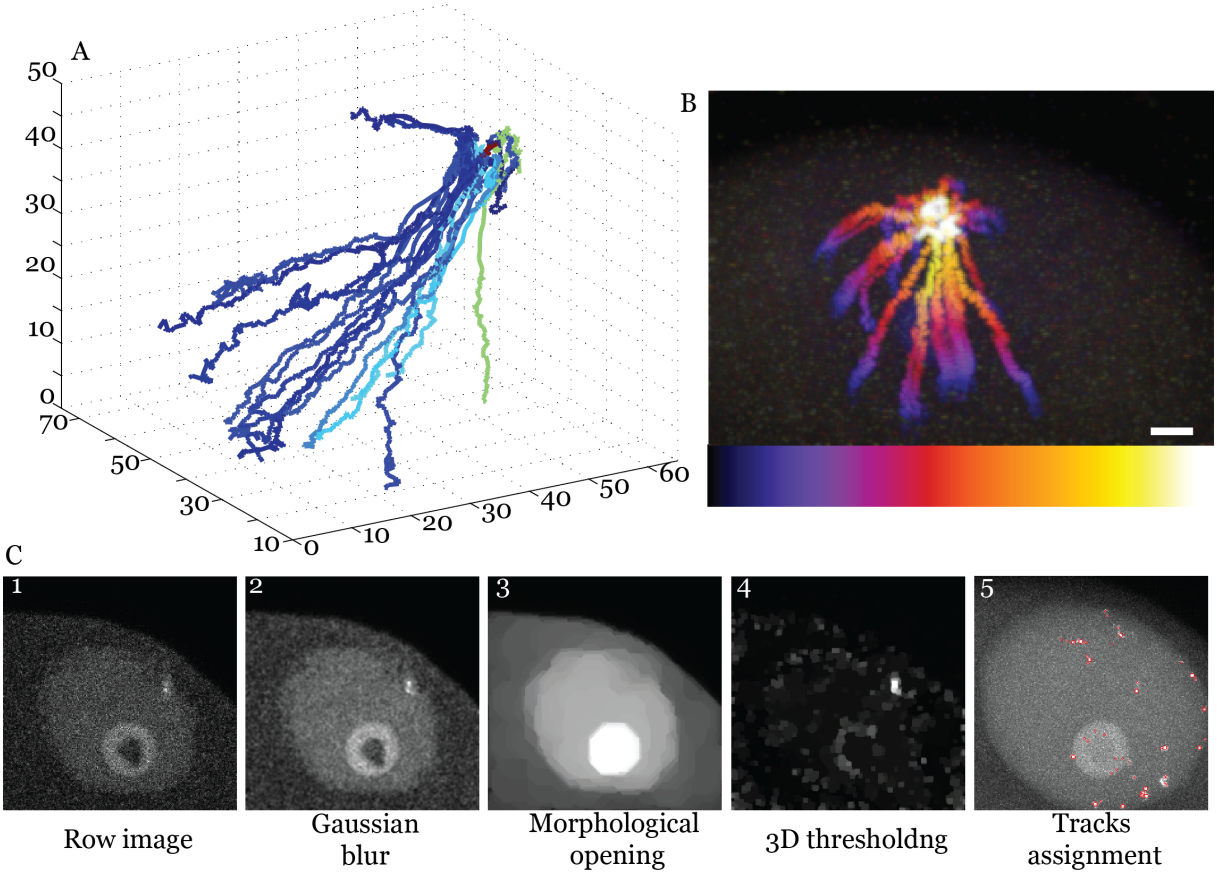

Figure 3.3. The principle of the 3D chromosome tracking algorithm. A. Trajectories of all chromosomes in the oocyte automatically tracked in 3D over time. **B.** Chromosome trajectories in 3D visualized according to the temporally color-code: 3D projection of the nuclear region of an oocyte expressing H2B-mEGFP3, labeling the chromosomes. Time step 5 sec. Single confocal slice. Scale bar 10 µm. C. 1. Raw images are imported and displayed via automated Matlab algorithm for chromosome tracking. 2. A small Gaussian blur is applied to remove high-frequency noise. 3. A

morphological opening filter is used to find the large objects like the nucleolus and the outline of the nucleus area. 4. Image 3 is subtracted from Image 2 and thresholded in 3D with the automated threshold filter. Chromosomes as identified as small bright objects. 5. In the subsequent frames of the time series, identified chromosomes are assigned into the tracks based on their respective position and velocity.

In starfish oocytes, chromosome congression is a two-stage process (Lénárt et al., 2005; Mori et al., 2011). The actin phase is slower and characterized by jittery chromosome motion. Microtubule-driven chromosome transport is faster and directed. When imaging with high speed (5 seconds per Z stack or less), for some chromosome trajectories, one can detect the pause between these two modes of transport. Furthermore, the direction of the chromosome transport is sometimes changed upon transition from the actin to the microtubule driven transport. I have manually identified the transition points between actin and microtubule-drive phases for each chromosome and from here on will call them *chromosome capture events*. These events are identified as the first moment of fast chromosome motion. The transitions between the two transport phases were defined strictly based on the following criteria:

1. rapid change in the chromosome pole-ward velocity (required);
2. chromosome transient 'dwelling' between the two phases;
3. change in chromosome motion direction.

Specifically, after the automated chromosome tracking was finished, chromosome trajectories were plotted in 3D and 2D as chromosome pole-ward velocities. The 'pole' was determined manually as an average point in 3D, corresponding to the full chromosome congression based on their trajectories. In physiological terms, the 'pole' corresponds to the average position between the two microtubule asters, close to the animal pole. Chromosome pole-ward velocity was calculated as a distance between the 'pole' and the chromosome position in 3D at every given moment of time. Furthermore, chromosome trajectories were overlaid with the original movies using the MtrackJ plugin in Fiji/ImageJ, checked in single slices and on the maximum - intensity projected images (fig.3.4.).

The resulting parameter, referred to as a *chromosome capture event,* is used further to analyze the kinetics of the chromosome capture by microtubules in the control and under a variety of conditions.

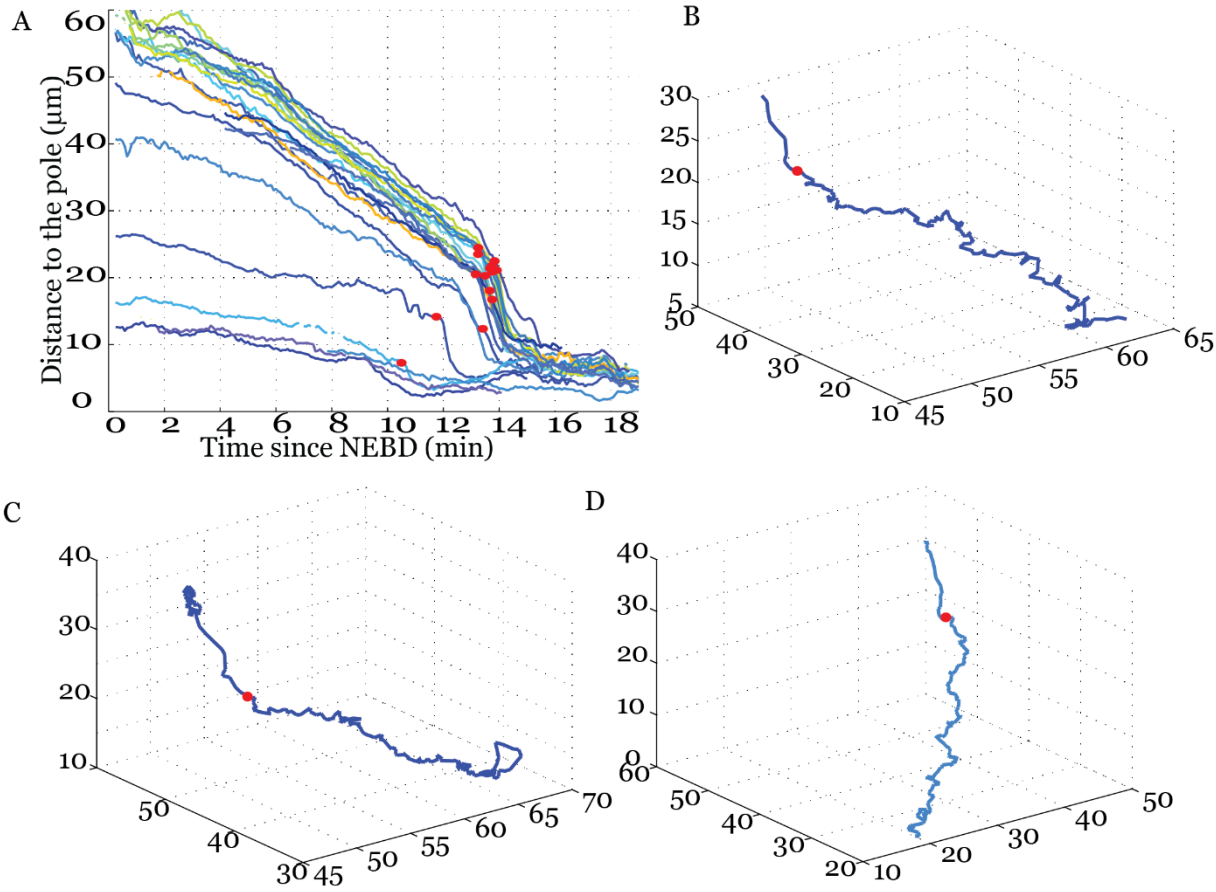

Figure 3.4. Defining the chromosome capture events as a transition point between actin- and microtubule-driven chromosome transport. A. Pole-ward Chromosome velocity, calculated from the chromosome trajectories derived by the automated tracking algorithm (see fig. 3.3.). Pole-ward velocity was calculated as distance to the asters vs. time. Each colored dot represents a capture event for an individual chromosome. **B-D.** Trajectories of the individual chromosomes in 3D, with the capture event defined manually based on the changes in the chromosome velocity and motion direction.

3.9. Oocyte chemical fixation and immunostaining

To describe the morphology of the microtubule asters and actin meshwork during meiosis, I performed oocytes chemical fixation and immunostaining. For the single microtubule labeling, I used an anti-tubulin antibody (DM1A Sigma-Aldrich) that recognizes tubulin in a wide range of species. The aldehyde fixation protocol was generally adopted from George von Dassow for echinoderm oocytes and embryos (Strickland et al. 2004), and further optimized for high-spatial resolution imaging.

The oocytes, matured by hormone 1-MA addition, were chemically fixed at specific times with a fixative buffer at room temperature. For that, sea water was aspirated and the buffer quickly added to the oocytes and mixed immediately by flipping the tube. Generally, fixative was added in 20-40 fold excess to the volume of oocytes in the remaining sea water on the bottom of the tube.

Fixative (100 mM HEPES pH =7.0, 50 mM EGTA, 10 mM $MgSO_4$, 0.5 % Triton-X100, 1 % formaldehyde, 0.1 % glutaraldehyde), is buffered to match the pH and salinity of the sea water, thus preventing cell cortex damage and bursting of the oocytes. In

addition, it contains a low amount of detergent for the chemical permeabilization of the membranes. Fixation was performed at the room temperature for 15 minutes, while the oocytes were gravity-sedimenting.

In the following step, the fixative buffer was aspirated and replaced by a PBS-T buffer (standard PBS solution with 0.5% Triton-X100). Fixed oocytes were permeabilized in PBS-T at room temperature for at least 2 hours or overnight. Prolonged incubation with the detergent in this step is required for the permeabilization and removal of all oocyte membranes. This is a requirement for efficient antibody penetration, as starfish oocytes are very large, and simple Brownian motion of the antibodies is restricted.

To increase the signal-to-noise ratio for the antibody staining, an extra step of background blocking was performed with an Image-iT reagent for 10 minutes (Image-iT®FX Signal Enhancer). This reagent abolishes weak electrostatic interactions in the sample, and thereby greatly reduces non-specific interactions of the antibodies.

An anti-tubulin antibody (DM1A Sigma-Aldrich) was added after a washing step with PBS. Antibodies were applied in a high titer (1:400) and for an extended period of time: minimum overnight, preferably for two or three days with constant rotation at +4°C. Secondary antibodies (goat-anti-mouse IgG Alexa488, dilution 1:500) were applied overnight as well. Simultaneously, the oocytes were stained for chromosomes with Draq5 (Biostatus), and F-actin with Phalloidin-A568. Phalloidin from stock, dissolved in methanol, was reconstituted in PBS, as described before (section 3.4.2). Oocyte incubation in the primary and secondary antibodies was done in a 3% BSA (Bovine Serum Albumin, Sigma) solution to further prevent unspecific antibody binding. Lastly, samples were mounted in an anti-fade mounting medium (ProLong® Gold Antifade Mountant), between the glass and a cover slip spaced with a single layer of double-sided sticky tape. The samples were kept overnight in darkness for the mounting medium to solidify, and to prevent light bleaching. Imaging was performed as described above.

3.10. Computational modelling in *Cytosim*

Cytosim (Cytoskeletal simulator) is a modelling software developed by François Nédélec at EMBL (http://www.cytosim.org). *Cytosim* is designed to model large systems. The key elements in the simulations are fibers and proteins associated with them. A fiber can be dynamic and/or flexible. Other objects in the simulation, such as beads, can be applied to compose complex assemblies. All elements in the simulation follow Brownian dynamics laws. Altogether, the modular principle of *Cytosim* allows modelling of a huge variety of cellular behaviors with great flexibility.

All properties and parameters used in a simulation are set-up and summarized in a single configuration file. Simulations were performed either on a desktop computer or

on the EMBL HPC Cluster. The configuration files are shown in the Appendix chapter. The final analysis of the computer modelling was performed in Matlab (MathWorks® Inc).

3.11. Correlative light-electron microscopy of starfish oocytes

3.11.1. Sample preparation

For the visualization of the chromosome ultrastructure with CLEM, chromosomes or microtubules were labeled with fluorescent proteins and imaged with a confocal microscope (Leica SP5) right after chemical fixation. Simultaneously with the protein injection, the oocytes were injected with several small oil droplets. These oil droplets served as reference points for the correlative map of each oocyte. While injecting oocytes, the microinjection needle was loaded with several repetitive bands of the protein and silicone oil, thereby, introducing several small oil droplets (typically, between 5 and 7) of different size, positioned in the cytoplasm as close to the nucleus as possible.

3.11.2. Oocyte chemical fixation

Oocytes injected with H1-A648 or Cy3-tubulin proteins and oil droplets were matured by adding 1-MA hormone and fixed at 5 to 8 minutes after NEBD. The NEBD onset was checked with transmitted light and under the confocal microscope. Some oocytes were also labeled with Cy3-Tubulin and fixed when the spindle was fully formed.

Each oocyte was fixed separately in a small well plate (Ibidi µ-slide for angiogenesis, volume 100 µl) by mixing 20 µl of double-concentrated fixative buffer with 20 µl of filtered sea water containing one oocyte. The fixative buffer in the final dilution had the following composition: 1% glutaraldehyde (Electron Microscopy Sciences), 2% formaldehyde (Electron Microscopy Sciences) and 0.1M PHEM buffer (60 mM PIPES, 25 mM HEPES,10 mM EGTA, 2 mM MgCl2 pH = 6.9). Oocytes were fixed with the fixative buffer at room temperature in small well-plates for 20 minutes (1:1 mixture of the fixative buffer and filtered sea water), and subsequently transferred into 3 cm Petri dishes with 2 ml of pure 1x fixative and stored at 4˚C overnight or until the following processing steps. Each oocyte was stored in separate petri-dishes to avoid mixing them up during EM-processing and hindering the future correlation steps.

3.11.3. Sample processing and resin infiltration

After the overnight fixation, the oocytes were transferred and washed in cacodylate buffer (pH = 7.4). The first post-fixation was performed with 1% OsO_4 (Electron Microscopy Sciences) and 1.5% $K_4Fe(CN)_6$ (Merck) in cacodylate buffer (0.1 M), followed by the second post-fixation step with 1% OsO_4 in cacodylate buffer (0.1 M). Next, the samples were treated with uranyl acetate aqueous solution (Serva

Electrophoresis GmbH, Heidelberg, Germany). Water in the samples was replaced with ethanol in gradual steps (from 25% to 100 %). Next, the oocytes were infiltrated with Ephon in ethanol solution (from 25% to 100 %) and transferred into the resin molds for polymerization for 3 to 4 days at 60˚C. These processing steps were performed in a laminar flow hood in a PELCO Biowave Pro microwave (Ted Pella, Redding, CA) to accelerate the sample preparation process. Afterwards, the front-face of the polymerized resin blocks were trimmed with a trimming-diamond knife (90˚, Diatome AG, Biel, Switzerland). Three out of four sides of the resin-block were also trimmed, making the block asymmetrical which helped orienting the sample during further processing steps.

3.11.4. MicroCT imaging

Before the serial sectioning, the fully-processed oocyte samples were scanned using microscopic X-ray computed tomography (microCT) in a Phoenix Nanotom m (GE Sensing & Inspection Technologies, Fairfield, CT) running under Phoenix datos|x 2 and xs control software (GE Sensing & Inspection Technologies Fairfield, CT). For that, the sample embedded in the resin block was mounted as close as possible to the X-ray source, in order to obtain a higher resolution image. The resulting microCT volume was obtained using Phoenix datos|x reconstruction software (GE Sensing & Inspection Technologies Fairfield, CT). The 3D volume was processed with VGStudio MAX software (Volume Graphics, Heidelberg, Germany). Following this, the microCT 3D images were analyzed in Amira (FEI company, www.fei.com/software/amira-3d-for-life-sciences). The voxel size of the obtained microCT datasets was typically around 0.5 x 0.5 x 0.5 μm.

3.11.5. Image registration with Amira software

Corresponding fluorescence and microCT images were loaded in Amira virtual space for their registration in 3D. Both datasets were segmented to visualize the outline of the resin block (microCT only), oocyte, oil droplets and chromosomes (FM only) and stored in separate label files. In order to facilitate the segmentation, the images were processed with a Gaussian filter, and several thresholding steps enabled to create a surface mask of the oocyte. Processing artifacts were corrected manually using the brush and interpolation tools. Chromosomes on the fluorescence images were segmented by the thresholding and/or manually drawing. After the segmentation, the two 3D datasets were superimposed and fitted into the microCT image, using the oil droplets as landmarks on which the correlation was based. If simple 3D rotation was not sufficient to precisely dock the two datasets, the fluorescent image was isotropically shrunken or expanded in order to match the microCT dataset. Chemical fixation and EM processing of biological samples results in size/shape changes, resulting in dimensional differences between the FM and microCT datasets of the oocytes. Based on the final 3D registration, an oocyte distance map was built for the thin serial

sectioning. Typical targeting precision of the region of interest (ROI) was in a range of 10-15 μm.

3.11.6. Sample trimming, serial sectioning and EM imaging

Using the distance map created in Amira software, part of the resin block was trimmed up to the ROI using a diamond knife (Diatome, 90° trimming diamond). For that, the sample was mounted on a Leica Ultracut UC7 ultramicrotome (Leica Microsystems, Wetzlar, Germany). Starting 5 μm away from the ROI, thereby leaving a buffering zone that allows to compensate for registration and trimming imprecisions, the oocyte sample was processed for transmission electron microscopy (TEM) by obtaining thin serial sections (typically 70 nm). The serial sections were additionally contrasted by post-staining with 2% uranyl acetate in 70% methanol and lead citrate prior to TEM imaging. For the visualization of the chromosome ultrastructure, serial sections were imaged with a Biotwin electron microscope (120kV Transmission Electron Microscope, FEI company).

Acknowledgements

This work would not have been possible without support from a large number of people. I had a lot of help while accomplishing this project, concerning either reagents and protocols, or advice on imaging and quantitative data analysis. Individual contributions are listed here:

Péter Lénárt started teaching me the Matlab. I also had a lot of support with Matlab from Philippe Bun, who also provided his script for chromosome pair-wise velocity calculation.

Nilah Moonier, who wrote the Matlab algorithm for automated chromosome tracking in 3D. She taught me how to use it (over skype!) and fixed the only bug, that later unveiled itself in this script.

The EMBL imaging facility, providing the opportunity to work on the newest microscopes, and particularly to Aliaksandr Halavatuy for supporting my work on the Zeiss LSM800 AiryFAST-microscope, which was very useful to my project.

The immunostaining protocol used in this project was developed only due to great advice from Martin Wür and Scilard Szicoka. It was further improved together with Natalia Wesolowska.

Kalman, the first technician of the Lénárt lab, who teached me all the basic techniques and helped with the design and cloning of the pGEM-HE-H2B-mEGFP3 construct.

Andrea Callegari, the second Lénárt lab technician, who provided constant support and discussions, as well as supervising Michal Fleszar, trainee at the Lénárt lab, who helped with my project. Together, they synthesized and tested several mRNA samples.

Correlative light-electron microscopy was performed in collaboration with Matthia Karreman. She performed all the sample processing, serial sectioning and most of the image acquisition. Part of the oocyte segmentation and EM imaging was done by Michal Fleszar.

Mathematical modelling in *Cytosim* software was performed in collaboration with and under supervision of François Nédélec. Furthermore, Serge Dmitrieff assisted with data handling and plotting.

Katarzyna Tarnawska provided Cy-3 tubulin. The GFP-Ndc80 protein was a gift from Stefano Maffini (Musacchio lab, MPI Dortmund).

Kresimir Crnokic, who took care of all the starfish in the EMBL animal house.

4. Results

4.1. Phases of chromosome congression in starfish oocytes

During division of the small somatic cells, chromosomes are captured by dynamic microtubules nucleated from the centrosomes. Astral microtubules, spanning the volume of the whole cell, are stochastically growing and shrinking and, thereby, able to reach and capture all chromosomes in the cell. As soon as a kinetochore of a chromosome is attached to a microtubule, this chromosome is transported either to the spindle pole or to the spindle equator. Nowadays, several mechanisms are known to facilitate the chromosome search, rendering it a fast and efficient process in somatic cells (see *Introduction*). However, the size and geometry of the oocytes is very different from that in somatic cells. How chromosomes are captured and delivered to the small meiotic spindle in these specialized divisions with chromosomes scattered in a volume orders of magnitude larger than in somatic cells remained poorly understood. Therefore, I set out to characterize the complete process of chromosome congression in starfish (*Patiria miniata*) oocytes, well suited to image the entire process live.

Starfish oocytes are 180 μm in diameter with a 70 μm large nucleus (fig. 4.1). In prometaphase, as described previously, chromosomes are first transported towards the animal pole by the contractile actin meshwork that forms within the volume of the nucleus and congresses the chromosomes into approximately half of their initially occupied volume (see *Introduction*). Interestingly, this area almost exactly corresponds to the microtubule capture range – the maximal length that spindle microtubules can reach in the first meiotic division. Simultaneously with chromosome transport by the actin meshwork centrosomes at the animal pole are nucleating dynamic spindle microtubules, searching for the chromosomes. Once a chromosome is captured by a microtubule, it is transported towards the centrosomes at the center of the asters. In starfish oocytes bi-orientation is separated in time, and only minutes later the spindle starts forming the metaphase plate. As a result, in approximately half an hour after NEBD, a small meiotic spindle is formed, which is comparable in size to those in somatic cells (approx. 20 μm in length). The assembly of a small spindle located at the cell cortex is the prerequisite for an asymmetric cells division, forming a small polar body (10-15 μm in diameter) and a large oocyte. After the second meiotic division, the oocyte will become a mature egg ready for the fertilization with reduced genomic content and containing all nutrients deposited for supporting the further embryonic development.

Chromosome congression by the actin meshwork ensures capture of all the chromosomes scattered in the large nucleus and transports them into the capture range of a small spindle. The two phases of the chromosome transport can be distinguished on chromosome tracks (for details of 3D imaging and tracking chromosome motion see *Materials and Methods*): chromosome motion mediated by

the contracting actin meshwork is slower and jittery, compared to the directed and much faster chromosome motion along the microtubules during the following step (fig.4.1.B). This allowed me, based on the difference in chromosome velocity and direction of the motion, to identify with high confidence the transition between actin- and microtubule-driven transport for each chromosome individually (fig.4.1.C). These transitions, in following referred to as *chromosome capture events*, are identified as the first moment of accelerated chromosome motion along the microtubule.

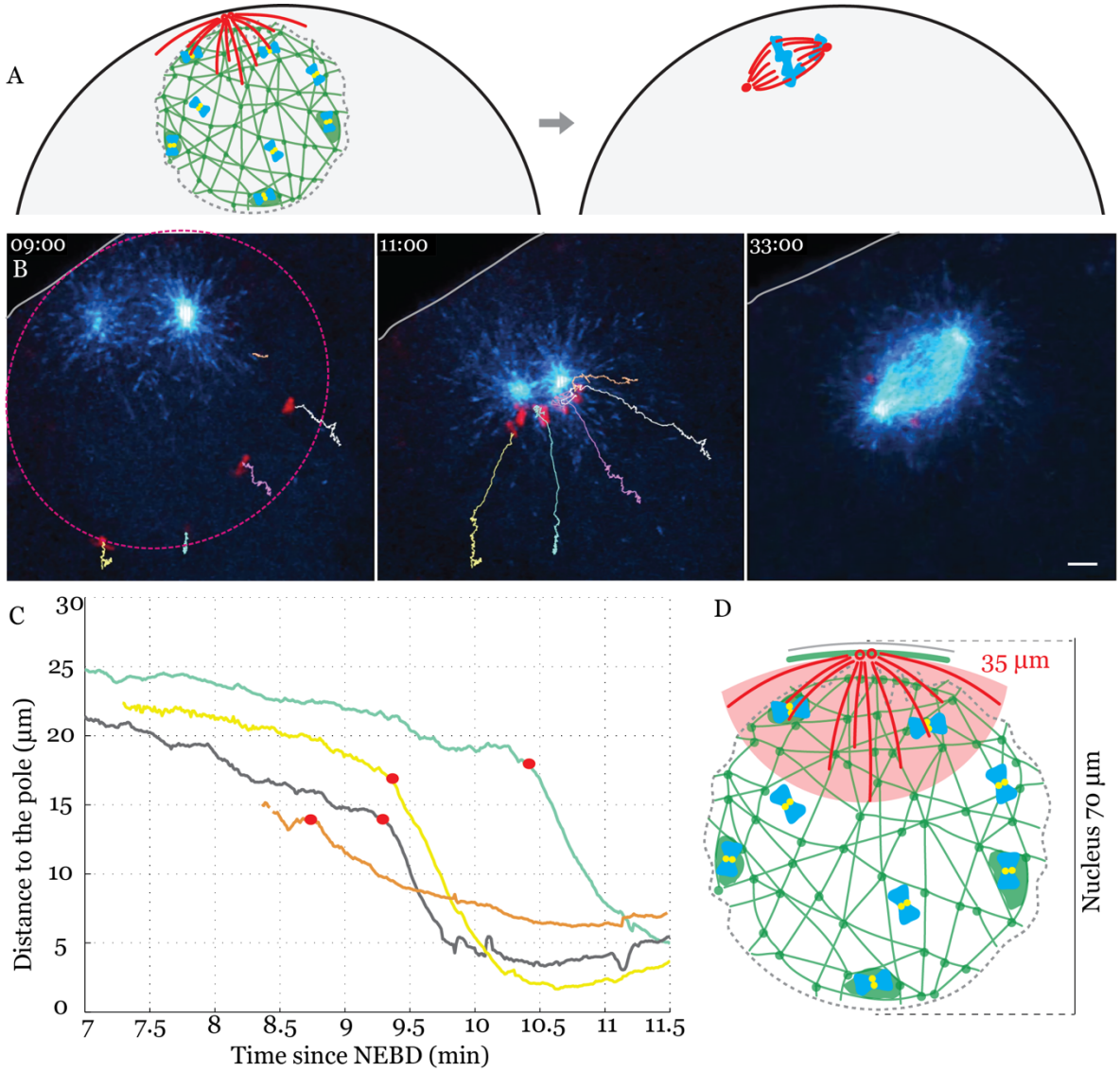

Figure 4.1. Overview of the chromosome congression process from NEBD until spindle formation. A. Scheme of the oocyte: nucleus is anchored off-center at the animal pole, where the centrosomes nucleate microtubules in the prometaphase. Actin meshwork transports the chromosomes into microtubule capture range. Next, a small spindle is formed. **B.** Selected frames from a time series in an oocyte expressing H2B-GFP (red) labeled chromosomes and EB3-mCherry (cyan) labeling microtubule plus-ends. Time step 0.7 sec. Single confocal slice. Scale bar 5 µm. Derived chromosome trajectory is overlaid with the images. Trajectory is plotted till the present time, as indicated. Time relative to NEBD. Pink circle corresponds to microtubule capture range. **C.** Chromosomes pole-ward velocity, calculated as the distance between the animal pole and chromosome at every given moment of time. Red dot on the chromosome tracks, corresponding to the transition between actin and microtubule driven chromosome transport. Color-code of the individual chromosome trajectories corresponds in B and C is preserved. **D.** Scheme: microtubule capture range covers only part of the nucleus. Chromosomes are congressed there by the actin meshwork.

As revealed by high resolution imaging of the microtubule plus tip marker EB3, and subsequent quantitative analysis, during the first meiotic division each centrosomal aster consists from several hundred microtubules. Each of the two asters is located 5-7 μm away from the cell cortex and nucleates microtubules in all directions. Those microtubules, growing towards the cell interior, reach up to 25 μm in length. Thereby, the length of microtubules define a chromosome *capture range* of 30 μm, which is fully consistent with the maximal chromosome capture distance identified in the chromosome tracking assay (fig. 4.1).

Additionally, I observed that some microtubules are nucleated from the wall of existing microtubules, like shown in fig. 4.2. These observations suggest, that branched microtubule nucleation pathway mediated by the Augmin and TPX2 (Petry et al., 2013), is active in starfish oocyte meiosis. Microtubule branching has been proposed to be particularly important in large cells like oocytes, as one of the mechanisms facilitating chromosome capture: microtubule-nucleated microtubules can increase microtubule density, thereby increasing the efficiency of the microtubule search (Ishihara et al., 2014).

I then performed high resolution imaging of fixed oocytes to reveal the detailed morphology of actin meshwork forming within the whole nuclear volume, thereby, partially overlapping with the microtubule asters. This raises the question of how the microtubules grow through the contracting actin meshwork and whether actin meshwork hinders the chromosome capture by the astral microtubules. On figure 4.2.B, an astral microtubule, growing towards the chromosome, is partially co-aligned with the bundle of the actin meshwork. On the same image, most of the other astral microtubules are not co-localizing with the actin meshwork and reaching the chromosomes. However, at the oocyte animal pole, the molecular environment may be so crowded that the observed partial co-alignment between microtubule and F-actin bundle is co-incidental. Overall, based on microtubule morphology on high-resolution images of immunostained oocytes, microtubules grow unconstrained in-between the actin filaments: no exclusion of the microtubules was detected inside the actin meshwork area, as compared to outside the meshwork.

More detailed analysis of the immunofluorescently stained oocytes revealed many chromosomes ($n > 100$) located in direct proximity to microtubule walls (fig. 4.2.A, chromosome 1), suggesting that chromosomes form lateral attachments with the microtubules during the initial pole-ward chromosome transport. This includes chromosomes surrounded by an actin patch, that also seem to be attached to astral microtubules (fig. 4.2.B). Actin patches form simultaneously with the F-actin shell around the chromosomes located near the nuclear envelope. Although they appear as very dense F-actin structures, nucleated by the Arp2/3 complex, microtubules seem to be able to grow through them and capture chromosomes. Non-captured chromosomes

(chromosome 3 on fig. 4.2.A) are loosely entrapped into the actin meshwork and s seem to be accessible to astral microtubules.

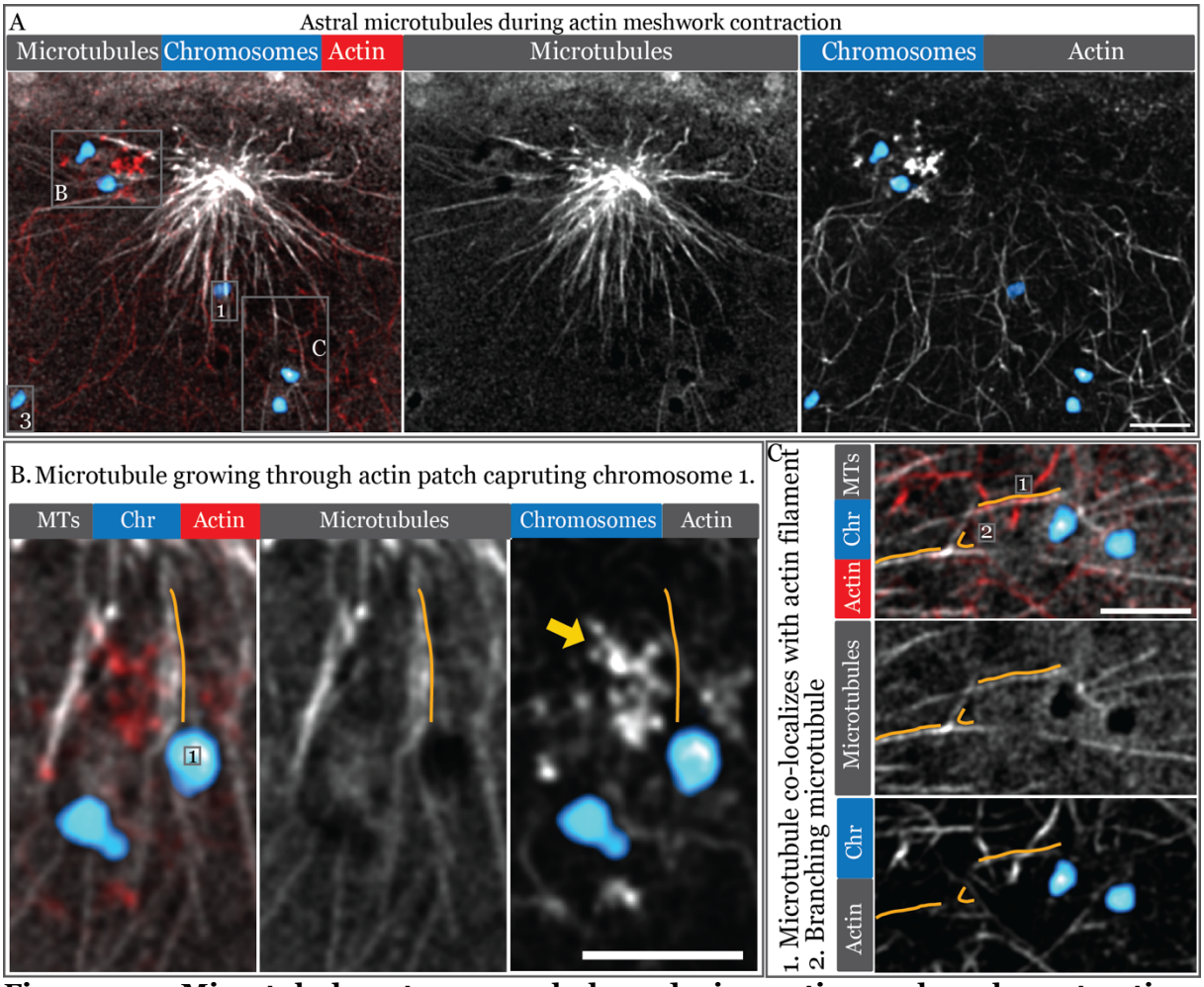

Figure 4.2. Microtubule asters morphology during actin meshwork contraction. Confocal image of a matured oocyte, chemically fixed 5 minutes after NEBD and immunostained. Microtubules (α-tubulin antibody) in gray; Actin meshwork (Phalloidin A561) in red; Chromosomes (Draq5 staining) in cyan. Scale bar, 5 µm. Single confocal slice. Z step = 130 nm. Pixel size = 38 nm. Single slice from the confocal stack, deconvolved. Panels B and C are enlarged images from A. In order to resolve individual microtubules and microtubule bundles, the protocol for oocyte chemical fixation and immunostaining was optimized: higher concentrations of antibodies applied and prolonged incubation time, sampling with the high density in the Z - stack.

Taken together, data obtained by immunostaining provides a very detailed single filament resolution description of the microtubules and actin meshwork during the process of chromosome congression. Based on these data, I conclude that microtubules *grow unconstrained by the actin filament meshwork*, although I observed occasional co-alignment of filaments. Capture of the chromosomes appear to occur through lateral chromosome-microtubule attachment.

4.1.1. Initial chromosome-microtubule attachment is lateral

According to the morphological description in the previous section, astral microtubules, upon chromosome capture, form lateral chromosome-microtubule attachments. These initial attachments are known to be formed in the prometaphase and tether the kinetochore to the wall of a single microtubule. This is followed by a rapid transport of the chromosome towards the microtubule minus-end (Rieder and Alexander, 1990). In addition to the images of immunostained oocytes (fig. 4.2), according to the individual chromosome trajectories (fig. 4.1), there is no pausing time between actin - and microtubule - driven congression phases. Altogether, this suggested that once a chromosome is captured by a microtubule, the lateral attachment is established and the chromosome is immediately transported along a single microtubule.

In order to characterize in detail the process of chromosome attachment and transport, I performed high spatio-temporal resolution live-imaging (pixel size 130 x 130 nm every 0.7 seconds) of chromosomes and microtubule tips simultaneously, starting at NEBD and until spindle formation. Specifically, I focused on chromosome-microtubule capture events, imaging the growth of individual microtubule plus-tips, labeled with EB3-mCherry3, emerging in the direct proximity of chromosomes, co-labeled with H2B-mEGFP3 (fig. 4.3). Chromosome trajectories, automatically tracked as described in chapter 3.8, have the characteristic fast movements, corresponding to the microtubule transport. These accelerations in the chromosome motion towards the aster precisely coincide with the appearance of the EB3 comet tip growing from the centrosome and co-aligning with the chromosome. Notably, in the subsequent moment after the EB3 comet tip appears, the chromosome moves faster in the direction of the centrosome (fig. 4.3.A). Although it is very difficult to visualize these very fast capture events in the large 3D volume, I was able to visualize such chromosome and microtubule tip behavior for six chromosomes in four different oocytes. Based on these observations, I conclude that initial chromosome-microtubule attachment is lateral and immediately followed by the chromosome transport along the microtubule.

Surprisingly, in one of the time-lapse examples (fig.4.3.B), I have observed two sequential microtubule capture events by two different microtubules for a single chromosome. Presumably, the chromosome is being captured and transported by one microtubule, released, and then captured by another microtubule after a short pause. This pause lasts several seconds (up to 10 seconds) until the next capture event. Thereby, towards the center of the aster, chromosomes are transported along the microtubules in several steps.

Altogether, these data directly visualize, that in prometaphase, chromosomes form lateral attachments with the microtubules and are rapidly transported toward the centrosomes. These observations are consistent with prior research of the initial

kinetochore-microtubule attachments, that form by the same mechanism in somatic cells (Rieder and Alexander, 1990).

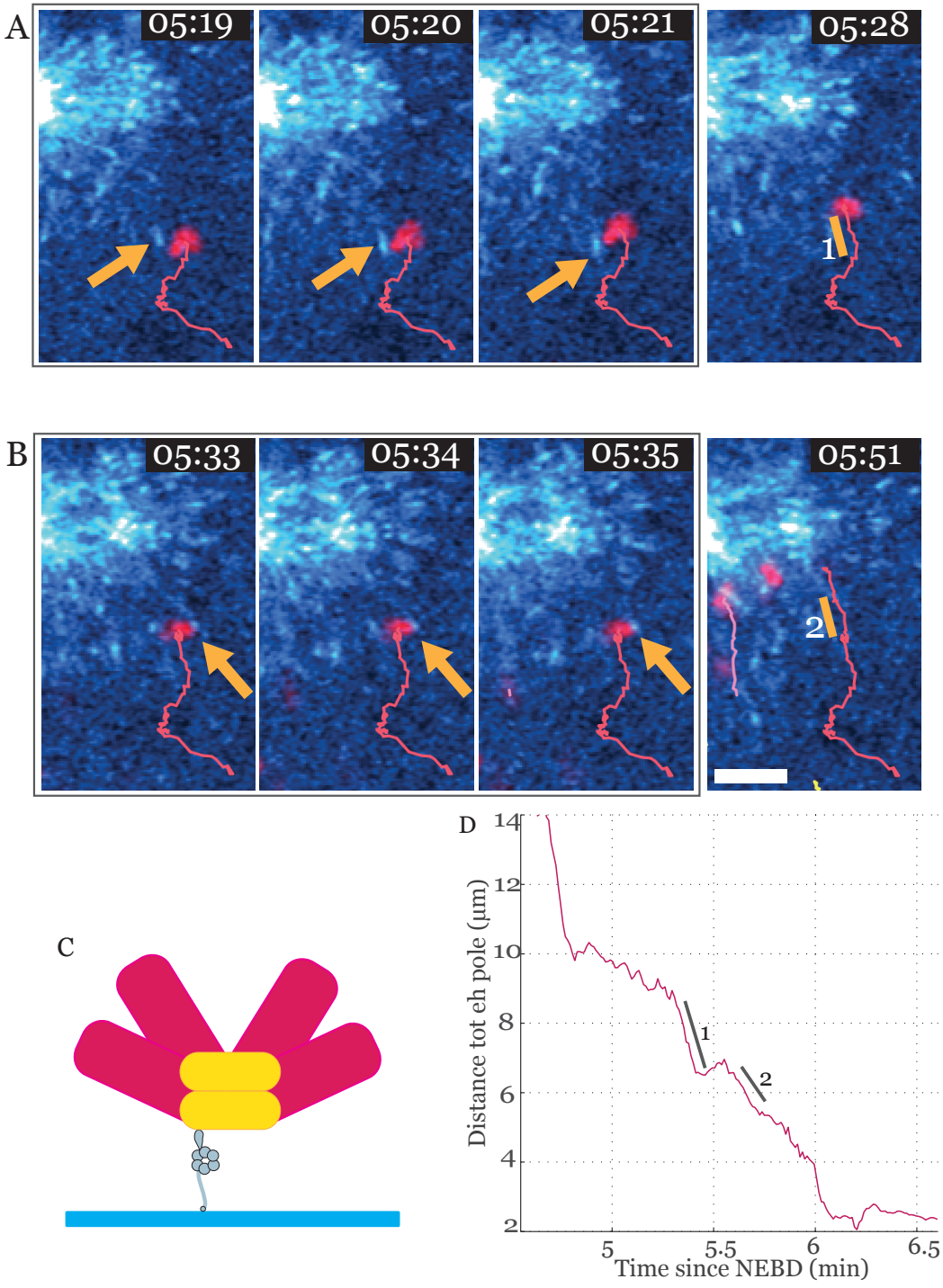

Figure 4.3. Microtubules attach laterally to the chromosomes and immediately transport them to the animal pole. A-B. Selected frames from a time series in an oocyte expressing H2B-GFP (red) labeled chromosomes and EB3-mCherry (cyan) labeling microtubule plus-ends. Imaging performed with the Zeiss LSM 880 microscope with AIRY Fast option. Time step 0.7 sec. Single confocal slice. Scale bar 5 µm. Derived chromosome trajectory is overlaid with the images. Trajectory is plotted till the present time, as indicated. Time relative to NEBD. **C.** Scheme of a lateral kinetochore (yellow) to microtubule(blue) attachment. Dynein is transporting the chromosome to the microtubule minus-end. **D.** Single chromosome pole-ward velocity plot.

Arrows indicate the beginning of the microtubule-driven transport. Timing correlates with the appearance of the EB3-comet.

4.1.2. Dynein transports laterally attached chromosomes along the microtubules

Molecular motors transporting chromosomes during the stage of the lateral kinetochore attachment are dynein and CENP-E (Barisic et al., 2014). In starfish oocytes, due to the specific geometry of the cell, all chromosomes are initially transported to the microtubule minus-ends to the center of the asters. Thus, initial microtubule transport must be mediated by dynein. To test this hypothesis, I inhibited dynein activity through a specific small molecule inhibitor.

Treatment with dynein inhibitor Ciliobrevin D completely abolished the microtubule-driven phase of chromosome transport, while the actin-dependent transport remained unperturbed (fig. 4.4). Chromosomes were congressed by the contractile actin meshwork into microtubule capture range. However, in contrast to the control, the microtubule-driven chromosome transport was completely abolished and the chromosomes remained scattered in a small area close to the animal pole. According to the chromosome trajectories obtained in 3D, after the actin meshwork transport was completed, the chromosomes slowly diffuse in the cytoplasm.

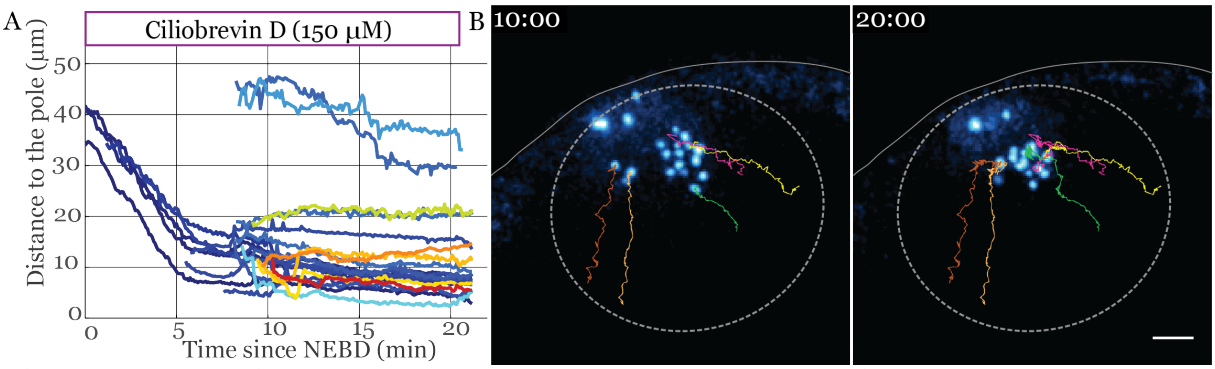

Figure 4.4. Dynein transports chromosomes along the microtubules. Chromosome tracking assay in 3D in the oocyte treated with Ciliobrevin D (150 µM). **A.** Chromosomes pole-ward velocity plot. Chromosomes are transported by actin meshwork in the approx. first 8 min after NEBD. The microtubule-driven transport is abolished, chromosomes diffuse in the nuclear volume. **B.** Selected frames from a time series of the nucleus area of an oocyte expressing H2B-GFP (cyan) labeled chromosomes. Time step 5 sec. Z-projection of 60 µm thick confocal slice. Scale bar 10 µm. Derived chromosome trajectories overlaid with the images, plotted up to the current time. Time relative to NEBD. Number of oocytes in the experiment: 6.

In conclusion, dynein is the main molecular motor transporting laterally attached chromosomes to the centrosomes in starfish oocytes. This data, together with the high spatial-temporal resolution live-imaging (fig. 4.3) indicates that in the prometaphase of the first meiotic division, *chromosomes form lateral attachments to the microtubules, and then are rapidly transported by dynein* toward the centrosomes.

4.1.3. No chromosome-mediated microtubule nucleation detected in early prometaphase

Astral microtubules, nucleated from the centrosomes, capture chromosomes within the microtubule capture range. However, microtubules can also be nucleated from the chromosomes (Karsenti et al., 1984), as well as kinetochores (Witt et al., 1980). Microtubule nucleation, as well as their plus-ends stabilization, is promoted by RanGTP on the chromatin (Carazo-Salas et al., 1999), thereby facilitating chromosome capture (Maiato et al., 2004). In starfish oocytes, actin meshwork greatly facilitates chromosome capture by transporting them into microtubule capture range. However, the role of the other known facilitation mechanisms in starfish remained unexplored. Particularly, microtubule nucleation from the chromatin, since in the other model systems like mouse and *Xenopus* oocytes, this is the predominant pathway of spindle assembly. Here, I tested whether microtubule nucleation from the chromatin takes place in starfish oocytes using high spatial - resolution imaging.

Oocytes, chemically fixed 5 to 8 minutes after NEBD and immunostained with α-tubulin antibody, were imaged at single microtubule resolution (fig. 4.5). While the astral microtubules were visualized quite well, no specific microtubule staining was detected co-localizing directly or in the proximity to the free chromosomes, yet not captured by centrosomal microtubules. The same effect was observed both in the control case (treated with DMSO), as well as upon complete disruption of the actin meshwork in the cell (Cytochalasin D, 40 μM added 30 min before the NEBD). Furthermore, oocytes were treated with the microtubule depolymerizing drug Nocodazole (3.3 nM, applied 5 min before NEBD) as the negative control of the microtubule nucleation (fig. 4.5.D). Under this condition, immunostaining with the α-tubulin antibody gave similar non-specific background staining, as in the other oocyte groups. Neither chromatin-outgrown microtubules, nor specific α-tubulin staining was detected near or in co-localization with the non-captured chromosomes. Altogether, at the given spatial resolution, in starfish oocyte no microtubule nucleation from the chromatin was detected.

In conclusion, based on the morphological observations, as well as live-microscopy data (fig. 4.1 and 4.3), no chromatin-nucleated microtubules were detected in early prometaphase. Thus, *chromosomes are captured and incorporated into the spindle by astral microtubules* nucleated from the centrosomes.

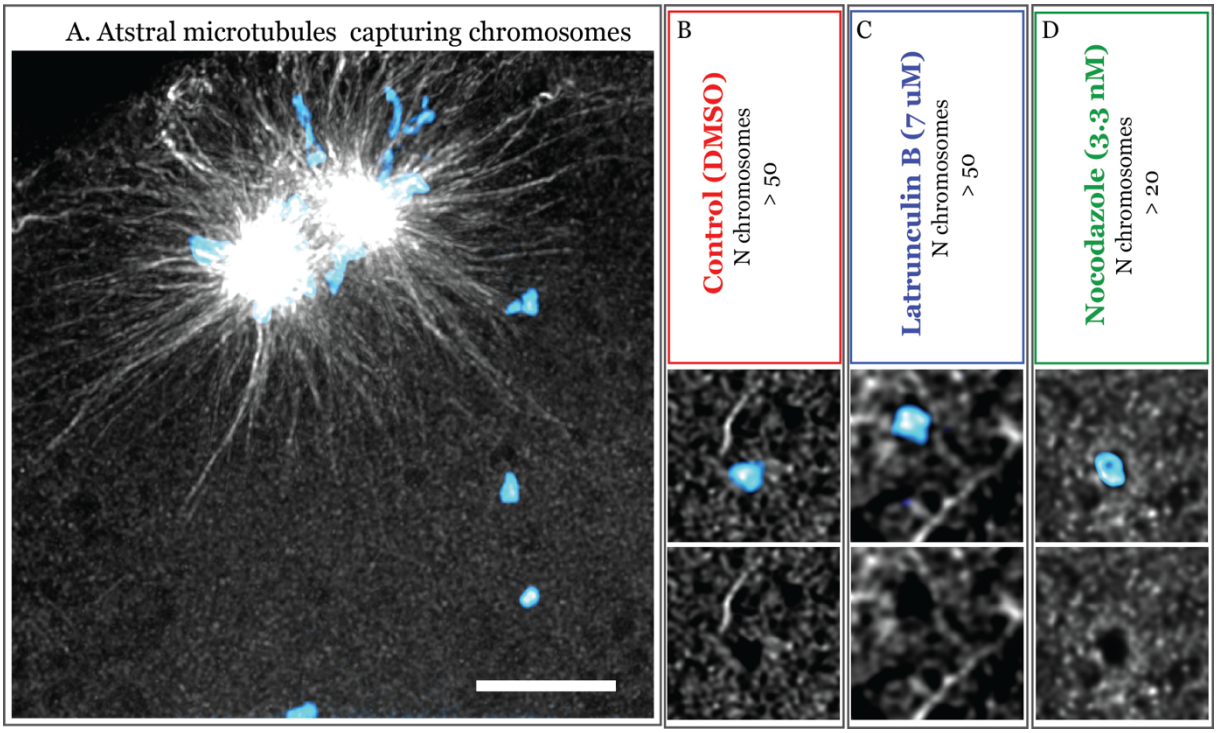

Figure 4.5. Microtubule nucleation from chromatin. Microtubules (α-tubulin antibody) in gray. Chromosomes (Draq5 staining) in cyan. Scale bar, 10 µm. Single confocal slice. Z step = 130 nm. Pixel size = 38 nm. Single slice from the confocal stack, deconvolved. **A.** Confocal image of a matured oocyte, chemically fixed 8 minutes after NEBD and immunostained. Microtubules are nucleated only from the centrosomes, but not from the chromosomes. **B-D.** Non-captured chromosomes in the control, Cytochalasin D and Nocodazole treated oocytes.

4.2. Cooperation between actin and microtubules during chromosome congression

4.2.1. Actin synchronizes chromosome capture by microtubules

During chromosome congression within the contracting actin meshwork, chromosomes are sterically entrapped in the meshwork and brought into the microtubule capture range. Once an astral microtubule captures a chromosome, a lateral attachment is established and the chromosome is immediately transported towards the centrosomes (Mori et al., 2011 and chapter 4.1). However, the cooperation between these two cytoskeletal systems, how chromosomes are transferred from the actin meshwork to microtubules remained unknown. Here, I investigated whether this actin-driven mechanism merely functions to transport chromosomes closer to microtubule asters, or whether there is additional synergy between actin meshwork and microtubules. To accomplish this, I performed chromosome tracking in 3D in the presence or absence of the functional actin meshwork. This allowed me to study the kinetics of the individual chromosome capture events in the live oocyte under different conditions with high temporal resolution.

To assess the role of actin meshwork, all actin structures in the oocyte were depolymerized with Latrunculin B. Importantly, the drug was applied at NEBD onset, therefore all previously formed actin structures were unperturbed, including formation of the F-actin shell, but specifically prevented the formation of the actin meshwork and actin patches, minimizing potential artefacts. The congression process of all the chromosome in the nucleus was imaged in 3D with the temporal resolution of 3 seconds per Z-stack (fig 4.6.A). Such high acquisition speed allowed to precisely identify when and where a chromosome was captured by a microtubule individually for each chromosome in the nucleus (fig 4.6.C-D). Each chromosome capture event was identified manually based on the difference in the speed of transport, as described in the *Materials and Methods* and 4.1 chapter.

While in the control untreated oocytes all chromosomes congress to the animal pole, upon actin disruption, chromosomes first diffuse around their initial positions (fig.4.7.A). Due to the very large size of the nucleus, microtubule capture range covers only approximately one third of the nucleus area. Only those chromosomes, that happen to be initially located in in the microtubule capture range will be captured by microtubules and incorporated into the spindle. Meanwhile, distally located chromosomes remain in their original positions and are subsequently lost: not incorporated into the spindle until chromosome segregation is initiated, as there is no spindle assembly checkpoint active during meiosis (fig.4.7.C-D).

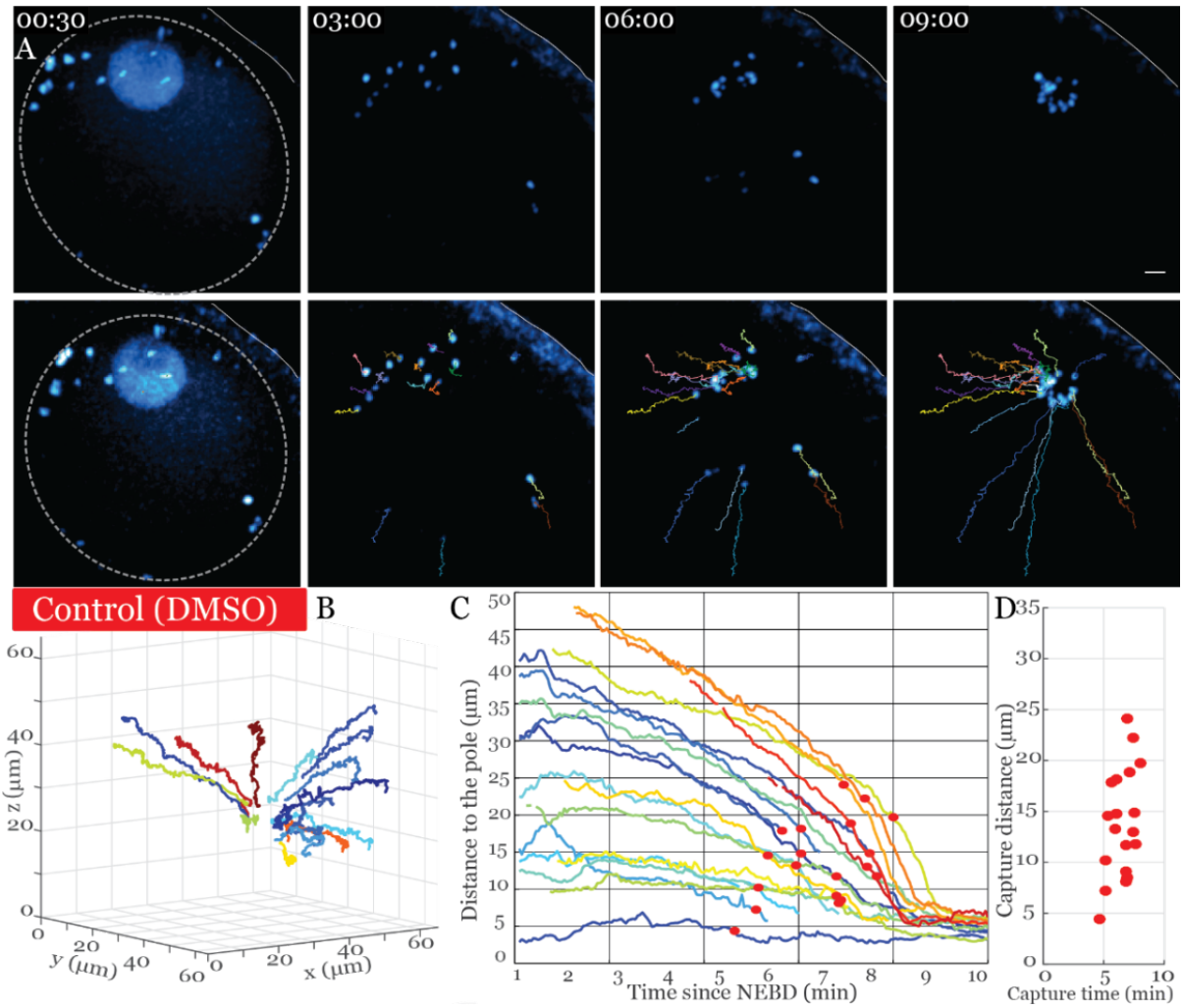

Figure 4.6. Chromosome capture kinetics in starfish oocyte. A. Selected frames from a time series of the nucleus. Oocytes are expressing H2B-mEGFP3 (cyan) labeling chromosomes. Time step 3 sec. Z-projection of 60 µm thick confocal slice. Z step 1.2.µm. Scale bar 10 µm. Derived chromosome trajectories overlaid with the images, plotted up to the current time. Time relative to NEBD. **B.** Chromosome trajectories plotted in 3D. One color represents one chromosome. **C.** Chromosome pole-ward velocity plot. Each capture event is plotted as a dot. Pole defined as an average position of all the chromosomes after the full congression. **D.** Chromosomes capture distance-time plot. Each dot represents a capture time and distance for an individual chromosome.

Normally, the number of chromosomes located within microtubule reach, which are, therefore, still captured upon actin disruption, is quite small (3 or 4 out of 22 chromosomes, approximately 18%). However, the number of chromosomes initially positioned within the microtubule capture range can be enriched by a simple 'gravity settlement' treatment. In 2013 Feric and Brangwynne demonstrated that in the *Xenopus* oocytes gravity becomes a substantial force (Feric and Brangwynne, 2013), causing aggregation of the multiple nucleoli in the oocyte nucleus. We observed a similar effect in starfish oocytes as well. Thereby, by letting the chromosomes undergo gravity settling in the nuclei of the oocytes, loaded into the chamber and prepared for the experiment (fig. 4.8), the total number of chromosomes located in the microtubule capture range and, therefore, captured upon actin disruption increased from 18% to 41% (8-10 chromosomes out of 22). Hereafter in the project, I will focus only on the

completed chromosome-microtubule capture events, and ignore the lost chromosomes in the analysis.

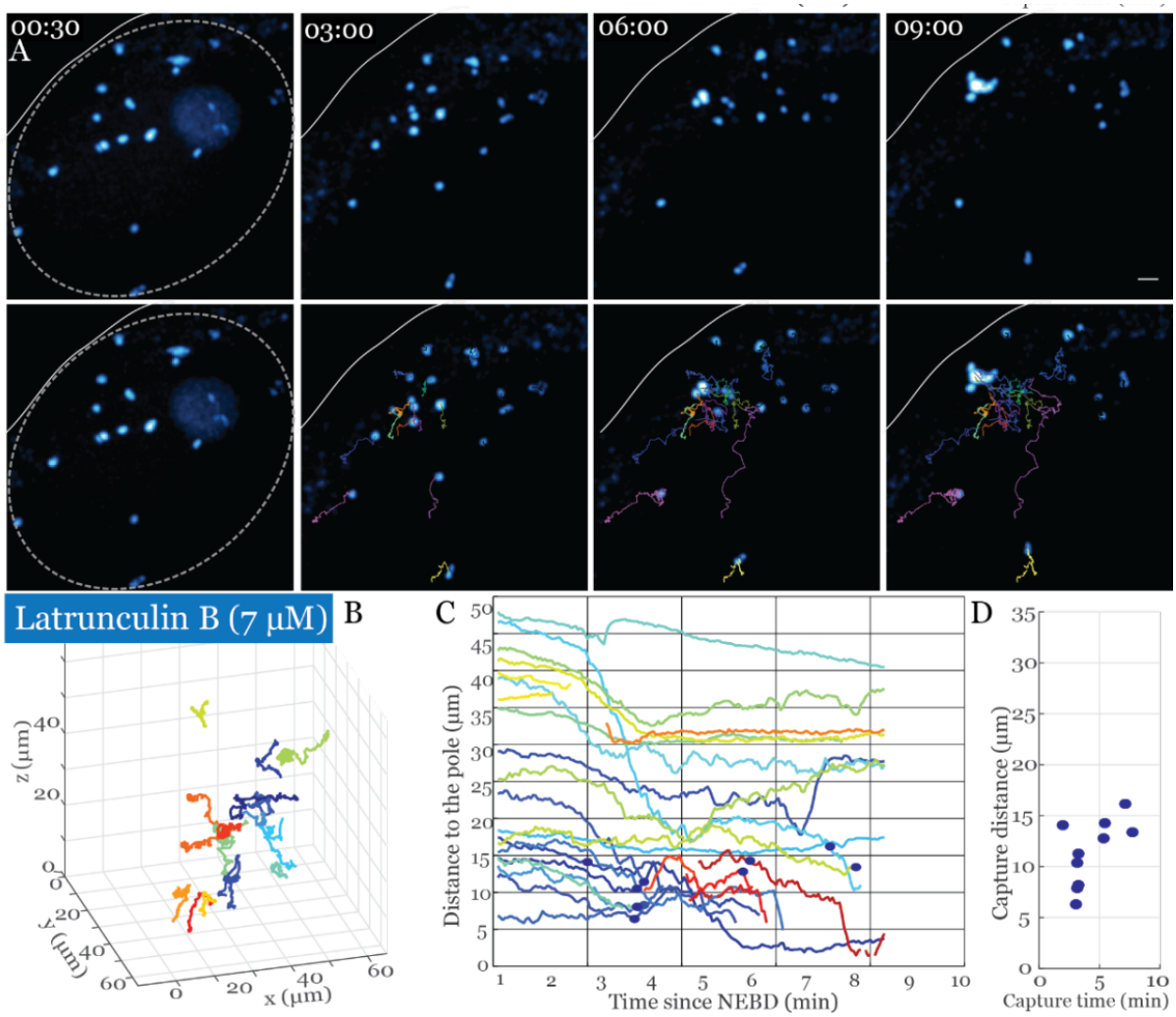

Figure 4.7. Chromosome capture kinetics upon actin disruption. A. Selected frames from a time series of the nucleus area of an oocyte treated 7 µM Latrunculin B. Oocytes are expressing H2B-mEGFP3 (cyan) labeling chromosomes. Time step 3 sec. Z-projection of 60 µm thick confocal slice. Z step 1.2.µm. Scale bar 10 µm. Derived chromosome trajectories overlaid with the images, plotted up to the current time. Time relative to NEBD. **B.** Chromosome trajectories plotted in 3D. One color represents one chromosome. **C.** Chromosome velocity plot. Each capture event is plotted as a dot. **D.** Chromosomes capture distance-time plot. Each dot represents a capture time and distance for an individual chromosome.

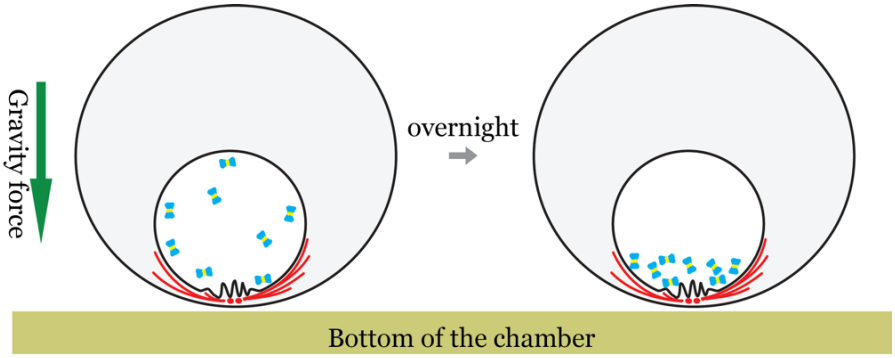

Figure 4.8. Scheme of chromosome gravity settlement in the oocyte. Oocytes were kept is the vertical position, as illustrated. Overnight chromosomes predominantly oriented in the bottom of the nucleus, thus, close to the microtubule asters. Only oocytes with the animal pole oriented down to the bottom of the chamber were injected with the mRNA of interest. On the next

day, confocal imaging was performed: chambers were positioned above the objective (top view on this scheme) and matured immediately.

In the presence of the functional actin meshwork, capture of all the chromosomes occurs in a short time-window (5 to 10 minutes after NEBD). As expected, actin meshwork facilitates the capture of more distantly-located chromosomes by bringing them into microtubule capture range. Notably, no chromosome captures were observed in the first five minutes after NEBD. Several chromosomes, initially positioned within the microtubule capture range, are captured simultaneously with those chromosomes, which were transported by the actin meshwork through the whole nuclear volume. Thus, capture of all the chromosomes occurs rather synchronously and is distance-independent (fig. 4.9.A). In contrast, without the actin-dependent chromosome transport, chromosome capture events are more spread in time. Thus, capture of the chromosomes located on the border of the microtubule capture range occurs later, than in the control. Notably, upon the drug-disruption of the actin meshwork, microtubule capture of the closely located chromosomes starts very early on, already at 2-3 minutes after NEBD, significantly earlier than in DMSO treated controls. Along with this, chromosomes located distantly from the microtubule asters are captured later or remain lost on the nucleoplasm. (fig. 4.9.B). Altogether, these observations clearly indicate that actin network synchronizes chromosome capture not only by transporting the far-located chromosomes, but through the delay in the capture of the chromosomes initially located within the microtubule capture range (fig. 4.9.C).

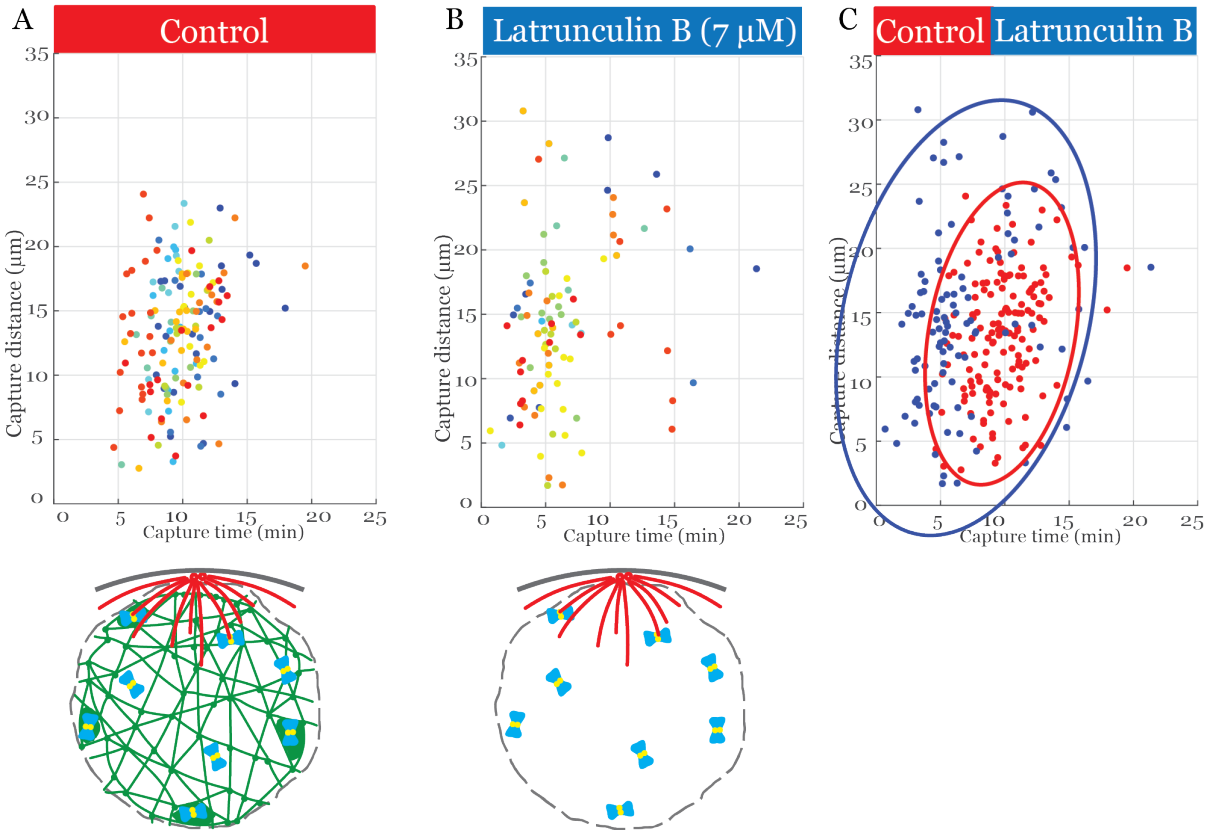

Figure 4.9. Actin synchronizes chromosome capture. Chromosome capture events were identified for 13 pairs of control (**A**) and Latrunculin B (**B**) treated oocytes correspondingly. Experiments were performed on the same day with the oocytes from the same starfish animal to

have the best possible comparison. All chromosome captures for each of the oocytes are plotted in a separate color. **C.** Data from the control oocytes (A) and Latrunculin B treated (B) oocytes plotted over together. Red and blue lines represent 95% confidence interval for control and drug-treatment data accordingly. Below is the scheme of the experiment: Latrunculin B depolymerizes all the actin structures in the oocyte.

From the observation of capture kinetics in several oocytes I conclude that contracting actin meshwork, while transporting the chromosomes across the nuclear volume simultaneously prevents microtubule capture of those chromosomes, located within the microtubule capture range early on right after NEBD. The initial chromosome position at the NEBD onset is disconnected of both the time and the distance of the microtubule capture event for this chromosome (fig 4.12). Thereby, microtubules capture occurs independently of the chromosome travel range within the actin meshwork.

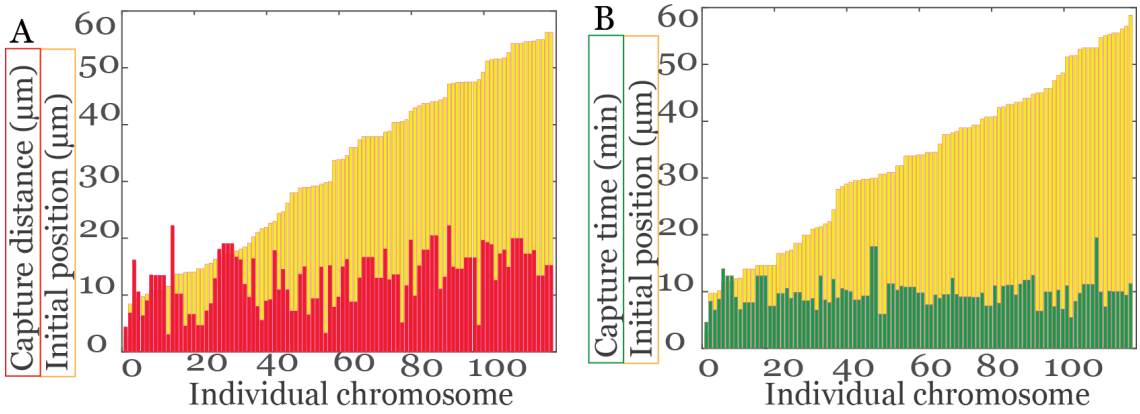

Figure 4.10. Chromosome capture time and capture distance are independent from the chromosome initial position. Data from the figure 4.11. Each yellow bar represents a distance between the center of the microtubule asters and chromosome position at the onset of NEBD. Red bars are the capture distance for the corresponding chromosome. Green bars are the capture time for corresponding chromosome (in minutes).

In conclusion, within the contractile actin meshwork chromosomes are delivered into microtubule capture range, which synchronizes the capture of the far-located chromosomes. Simultaneously, capture of the chromosomes initially located within the microtubule reach, is prevented and only occurs later, occurs simultaneously with the far-traveling chromosomes. Thus, *actin network synchronizes chromosome capture in addition to delivering distal chromosomes to the capture range, by delaying capture of the chromosomes* initially located in the microtubule capture range. Therefore, capture by microtubules is synchronous and distance independent.

The biological function of the actin meshwork to deliver chromosomes into the microtubule capture range is clearly understood (Lénárt et al., 2005). Here I demonstrated, that the meshwork synchronizes capture of chromosomes by additionally delaying the capture of the proximal chromosomes. The mechanism of this delay is not known, therefore in the following I investigated several hypotheses to explain the chromosome capture delay.

4.2.2. Microtubule dynamics is not affected by the actin meshwork

Actin meshwork, while transporting the chromosomes, could potentially prevent access of the microtubules to the kinetochores. Thereby, temporal delay in the capture of the closely-located chromosomes, described in the above chapter, could be caused by the altered microtubule behavior in the presence of the functional actin meshwork. Images of the fixed and immunostained oocytes did not reveal any exclusion of the microtubules from the area occupied by the actin meshwork (fig. 4.2), however, immunostaining does not provide any information on the temporal dynamics of this processes. Therefore, here I tested whether microtubule behavior is affected by the actin meshwork using live-imaging of the dynamic microtubule tips, on a single confocal slice with high spatio-temporal resolution.

Microtubule asters, labeled with EB3-mCherry3, were imaged from the NEBD onset until the full chromosome congression (approx. 15 minutes after NEBD). The distances between the centrosome and the growing microtubule tips was measured manually for several consecutive time points for several oocytes in control and Latrunculin B treated oocytes (fig. 4.11.A). At the NEBD onset microtubule asters start nucleating dynamic microtubules and reach their full-grown size at approximately 3 minutes. In the following microtubules asters maintain the same size, while capturing the chromosomes. No statistically significant difference in the microtubules asters behavior was detected in the oocytes with functional or depolymerized actin meshwork (fig.4.12). Microtubules seem to be able to grow unperturbed through the contracting actin meshwork and, consequently, to capture chromosomes within the microtubule capture range right after the NEBD onset.

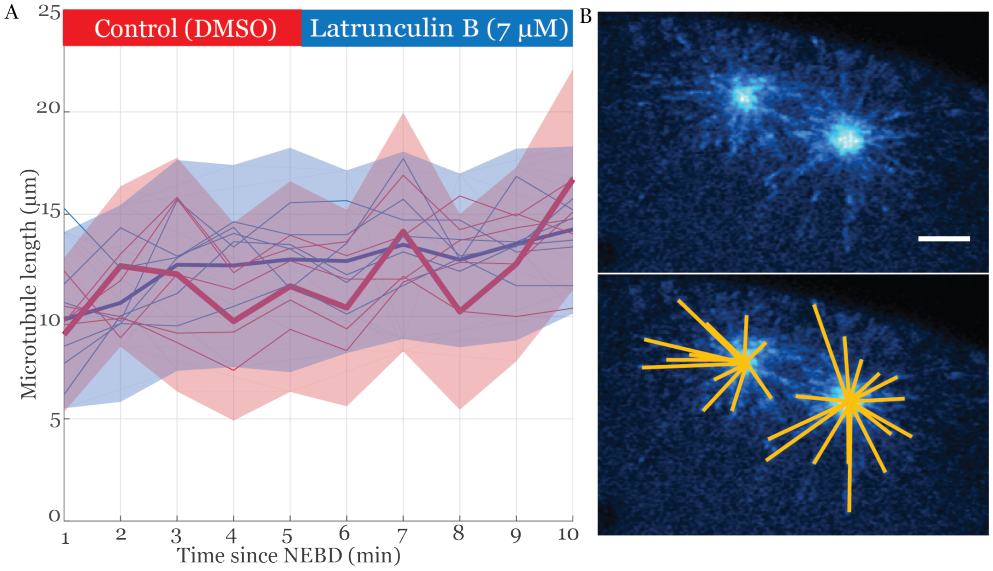

Figure 4.11. Microtubule behavior is not affected by actin meshwork. A. Histogram displaying microtubule length profile illustrating the aster growth, starting at 1 min after NEBD for 10 min. On the x-axis – time since NEBD; on the y-axis – mean value of microtubule length at given time for the control oocytes (red) and treated with Latrunculin B (blue). Thin lines – data from a single experiment. Thick lines – mean value for 6 oocytes in each group. Shaded red or blue represents standard error deviation for control and drug-treated oocytes, accordingly. **B.**

Microtubule tips labeled with EB3-3mCherry (cyan) were imaged every 2 seconds on a single confocal slice. Microtubule length was measured manually (orange lines) every minute starting from 1 minute after NEBD.

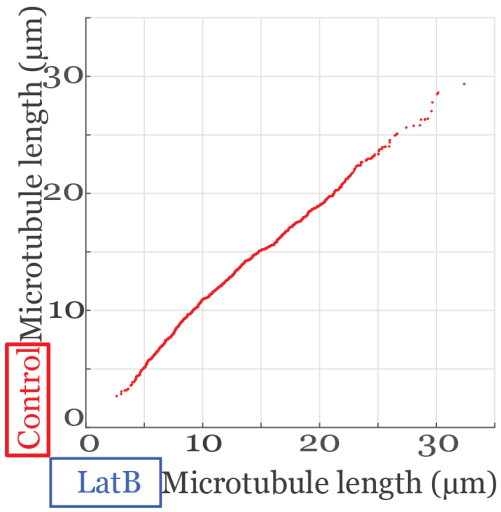

Figure 4.12. Comparison of the microtubule tips lengths with and without the functional actin meshwork. Comparison of all microtubule lengths in the control oocytes (y-axis) vs. Latrunculin B treated oocytes (x-axis).

To conclude, *microtubule dynamics as measured by the length of microtubules is not affected by the actin meshwork*, implying non-microtubule dependent mechanism preventing early chromosome capture events in the presence of actin meshwork described above. This hypothesis is further supported by the fact, that chromosome capture occurs wile actin meshwork is still contracting.

4.2.3. Chromatin is not directly interacting with the actin meshwork

Chromosome capture kinetics by microtubules, described by the chromosome tracking assay, revealed a delay in the chromosome captures of those chromosomes, initially positioned within the microtubule capture range. However, based on the chromosome tracking assay it is not possible to distinguish, whether this delay effect is caused by a deficiency in establishing an attachment or block of transport by microtubules.

Knowing that microtubule length is not affected by the contractile actin meshwork (fig.4.12), the delay could be caused by the hindered chromosome transport through the actin meshwork at the early prometaphase. According to this hypothesis, kinetochore-microtubule attachments are formed in time, however, chromosomes fail to be transported through the actin meshwork due to the interaction between the chromosomes and filaments of the actin meshwork.

The interaction of the chromosomes with the actin meshwork remained poorly characterized. The physical nature of the chromosome transport by the actin meshwork was tested by injecting fluorescent beads into the nucleus before NEBD. These experiments showed that inert beads of a size comparable to chromosomes (2 µm) are entrapped into the actin meshwork, and congressed with dynamics similar to chromosomes. Meanwhile, beads of a smaller diameter (0.5 µm) are sieved through

the pores of the actin meshwork and freely diffuse in the cytoplasm (Mori et al., 2011). This observation suggests that steric entrapment is sufficient for the chromosome transport, but does not exclude that direct interactions also exist.

Here I specifically tested this hypothesis on the interaction between the chromosomes and actin meshwork. Oocytes were incubated with Zeocin, a drug inducing DNA double-strand breaks, thereby, causing the formation of smaller chromatin fragments from the chromosomes. Thus, if chromatin is directly or indirectly attached to the filaments of the actin meshwork, those small chromosome fragments will be congressed by the actin meshwork as well as full-sized chromosomes. However, if the interaction with the actin meshwork is only steric, these small DNA fragments will behave similarly to the small inert beads described above: will be sieved through the pores of the actin meshwork and diffuse in the nucleoplasm.

Treatment with Zeocin induced the formation of chromatin fragments down to 0.5 µm in size. During chromosome congression, these fragments are sieved through the pores of the contracting actin meshwork and freely diffused in the nucleoplasm (fig.4.13). Meanwhile, chromatin fragments of larger size and full-sized chromosomes are transported by the actin meshwork normally and incorporated into the spindle. These fragments must have had kinetochores. Whether the lost fragments contained kinetochores remains unknown. Altogether, the obtained results suggest that *chromatin per se is not interacting with the actin meshwork filaments*. However, based on only these observations I cannot exclude the possibility that the interaction with the actin meshwork is mediated specifically through the kinetochores. Unfortunately, in this assay, co-labeling and imaging kinetochores was not performed due to the imaging limitations.

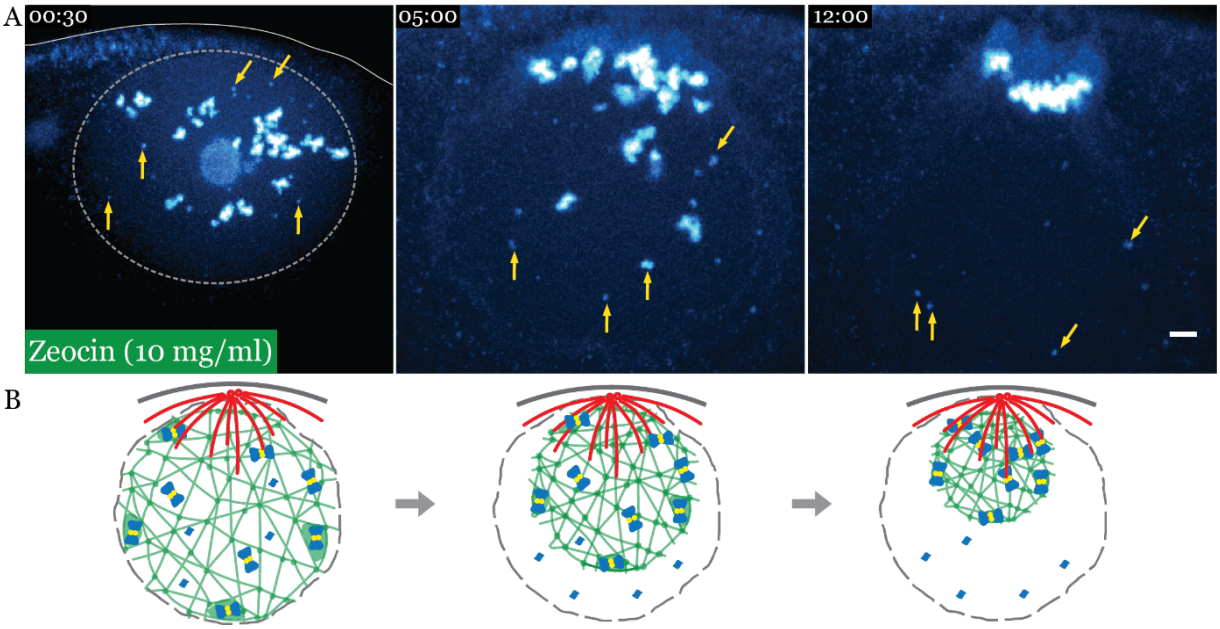

Figure 4.13. Chromatin is not directly interacting with the actin meshwork. A. Selected frames from a time series of a nucleus area of an oocyte treated with Zeocin for 3.5 hours. Oocytes are expressing H2B-mEGFP3 (cyan) labeling chromatin. Time step 30 sec. Z-projection of 60 µm

thick confocal slice. Z step 5 μm. Scale bar 10 μm. Yellow arrows mark chromatin fragments. Images 2 and 3 are enlarged from image 1. **B.** Schematic representation of the experiment: drug-induced chromatin fragments are sieved through the contracting chromosome meshwork and lost in the nucleoplasm.

4.2.4. Chromosomes can be captured and transported through the stabilized actin meshwork

Chromatin is not directly interacting with the filaments of the actin meshwork, since the small chromatin fragments were observed being sieved through the actin meshwork. Assuming that chromosomes and kinetochores are not attached to the meshwork, their transport along the microtubules could be hindered simply by the steric entrapment of the chromosomes in the actin meshwork, thereby, causing the delay in the chromosome capture onset, as observed on fig. 4.9. According to this hypothesis, kinetochore-microtubule attachments are established normally, however, microtubule transport in restrained due to the strong steric entrapment of the chromosomes in the contracting actin meshwork. Therefore, I aimed to stabilize the actin meshwork completely to the extent that its contraction is fully inhibited. Here, I tested whether microtubules are capable to transport the captured chromosomes through the completely stabilized actin meshwork.

Actin meshwork was artificially stabilized by microinjecting Phalloidin-A568 into the oocytes to the extent, that the meshwork was completely stabilized and almost no contraction was observed, as confirmed by the chromosome trajectories (fig.4.14). As described previously in chapter 4.2.1, oocytes were let overnight to gravity-settle in order to enrich for the number of chromosomes in the microtubule capture range. Capture events of the chromosomes, located within the microtubule reach area, occurred in the timing, similar to the control oocytes. Capture and transport of these proximally located chromosomes caused partial collapse of the stabilized actin meshwork, thereby shortening the distance between the microtubule asters and the distally located chromosomes. Thereby, in the given example, all the chromosomes were captured by the astral microtubules. Here individual chromosome captures occurred in the distance-dependent manner, however, in this experiment, this effect is caused rather by gradual entry of the chromosomes into the microtubule capture range due to the collapse of the frozen actin meshwork.

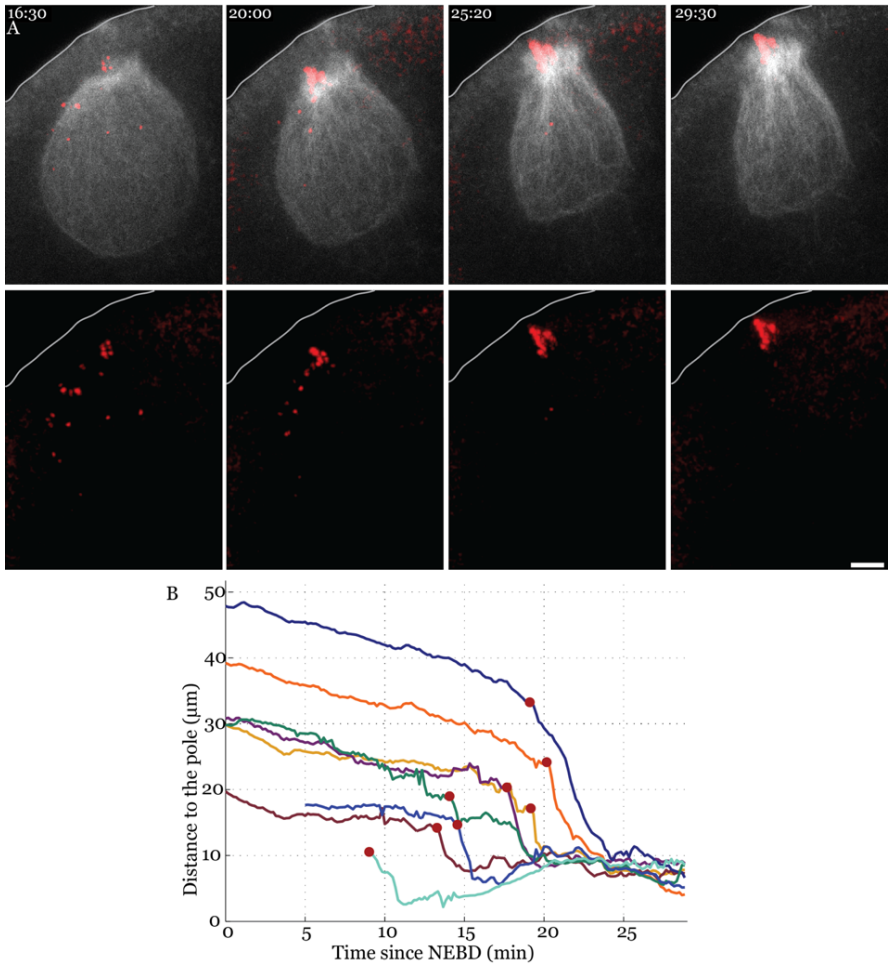

Figure 4.14. Chromosomes can be congressed through the completely stabilized actin meshwork. A. Selected frames from time series of the nucleus area of an oocyte injected with 30 units of Phalloidin-A568 after NEBD next to the nucleus area. Actin meshwork is stabilized and not contracting. Oocytes are expressing H2B-mEGFP3 (cyan) labeling chromosomes. F-actin labeled with Phalloidin-A568. Time step 10 sec. Z-projection of 60 µm thick confocal slice. Z step 2.3 µm. Scale bar 10 µm. Time relative to NEBD. **B.** Chromosome pole-ward velocity plot. Each chromosome capture event is plotted as a dot. Number of oocytes in the experiment: 7.

In summary, chromosome capture and transport along the microtubules can occur though the fully stabilized actin meshwork. This observation suggests that microtubule pulling force can overcome the steric entrapment of the chromosomes in the actin meshwork, as well as any direct or indirect interactions of the actin meshwork with the chromosomes and kinetochores. Thus, *entrapment of the chromosomes cannot explain the delay and prevention of the chromosome capture by microtubules*.

4.2.5. Actin meshwork contraction speed does not affect chromosome capture kinetics

The delay in the chromosome capture onset of the proximal chromosomes is actin-dependent and may be caused by the actin meshwork contraction rate. An important prediction of this hypothesis is that chromosome capture should be coordinated with the meshwork disassembly. According to this hypothesis, slower contraction rate would further delay the onset of the first capture events. In order to resolve this

mechanism, actin meshwork contraction rate was decreased through the F-actin stabilization with the Utrophin-CH domain protein.

Actin meshwork contraction speed can be altered through the artificial F-actin stabilization. Since the main contraction-driving force in the actin meshwork is linked to F-actin depolymerization (Philippe Bun, Lénárt lab, manuscript in preparation), injection of the actin stabilization factors such as Utrophin-CH protein domain decreases depolymerization rate, thereby a gradual response in the actin meshwork contraction speed can be achieved. A parameter, describing the speed of contraction, was developed in the Lénárt lab previously (described in Mori et al., 2011). *Chromosome approach rate* and can be calculated from the known chromosome trajectories. Since actin meshwork contraction is intrinsically homogenous, the speed for every chromosome during actin-driven motion in constant and proportional to the initial distance for each chromosome. Thereby, although every chromosome is travelling with a different speed, their pair-wise velocities are linearly dependent to each other and to the animal pole. The slope of pair-wise chromosome velocities is a function of their initial separation distance corresponds to the chromosome approach rate and, thereby, to the contraction rate of the actin meshwork (Mori et al., 2011). With the known approach rate, one can calculate the moment when all chromosomes are congressed into one point. *Full congression time* is reversed value of the chromosome approach rate. This parameter is useful when comparing the contraction speed under different conditions (Philippe Bun, Lénárt lab, manuscript in preparation).

Injection of the Utrophin-CH protein domain into the oocytes decreased actin meshwork contraction speed almost two – fold, compared to the control (fig. 4.15.C and 4.16.D). The full congression time was extended from 19 minutes in the control oocyte to 31 minute upon actin meshwork stabilization with Utrophin-CH. Upon this treatment chromosomes were entering the microtubule capture range with a significant time delay (fig 4.15.A-B).

Upon actin meshwork contraction rate decrease, chromosome capture events were detected much longer, up to 30 minutes after the NEBD onset, while in the control all the chromosomes are captured up to 13 minutes after NEBD. Furthermore, several chromosomes were lost in the nucleoplasm unable to reach the microtubule capture range. When actin meshwork contraction speed is decreased, chromosome capture events last longer, since chromosomes enter chromosome capture range slower. These 'delayed' chromosomes are captured as soon as they enter the microtubule capture range. However, the first chromosome – microtubule capture events occur almost simultaneously both in the control oocytes and upon actin meshwork stabilization with the Utrophin-CH protein. Importantly, the start of the chromosome capture events in

the oocytes with the slower actin meshwork contraction rate is not significantly delayed, compared to the control oocytes (fig.4.16).

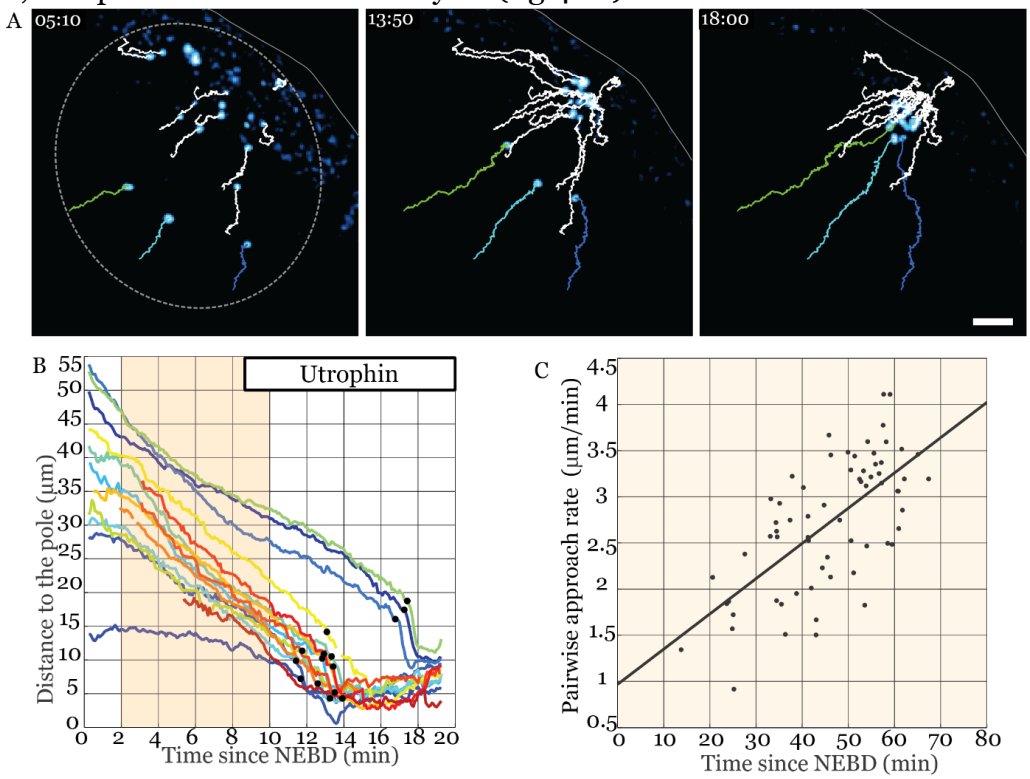

Figure 4.15. Decreasing actin meshwork contraction rate through the F-actin stabilization. A. Selected frames from a time series of a nucleus area of an oocyte injected with 40 units of Utrophin-CH domain protein 20 minutes before NEBD. Oocytes express H2B-mEGFP3 (cyan), labeling chromosomes. Time step 5 sec. Z-projection of 60 µm thick confocal slice. Z step 2.2 µm. Scale bar 10 µm. Derived chromosome trajectories overlaid with the images, plotted up to the current time. Time relative to NEBD. **B.** Chromosome pole-ward velocity plot. Pole defined as an average position of all the chromosomes after the full congression. Capture events represented as black dots on each chromosome track. **C.** Chromosome pair-wise velocity plot, calculated for minutes 2-10 after NEBD (shown in yellow in B and C).

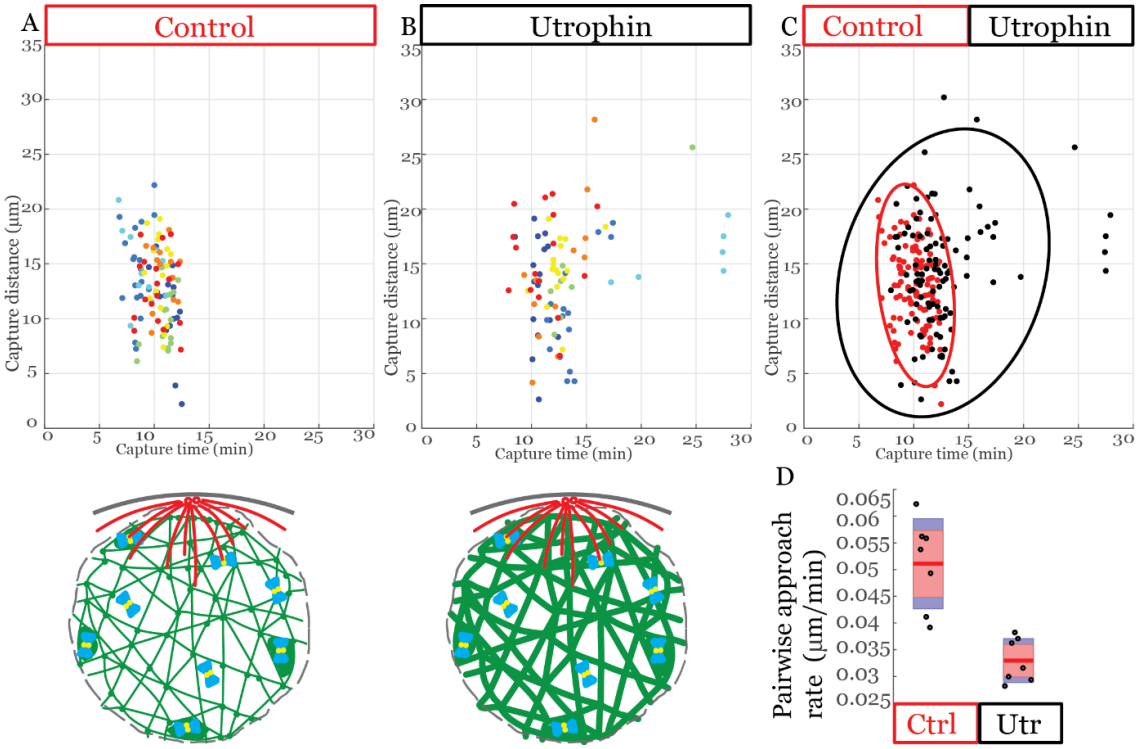

Figure 4.16. Chromosome capture through the stabilized actin meshwork. Chromosome capture events were identified for 7 control oocytes (**A**) and 7 injected with the Utrophin-CH protein (**B**). All chromosome captures for each of the oocytes are plotted in a separate color. **C.** Data from the control oocytes (**A**) and injected with Utrophin-CH protein (**B**), plotted over together. Red and black lines represent 95% confidence interval for control and experimental data, accordingly. Below is the scheme of the experiment: Latrunculin B depolymerizes all the actin structures in the oocyte. **D.** Chromosome approach rate (min^{-1}) of the control and Utrophin-CH injected oocytes comparison in the box-plot.

In conclusion, actin meshwork synchronizes chromosome capture by transporting distal chromosomes and delaying the capture of the proximal chromosomes. *Slowing down the meshwork contraction* desynchronizes capture by delaying transport and capture of the distal chromosomes, but *does not affect the capture kinetics* of the chromosomes, initially positioned within the microtubule capture range. Altogether, this suggests that actin meshwork contraction cannot alone explain the delay in the capture.

4.3. Computational model of the two-staged chromosome congression

4.3.1. Establishment of a mathematical model of chromosome congression and capture

To explore how actin meshwork synchronizes kinetochore-microtubule capture, I performed computer simulations to model the chromosome capture events in the live oocyte. Specifically, I aimed to precisely recapitulate the process of two-staged chromosome congression and chromosome capture kinetics in the control oocytes and upon actin meshwork disruption. Thereby, I wanted to validate the hypothesis whether initial chromosome capture events are delayed due to a failure to form kinetochore-microtubule attachments.

Simulations were performed in *Cytosim (Cytoskeletal simulator)*, in collaboration with François Nédélec, who lead the development of this modelling software at EMBL. Because many elements of the cytoskeleton are already included in *Cytosim*, I was able to model the two staged-chromosome congression process in 3D in realistic 3D geometry of starfish oocyte from the NEBD until chromosome congression is completed. The model included thousands of molecules and fibers. Most of the parameters were taken from my experimental observations, described in the preceding chapters, other microtubule dynamics parameters were taken from literature (Magidson et al., 2015).

Chromosome congression process during the early prophase was modelled in 3D. The system consisted of a sphere 70 μm in diameter, which corresponds to the oocyte nucleus. Microtubules were nucleated from the two centrosomes 4 μm in diameter, located in the fixed positions 3 μm inwards from the nuclear boundary (fig. 4.17). Each simulation started at NEBD with all microtubules being 3 μm long, starting to stochastically grow and shrink according to the standard dynamic instability model (Mitchison and Kirschner, 1884). Chromosomes, randomly positioned in the nucleus, were transported by the actin meshwork toward the animal pole. Once a chromosome gets captured, it was transported along the microtubule by dynein motor. Overall, chromosome trajectories precisely followed a two-staged chromosome congression, as in the experimental data.

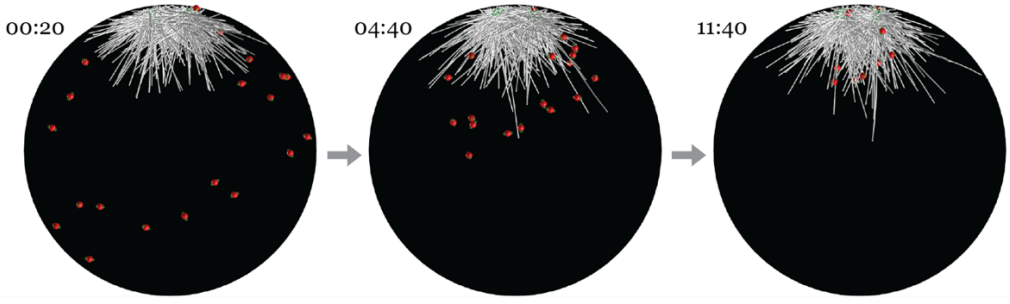

Figure 4.17. Simulation of the two-staged chromosome congression process in starfish oocyte. The nuclear sphere has a diameter of 70 μm. Chromosomes (red) with two kinetochores each (green) are transported with the contractile actin meshwork (modelled as an ad-

hoc force, of appropriate direction and magnitude to yield the measured speed). Upon kinetochore-microtubule capture, chromosomes are transported by dynein to the centrosomes.

Chromosomes were modeled as spheres 1.6 μm in diameter, with two kinetochores each, placed on the opposite sides of the chromosome. Kinetochores were represented as solid spheres 0.3 μm in diameter, according to the experimental images (fig. 4.18). Chromosomes were positioned within the nuclear volume randomly and in random orientation. A lateral kinetochore-microtubule attachment was established immediately once a microtubule tip or its wall reached a kinetochore. Dynein transported this chromosome to the microtubule minus-end. The speed of the dynein transport in the simulation was 1 μm/sec, which corresponds to experimental measurements of the chromosome transport (fig. 4.1, 4.3), as well as those published earlier (Rieder and Alexander, 1990).

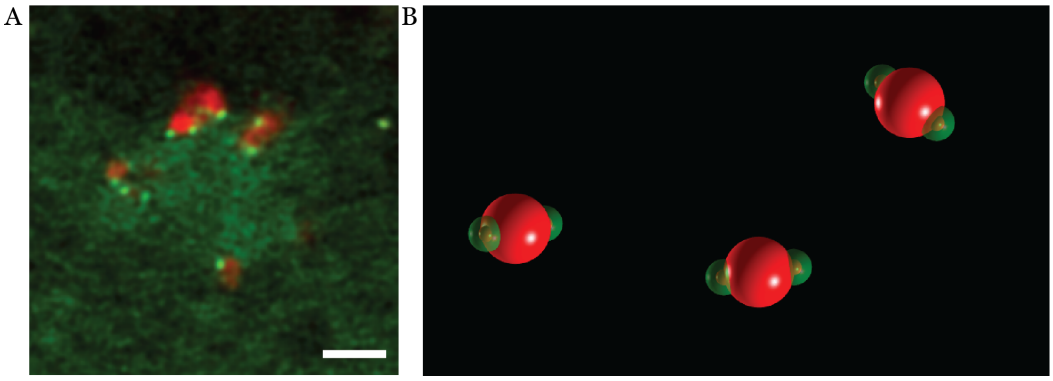

Figure 4.18. Chromosomes and kinetochores morphology in the experiment versus simulation. A. Selected frames from a time series of a spindle area during prometaphase. Oocytes express H2B-mEGFP3 (green), labeling chromosomes. Kinetochores are labeled by injecting 30 units of Ndc80-GFP protein (red). Single confocal slice, deconvolved. Scale bar: 5 μm. **B.** Simulation**.** Chromosomes are 1.6 μm spheres (red) each with two 0.3 μm large kinetochores (green) located on the opposite sites of the chromosome.

Microtubules in the simulation were represented as infinitely thin rods, growing and shrinking with a certain speed (all modelling parameters are listed in table 4.1.). Microtubules followed dynamic instability, with a catastrophe rate that increased linearly with microtubule length. No catastrophe rescue of the microtubules was permitted in the simulation. The rotational motion of microtubules was neglected in these simulations in order to decrease computational time, since experimental and modelling data suggests that microtubule pivoting is an essential factor only in small cells like yeast with the nucleus diameter of 3 μm (Cojoc et al., 2016). To verify this assumption, microtubule rotational motions were enabled in certain simulations, but extensively tests showed that this did not affect the results of the simulations. In addition, branched microtubule nucleation was neglected in the model as well. In the simulation, microtubules reaching the cell cortex undergo catastrophe event immediately, and no sliding occurs therefore.

Parameter	Value
Simulation time step	0.05 sec
Viscosity	0.1
Diameter of the nucleus	70 μm
Number of chromosomes	22
Chromosome size	1.6 μm
Diameter of a kinetochore	0.3 μm
Number of dynamic MTs from each centrosome	500
MT segments length	0.25 μm
MT growing speed	0.5 μm/min
MT shrinking speed	-1 μm/min
MT catastrophe rate	0.15
MT rescue rate	0
Dynein motor speed	-1 μm/min

Table 4.1. List of parameters used in the computational model.

Each of the centrosomes contained 500 nucleation sites, creating at most 500 microtubules. This number corresponds to the experimental measurements (see chapter 4.2.2). Briefly, the total number and length of astral microtubules, imaged in a single confocal plane, was calculated as a distance from the end of a microtubule tip to the center of the corresponding aster for several time-points. Next, this data was extrapolated to the 3D volume of the nucleus, assuming equal number of growing and shrinking microtubules co-existing during the dynamic steady-state of astral microtubules. Since EB3 protein labels only growing microtubule tips, the total number of microtubules was doubled, yielding a number of 500 microtubules nucleated by each aster. This number came in a good agreement with the other computational models (Paul et al., 2013; Magidson et al., 2015).

Next, the size of the fully - grown asters, thus, the microtubule length, was fitted to the experimental data. Specifically, a set of microtubule dynamic parameters was tested in the simulations, and the resulting microtubule length profile was compared to the experimental profile, where microtubule length varied between 4 and 34 μm. Due to the resolution limitations, the tips of the shortest microtubules (below 4 μm) were all blurred into a halo-like image at the aster center (fig. 4.11), suggesting that the total number of these short microtubules is very large and decreases with the microtubules getting longer. Therefore, I assumed that microtubule lengths could be described as an exponential function. Extensive screening of microtubule dynamic parameters, such as catastrophe rate as a function of microtubule length vs maximal length, gave a good fit and was used in the following simulations (fig. 4.19).

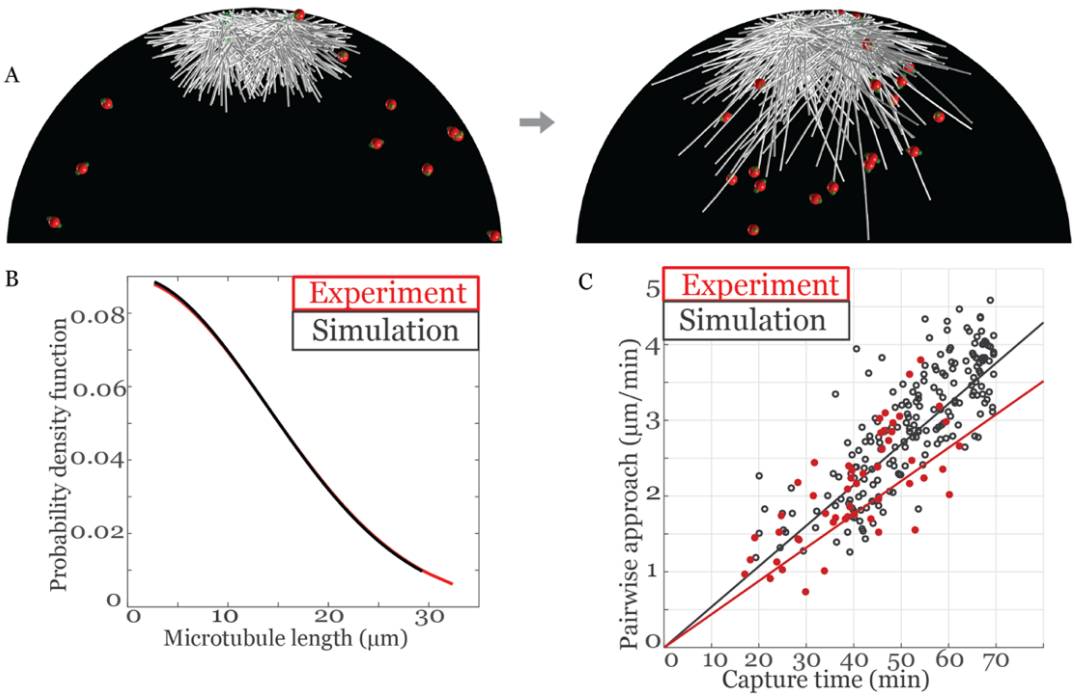

Figure 4.19. Comparison of the microtubule lengths in simulation and experimental data. A. Scheme illustrating microtubule asters growth in the first 3 minutes after NEBD. **B.** Microtubule lengths distribution of a full-size microtubule aster in the control oocytes (red) and simulation (black) fitted with the half-normal distribution function. Microtubules length was compared at time 3 to 10 min after NEBD, when aster reach the fully - grown size. **C.** Chromosome pair-wise velocity analysis. Comparison between experimental data (red) and simulation (black).

The contracting actin meshwork was not explicitly modelled, but a physical force was applied on the chromosomes, which transports them as observed *in vivo* into microtubule capture range (i.e. without explicitly modelling actin filaments). Actin meshwork contraction speed was calculated from the chromosome tracks, as described previously (chapter 4.2.5 and Mori et al., 2011). Briefly, every chromosome travels with a different, but constant speed, proportional to the distance between the chromosome and the asters at NEBD. Contraction is homogenous and the speed for each chromosome differs and yet is constant over time. As a consequence, all the chromosomes meet at the pole at the same time point, while velocities for each chromosome are linearly proportional to the distance to the pole. In control oocytes the average *chromosome approach time* is 0.067 min^{-1} (Mori et al., 2011). Chromosome *full congression time,* the moment when all chromosomes are congressed into one point, is obtained by inverting the chromosome approach rate. Thus, for the measured approach rate value of 0.067 min^{-1} full congression time is 14.92 min. In the simulation, full congression time was set to 15 minutes, while the actual time at which the contraction force was applied on the chromosomes was 12.5 minutes, which corresponds to all the chromosomes being congressed to a sphere of diameter 13.5 µm: given no microtubule capture, chromosomes occupy similar area at the animal pole. Pairwise velocity plot for every chromosome pair in the simulation were fitted with a line, as represented on fig 4.19.C.

4.3.2. Modelling predicts delay in chromosome capture caused by blocking the kinetochores

The two-staged process of chromosome congression in starfish oocyte was reconstructed *in silico*. The modelling precisely matches the experimental observations, described in chapters 4.1 and 4.2, for the control oocytes and oocytes, whereby actin meshwork is disrupted (fig. 4.20.A). Thus, in the simulation, chromosome poleward velocities display the two phases of the chromosome transport: a slower phase where the chromosomes are jittery within the actin meshwork and, then, rapid transport along the microtubules. All 22 chromosomes are captured by microtubules with the capture kinetics, similar to the experimental observations.

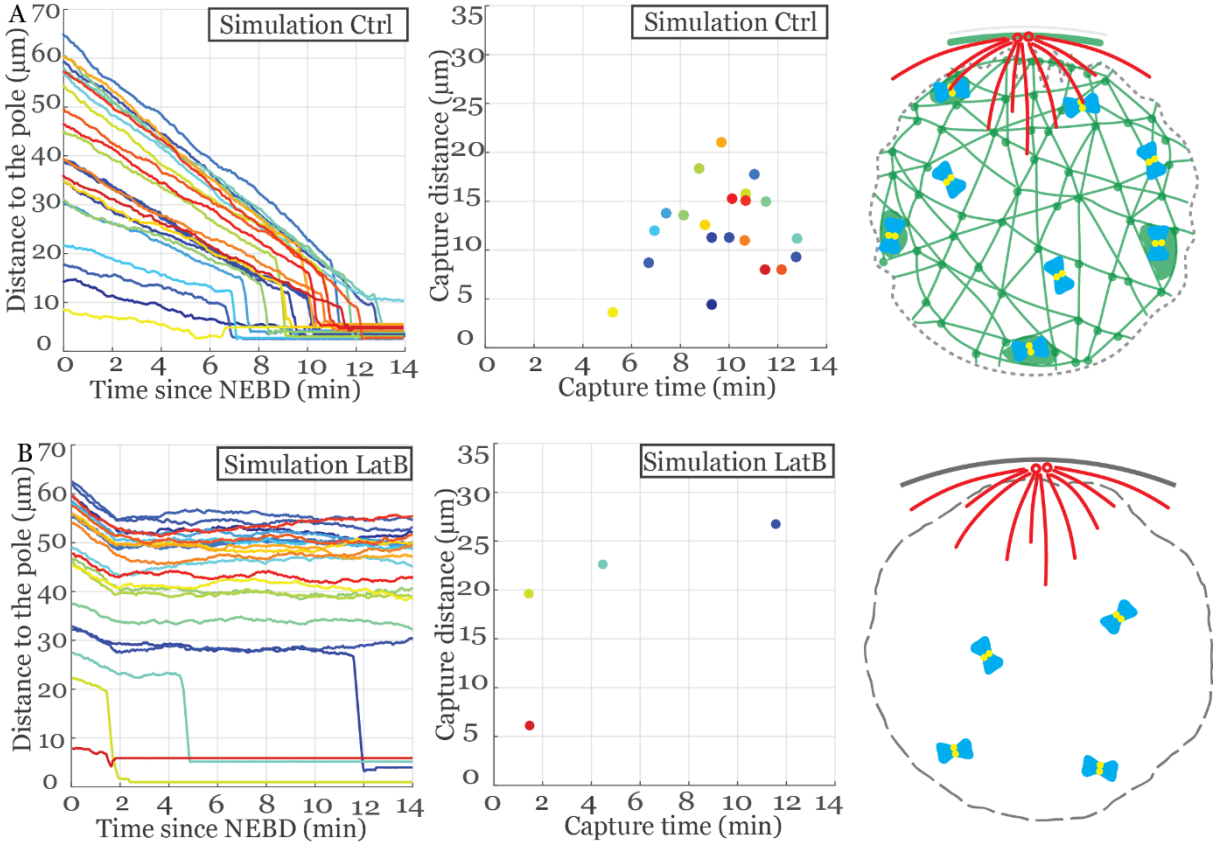

Figure 4.20. Modelling of the two-staged chromosome congression process. A. Chromosomes poleward velocity plot in the 'Control' scenario simulation. **B.** Chromosomes poleward velocity plot in the 'Actin disruption' scenario simulation. All simulations were performed starting at NEBD for 25 minute. Details on the simulation described in the main text. To the right, chromosome capture kinetics plot and scheme of the experiment.

In the simulations, recapitulating actin disruption experiments, chromosomes were simply diffusing in the cytoplasm (fig. 4.20.B). However, in these experiments, chromosomes, as well as all components of the nucleus, are congressed during the first minute due to the strong inward cytoplasmic flows occurring as the nuclear envelope disassembles. This short initial flow was also modelled in the simulations (fig. 4.20.B). One minute after NEBD, chromosomes are freely diffusing in the nucleoplasm. Only few chromosomes are captured by microtubules (3-4 out of 22). This number precisely

matches the experimental data, where the oocytes and the chromosomes contained in them do not undergo gravity-settlement (fig.4.8). Some chromosome capture events occur quite late in simulations and in the experiments (nearly 25 minutes after NEBD). Importantly, in the simulation and upon actual actin disruption the first chromosome capture events occur very soon after NEBD onset. When in the simulation actin meshwork brings chromosomes into the microtubule capture range (fig.4.21.B), those chromosomes initially positioned in the microtubule capture range, are being captured right after NEBD and more of them occur as soon as chromosomes enter the microtubule capture range. Only if the kinetochores are blocked from establishing the attachments to the microtubules in the first five minutes after NEBD, computer simulation precisely matches the chromosome capture kinetics of the control untreated oocyte (fig.4.21.C).

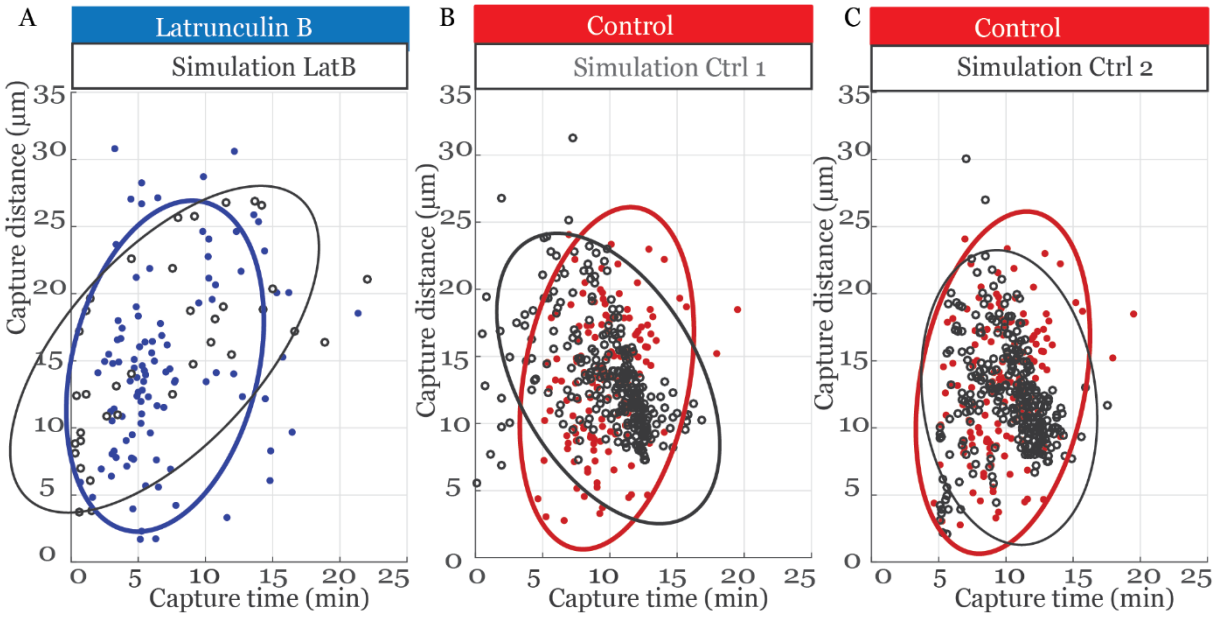

Figure 4.21. Modelling predicts, blocked kinetochores cause a delay of the chromosome capture in the control oocytes. A. Comparison of the chromosome capture kinetics of the oocytes, treated with Latrunculin B (blue) and simulation of the 'actin disruption' (gray). Ellipse draws 85% confidence interval. **B**. Comparison of the chromosome capture kinetics of the control oocytes (treated with DMSO, red) and modelled 'Control 1' scenario (gray). Ellipses indicate the 95% confidence interval. **C**. Comparison of the chromosome capture kinetics of the control oocytes (treated with DMSO, red) and simulation carried out with kinetochores blocked from the microtubules in the first 5 minutes after NEBD 'Control 2' (gray). Ellipses indicate the 95% confidence interval. Number of oocytes in each group (either simulation or experimental) = 13. Experimental data taken from figure 4.9.

In conclusion, computer modelling confirmed the hypothesis that the delay in the chromosome capture of the chromosomes within the microtubule reach can be due to the *failure to establish kinetochore – microtubule attachments* early on. Upon actin disruption chromosome capture events occur right after NEBD, suggesting an actin-dependent mechanism that prevents chromosome capture.

Summary of the results

Chromosome congression in starfish oocytes is a two-staged process. First, to collect all chromosomes in the large oocyte nucleus, a contractile actin meshwork forms in the nuclear region and transports embedded chromosomes into the microtubule capture range. Once in range, chromosomes are captured by astral microtubules by establishing lateral kinetochore-microtubule attachments and transported by dynein to the center of the asters. Interestingly, I find that chromosome capture occurs simultaneously, whereby capture of chromosomes initially located within the microtubule capture range is delayed until distal chromosomes travel through the nuclear area. I show that this delay is actin-dependent, as depolymerization of actin results in early capture of proximal chromosomes (graphical summary on fig. 4.22).

I show that microtubules grow unconstrained into the actin meshwork, and that microtubule dynamics is not affected by actin meshwork disruption, thus the delay in chromosome capture is not caused by exclusion of microtubules from the actin meshwork. Gradually slowing down the contraction speed of the meshwork has no effect on the onset of the first chromosome capture events, and chromosomes are still captured by microtubules even in a fully stabilized actin meshwork, indicating that the delay in capture is not due to the physical entrapment of chromosomes by the actin meshwork. Altogether, my results point to an actin-dependent mechanism, which prevents formation of the lateral kinetochore-microtubule attachments in the first five minutes after NEBD, thereby synchronizing chromosome capture. I validated this hypothesis by computational modelling that precisely recapitulated chromosome capture kinetics observed experimentally.

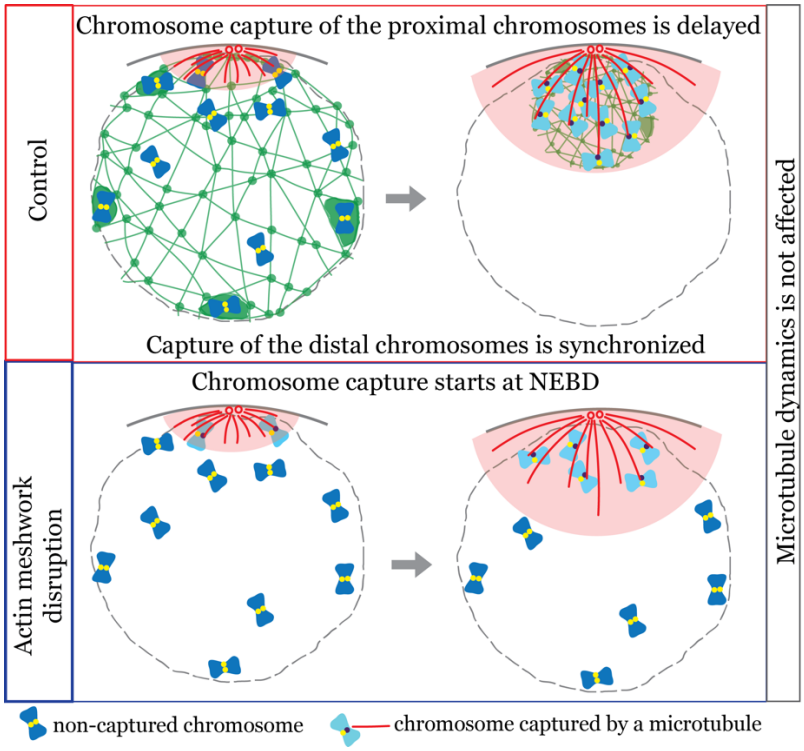

Figure 22. Graphical summary of the results.

5. Discussion

5.1. A coordinated action of actin and microtubules is required to prevent aneuploidy during chromosome congression in starfish oocytes

Aneuploidy, gain or loss of chromosomes during cell division, is the major cause of infertility and unviable or defective progeny. In somatic cells unbalanced number of chromosomes is thought to be one of the major triggers for cancerous transformation of the cells. Therefore, faithful capture, correct alignment and segregation of chromosomes are crucial steps during division of germ line, as well as somatic cells.

The initially proposed model of 'search and capture' by dynamic astral microtubules is still valid to explain chromosome capture, and has been extended by recent studies revealing additional mechanisms that facilitate capture by biased microtubule nucleation and stabilization in the proximity of chromatin and kinetochores. These mechanisms act together to ensure rapid and efficient capture of chromosomes in somatic cells.

In contrast, in large specialized cells like oocytes, chromosomes are often located much further from the microtubule asters. How chromosome capture occurs in these large cells remains poorly understood, as computational models predict 'search and capture' to fail over such extended distances. In starfish oocytes a contractile actin meshwork transports chromosomes to the microtubule asters, thereby, greatly facilitating the chromosome search and capture process. The details of how this actin-driven mechanism of chromosome transport is coordinated by capture by microtubules were not understood, but suggested an intricate interplay between actin meshwork and astral microtubules.

Here I present evidence that the actin meshwork while transporting chromosomes additionally synchronizes chromosome capture. While spatial microtubule search is very efficient, the kinetics of the chromosome capture is precisely coordinated by actin-driven transport by the means of preventing chromosome capture for the first five minutes after the NEBD onset. I show that an actin-dependent mechanism synchronizes chromosome capture by delaying the early chromosome capture events of the proximally located chromosomes, meanwhile the actin meshwork transports distal chromosomes into the microtubule capture range. To my knowledge, this is the first description of a mechanism for regulating and synchronizing microtubule 'search and capture' and the first indication for a regulatory role of actin in this process. While the detailed molecular mechanisms of how F-actin prevents chromosome capture remain to be explored, I will discuss here possible hypotheses and propose experiments for testing these.

As detailed in the *Results*, I have already excluded a number of hypotheses: chromosome capture by microtubules occurs while actin meshwork is contracting, but microtubule dynamics is not affected by the actin meshwork. Thus, microtubules are able to grow and reach the chromosomes though the contacting meshwork and they are not 'waiting' for chromosomes to enter the microtubule capture range to start capturing them.

Second, slowing down the contraction speed of the actin meshwork causes late entry of the distally located chromosomes into the microtubule capture range and their later capture by microtubules. However, this does not affect the onset of the first capture events for the proximal chromosomes. This indicates that the rate of the actin meshwork contraction is not causing the initial chromosome capture delay. Further, complete stabilization of the actin meshwork does not prevent microtubules from eventually capturing and transporting the chromosomes to the spindle area. This indicates that chromosome capture is not directly coupled with actin meshwork disassembly. Furthermore, these results suggest that microtubule pulling force can overcome the steric entrapment of the chromosomes in the actin meshwork, as well as any direct or indirect interactions of the actin meshwork with the chromosomes and kinetochores. Altogether, these results suggest that steric hindrance/ entrapment by the actin meshwork *per se* cannot explain the delay in the chromosome capture in the first five minutes after NEBD. At the same time, my data clearly show that the mechanism to delay chromosome capture is actin-dependent, since complete actin depolymerization abolished the synchronizing effect by delaying chromosome capture.

Upon chromosome capture, as I visualized it live with high temporal resolution, microtubules immediately form lateral attachments with the kinetochores and transport chromosomes to the centrosomes. I therefore propose that an *actin-dependent mechanism prevents microtubule attachment to kinetochores* to synchronize chromosome capture. Thereby, an actin structure could be sterically hindering microtubules from the kinetochore capture. Synchronous disassembly of these structures 'shielding' kinetochores would coordinate chromosome capture.

5.2. Chromosome capture by microtubules during the two-staged chromosome congression

Once captured, chromosomes establish lateral attachments to the wall of a single microtubule. After this lateral attachment is established, chromosomes are transported along the microtubules by dynein. I was able to visualize individual capture events in the oocyte live. I demonstrated that spatial microtubule search is very robust (see chapter 6.1). Overall, my data revealed that despite the very different geometry, the spatial capture range (approx. 30 um) and temporal kinetics (approx. 20 minutes) of the chromosome capture events in starfish oocytes, is remarkably similar to that in somatic cells. Indeed, my data also suggests that the underlying molecular

mechanism of later attachment followed by dynein-driven transport is also conserved. The major difference is that 'search and capture' is synchronized by an actin-dependent mechanism in order to coordinate actin-driven chromosome transport with capture by microtubules.

Altogether, in starfish oocytes chromosome capture by several means is more related to this process in somatic cells: chromosomes within the microtubule capture range are captured through lateral kinetochore-microtubule attachments very efficiently in a time scale similar to that in somatic cells. At this stage, no chromatin-mediated microtubule assembly was detected in starfish oocytes, while this was clearly observed at later stages of spindle assembly.

5.3. Formins, possible molecular players coordinating actin and microtubules during the chromosome congression

The complex relationship between actin structures and astral microtubules in starfish oocytes is a fascinating example of the cross-talk between the different cytoskeletal systems working synergistically to ensure correct chromosome segregation in large cells.

One of the possible molecular players linking actin and microtubules is the family of formin proteins, directly binding both actin and microtubules. Formins are strong actin nucleators polymerizing long unbranched filaments. They are also known to stabilize growing plus- ends of microtubules. Several *in vitro* studies demonstrated a direct link between actin and microtubules (Henty-Ridilla et al, 2016; Preciado Lopez et al., 2014). Recently, a group of Mao suggested formin mDia3 to be involved in stabilization of the microtubule plus-end tips in the end-on kinetochore attachment (Mao et al., 2011) (fig. 1.12).

Formins are involved as actin nucleating factors during several stages of cell division, specific for the oocyte meiosis. For example, in mouse oocytes, formin-2 is essential for the positioning of the already assembled spindle at the cortex (Schuh and Ellenberg, 2008). In starfish oocytes, formins are required during the later stages of cell division for the cleavage furrow closure during the polar body formation (Ucar et al., 2013). Furthermore, formin family of actin nucleators is the major candidate for the assembly of the actin meshwork in starfish oocytes as filaments of the actin meshwork reach several micrometers in length, what is in good agreement with morphology of the other formin-nucleated structures, such as filopodia and actin-stress cables (reviewed in Goode and Eck, 2007).

Due to these dual roles in regulating both actin polymerization and microtubule dynamics, formin proteins could directly or indirectly link actin meshwork contraction with chromosome congression. According to this hypothesis, right after NEBD onset formins are involved in the actin meshwork assembly. At some point during the

chromosome congression process their activity may shift to stabilize microtubule plus-tips, thereby, synchronizing the onset of chromosome capture.

Unfortunately, the role of formins is difficult to access experimentally, since they compose a large family (estimated 15 formins in starfish) of large proteins that could have redundant functions upon knock-down of one of their genes. The existing small molecule inhibitor SMIFH2 targets the actin assembly activity of the formin FH2 domain, domain conserved for the whole protein family. However, efficiency and specificity of the SMIFH2 drug remains controversial (Lénárt lab, unpublished data).

5.4. Depolymerization of 'actin patches' correlates with chromosome capture

I demonstrated that in starfish oocytes during chromosome congression chromosome capture does not occur in the first five minutes after NEBD. The obtained results suggest, that *formation of kinetochore-microtubule attachments is prevented in an actin-dependent mechanism*. I propose that this may be explained by kinetochores being sterically 'shielded' from the microtubules by an actin structure for this time period following NEBD. According to this hypothesis, synchronous disassembly of these actin structures exposes kinetochores and thereby synchronizes chromosome capture. Intriguingly, in starfish oocytes prominent *actin patches*, form around chromosomes at the contact with the nuclear envelope, which may be the structures responsible for delaying chromosome capture.

Those chromosomes located in direct contact with the nuclear envelope are surrounded by the actin patches (fig. 5.1). These are dense structures formed simultaneously with the actin shell (Mori et al., 2014) in an Arp2/3 dependent manner. Actin patches surround only chromosomes located at the nuclear periphery. Similar to the actin shell, their formation requires Arp2/3 nucleation activity, as well as direct contact to nuclear membranes and RanGTP activity (Lénárt lab, unpublished data). In the following, actin patches are incorporated into the actin meshwork and transported together with the chromosomes. Presumably, they facilitate the process of chromosomes detachment from the nuclear membranes at NEBD, however their precise role remains unknown as the first known example of F-actin polymerization from chromatin (Lénárt et al., 2005). Most interestingly, depolymerization of the actin patches is well correlated with the onset of the microtubule-driven transport (Lénárt et al., 2005) (fig. 5.1). On the chromosome trajectories, the fast microtubule-driven phase occurs soon after the gradual depolymerization of the actin patch is finished.

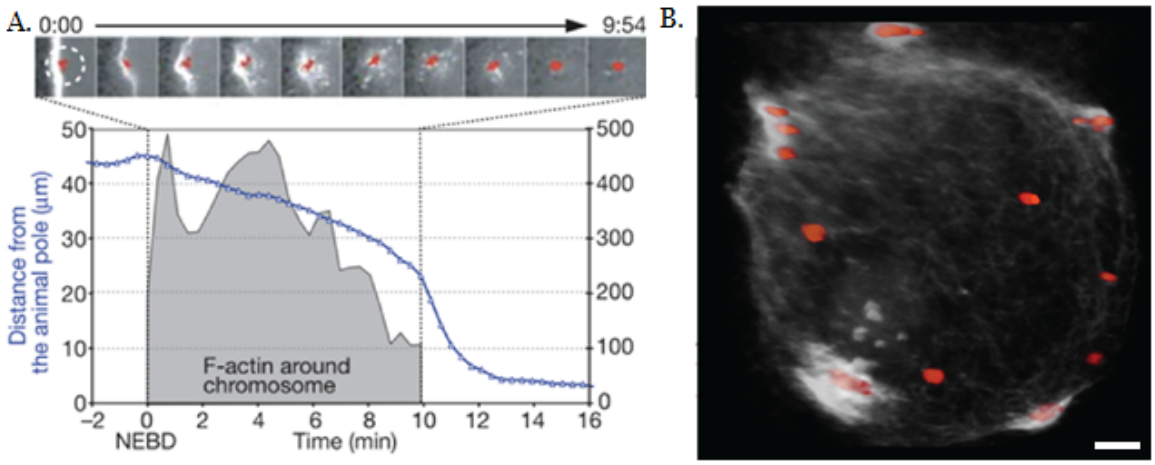

Figure 5.1. Actin patch depolymerization is synchronized with the chromosome capture. A. Gradual depolymerization of a chromosome, marked with a circle, correlated to the chromosome pole-ward velocity. Fast microtubule-driven phase starts when F-actin fluorescence is decreased to the background level. Figure and legend adapted from (Lénárt et al., 2005). **B.** Actin patches morphology during chromosome congression. Confocal image of a matured oocyte, chemically fixed 5 minutes after NEBD and immunostained. F-actin (Phalloidin A561) in gray; Chromosomes (Draq5 staining) in red. Confocal stack, 3D rendered. Scale bar 5 µm.

Although these features render chromosome patches an attractive candidate to synchronize chromosome capture, immunostaining of the matured oocytes with single microtubule resolution revealed that microtubules can actually grow through the actin patch and seem to laterally attach to chromosomes (fig. 4.2). However, the status of the attachment and whether microtubules are able to transport those chromosomes remains unknown. Furthermore, actin patches are formed only on a subset of the chromosomes in direct contact with the nuclear envelope leaving the other subset of the chromosomes in the nuclear interior and their kinetochores potentially accessible for the microtubule capture already after NEBD onset. Live imaging revealed, that chromosomes with and without actin patches are captured simultaneously (fig. 5.2).

Therefore, the actin patches are unlikely to explain the synchronized chromosome capture delay. However, a similar actin structure that is too small to be reliably detected could accumulate around every chromosome/kinetochore, shielding them from the microtubules as predicted by computer modelling of chromosome capture kinetics.

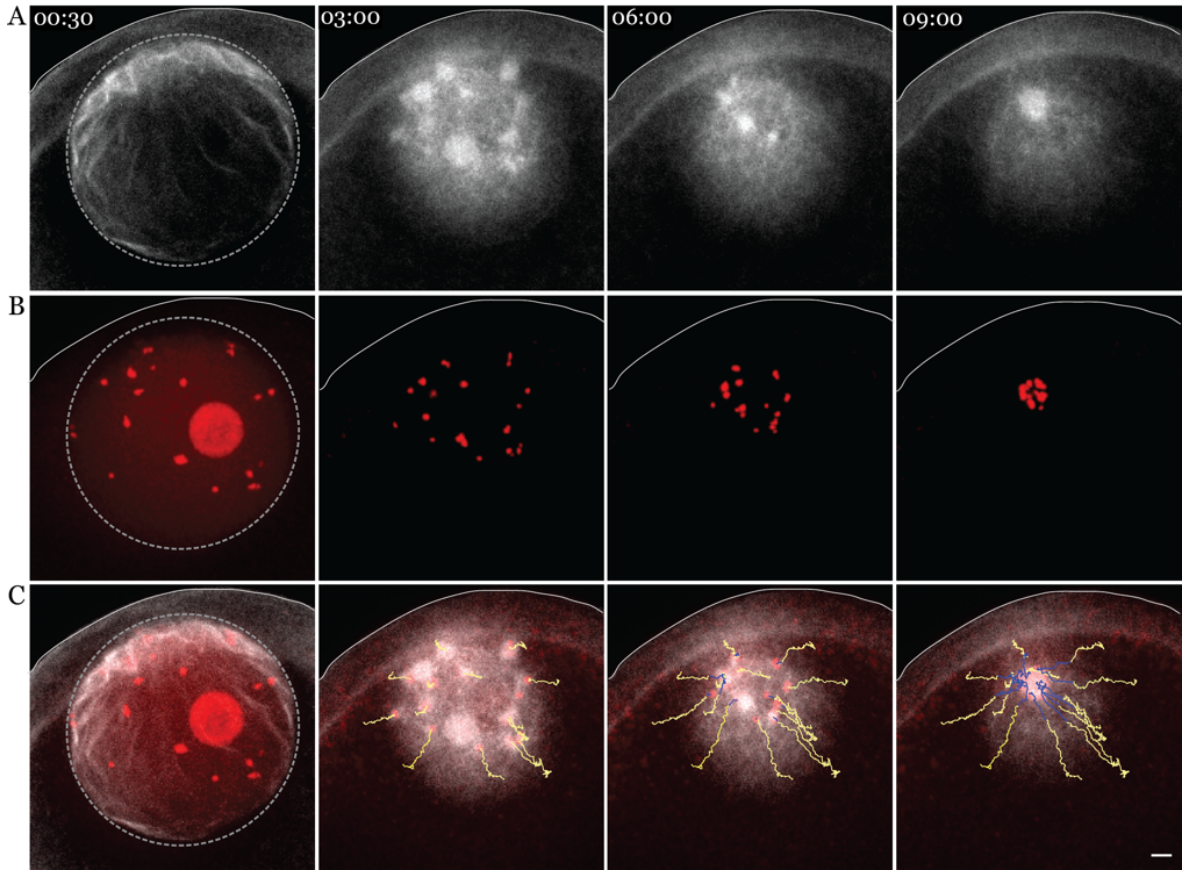

Figure 5.2. Structure and temporal dynamics of the actin patches around the chromosomes. Selected frames from a time series of through a nuclear region of the control oocyte expressing H2B-mEGFP3 (red) and Utrophin-CH-mCherry3 (gray). Time step 5 sec. Z-projection of 60 µm thick confocal slice. Z step 2.2 µm. Scale bar 10 µm. Derived chromosome trajectories overlaid with the images, plotted up to the current time. Time relative to NEBD. Upon capture trajectory line is changed from yellow to blue for each chromosome.

5.5. Suggested mechanism: actin structures shield kinetochores delaying microtubule attachments

Dense actin patches are formed only on a subpopulation of the chromosomes, and, chromosomes with and without an actin patch are captured with exactly the same kinetics. However, it is possible that while strong F-actin accumulation is only present on a subset of chromosomes, a smaller 'actin patch' is present on all chromosomes/kinetochores. However, due to a very small size of these actin structures, as well as kinetochores, these actin shields may be below the detection limit for the fluorescent microscopy. Thus, at the molecular level chromosome congression by microtubules could be prevented either by a *actin shielding structures on the kinetochores*, or due to the *failure to transport the chromosomes caused by a direct kinetochore attachment to the actin meshwork* filaments (fig.5.3).

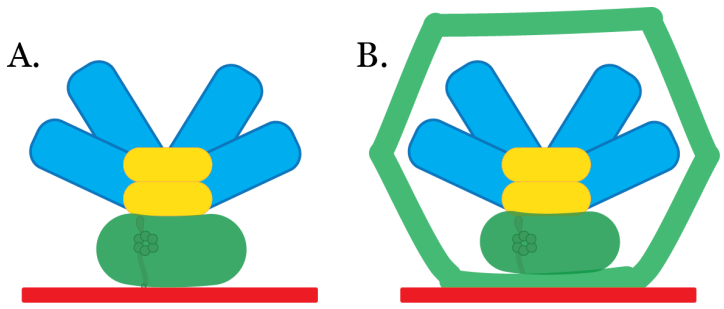

Figure 5.3. Hypothetical F-actin structures, shielding kinetochores from the microtubule attachment. A. F-actin shielding structure on the kinetochore. **B.** F-actin shielding structure attached to the actin meshwork filaments. Actin in shown in green, microtubules in red, chromosome in blue, kinetochore in yellow.

Since actin polymerization is induced on chromatin, this strongly suggests that these newly formed actin structures are firmly incorporated into the actin meshwork. Therefore, not only the formation of the kinetochore-microtubule attachments (fig.5.3.A), but also chromosome transport through the actin patches could be prevented by these actin structures (fig. 5.3.B).

According to this hypothesis (fig. 5.3.B), kinetochore is attached to filaments of the actin meshwork. Therefore, even if the kinetochore-microtubule attachment is made, this chromosome cannot be transported along the microtubule. Since actin meshwork contraction is driven through constant depolymerization and remodeling of the actin filaments, kinetochores at certain time could be 'liberated' from their entrapment under the pulling force of the attached microtubule through the depolymerization and/or remodeling of the actin structures around it.

Since chromosome capture by microtubules can occur while actin meshwork is contracting, it is more likely that kinetochore sites are sterically blocked from the microtubules (fig. 5.3.A). These actin - shielding structures on kinetochores could form at NEBD simultaneously with the actin shell and actin patches, and gradually disassemble along with the actin meshwork depolymerization. Since there is no new actin polymerization at these actin shields (unlike in the actin meshwork), kinetochores appear exposed to the microtubules while the meshwork is still contracting and in a synchronous manner.

5.6. Future directions: how to address role of actin in the chromosome capture

First, the ultrastructure of the actin structures blocking kinetochores, as well as lateral kinetochore-microtubule attachments can be revealed by imaging by electron microscopy. In collaboration with Matthia Karreman, we developed a novel method for correlative light-electron microscopy (CLEM) to precisely target the chromosome-microtubule capture events in starfish oocytes. Technical details and some preliminary data are described in chapter 6.1.

Second, combined with the high temporal resolution imaging, one could address the question, whether chromosome capture is prevented through the steric blocking of the kinetochores or failure to transport it. Quantitative analysis of the individual chromosome trajectories and estimation of the diffusional motion of a chromosome/kinetochore could potentially reveal the status of the early kinetochore-microtubule attachments. Thereby, unattached chromosome even within the actin meshwork will have higher diffusion coefficient, then the one, attached to the microtubule. In this way one can also estimate the role of the actin patches on the subpopulation of the chromosomes.

Third, functional role of the actin shielding structures, blocking kinetochore-microtubule attachments can be addressed by an experiment as illustrated on fig. 5.4. Formation of the actin parches can be induced or prevented around all the chromosomes simultaneously by fusing actin nucleation /depolymerization factors to the histone H2B, thereby, localizing them on the chromatin. Thereby, potent actin depolymerization factor, MICAL (Fremont et al., 2017), localized on the chromatin would prevent formation of all F-actin structures on all chromosomes. Upon disassembly of actin structures with MICAL protein, first chromosome capture events must occur without the delay. On contrary Utrophin-CH domain will induce formation of the actin structures, thereby, further delaying chromosome capture onset. If chromosome capture occurs synchronously, this suggests that kinetochore-microtubule capture occurs due to the depolymerization of the actin 'shielding' structures. Similarly, using Arp2/3 specific nucleating factor or inhibitor one can specifically address the role if the actin patches, formed at the nuclear rim: Arpin (Arp2/3 inhibitor) would prevent formation of the actin patches at the nuclear envelope (Dang et al., 2013); VCA domain of Wave, an Arp2/3 specific nucleation promoting factor (Campellone and Welch, 2010), would induce their polymerization around all the chromosomes in the cell. Expression of these constructs in the oocyte followed by high temporal resolution chromosome tracking and capture kinetics analysis will reveal the role of actin in the chromosome capture by microtubules.

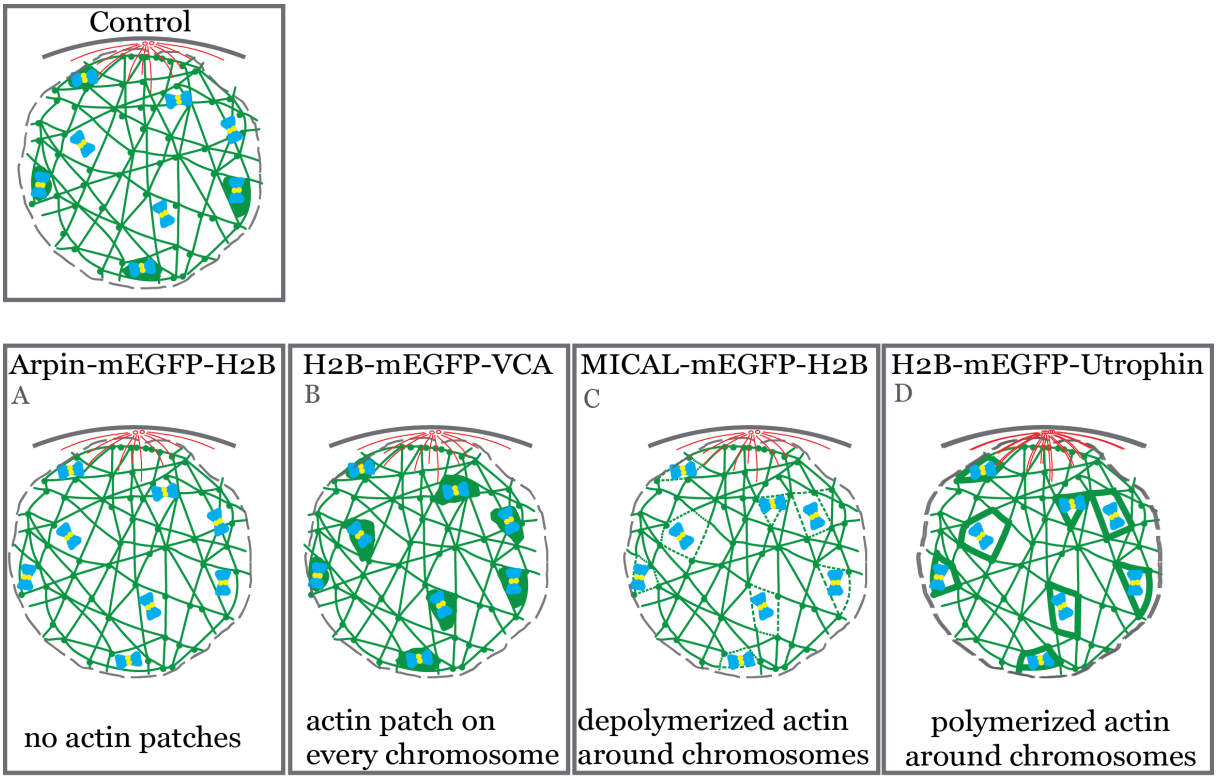

Figure 5.4. Scheme of the experiment addressing actin role in chromosome capture. Above: control oocyte. Below: different constructs, designed to: **A.** Arpin-mEGFP-H2B induces depolymerization of all Arp2/3 dependent structures around the chromosomes. This construct was designed according to (Maiuri et. al., 2015). **B.** H2B-mEGFP-VCA induces formation of the Arp2/3 actin structures around every chromosome, including those inside the nuclear area. This construct was designed as in (Chaigne et. al., 2015). **C.** MICAL-mEGFP-H2B is depolymerizing all possible actin structures around the chromosomes; N-terminal monooxygenase (FAD) domain of MICAL was designed according to S. Fremont personal advice. **D.** H2B-mEGFP-Utrophin-CH stabilizes F-actin around the chromosomes. Utrophin-CH domain constructs were available in the Lénárt lab previously.

6. Appendix

6.1. Visualization of chromosomes with correlative light - electron microscopy

During chromosome congression in starfish oocytes, chromosomes are brought into the microtubule capture range by a contractile actin meshwork. While actin meshwork transports the chromosomes to the spindle area, it additionally prevents microtubule capture of those chromosomes, initially located within the capture range. Based on the results of the actin meshwork perturbations (see *Results*), I concluded that the delay in the chromosome capture onset could be caused by the failure to establish initial lateral chromosome-microtubule attachments either due to the existing attachment of the kinetochore to the filaments of the actin meshwork, or a F-actin structure on the kinetochores, preventing microtubule attachment.

Resolution of the images obtained by light microscopy of the chemically fixed immunostained oocytes was not sufficient to reveal these chromosome-microtubule attachments. Therefore, I aimed to visualize the ultrastructural organization of the kinetochore-microtubule attachments using electron microscopy (EM). Ultrastructural details could ascertain the mechanism delaying microtubule capture of the proximally located chromosomes and visualize the nature of the kinetochore-microtubule attachments, as well as those structures, possibly hindering the kinetochore attachment sites.

Therefore, I set out to image individual chromosomes in starfish oocyte during the two-staged chromosome congression. For this study, it was required to use the fluorescence microscopy to 1) stage the event of interest in time, aiming to visualize the moment that the chromosomes are captured by the microtubules, and 2) to subsequently retrieve these areas inside the large oocyte and image the region of interest (ROI) at high magnification with transmission electron microscopy (TEM). However, due to the very large size of the cell (~180 μm in diameter), examining all the thin, 70 nm, serial sections of the entire oocyte to find the chromosomes with TEM is extremely time-consuming.

Correlative light-electron microscopy (CLEM) is a powerful approach that allows to combine live-imaging of fluorescently labeled samples with the high spatial resolution of EM. Generally, the sample is imaged first with fluorescence microscopy (FM) to identify the event of interest in space and time. Next, the sample is processed for EM and ROI is retrieved and imaged at high resolution. CLEM of relatively small objects like somatic cells is performed by direct correlation of the fluorescence and EM images. For example, somatic cells are often grown on the special surfaces with markings. The position of the ROI with respect to these markings is recorded during FM imaging, and subsequently function as a guide to retrieve the ROI in the electron microscope.

However, for samples larger than the somatic cells, introducing landmarks becomes non-trivial. On tissues, for instance, one of the typically used reference points are those artificially introduced by laser branding to mark the position of the ROI (Bishop et al., 2011; Maco et al., 2013).

Importantly, correlative microscopy relies on keeping track of the ROI when the sample is moved from one imaging modality to the next. To facilitate this correlation, reference points that are visible in both microscopy datasets can be used to map the sample and to retrieve the position of the ROI. However, during prometaphase, oocytes do not possess any special landmarks that would allow such correlation.

Recently, Matthia Karreman (Yannick Schwab group, EMBL) developed a novel approach of CLEM for large, 3-dimensional samples that includes an intermediate step of X-ray tomography (microCT) scanning of the EM-processed sample to determine to position of the ROI. This technology was proven in mouse brain biopsy samples (Karreman et al., 2016), as well as for centriole visualization in the polar bodies of starfish oocytes (Borrego-Pinto et al., 2016). Using microCT imaging, the sample can be visualized within the resin block, as well as other characteristic landmarks (blood vessels in a biopsy sample; polar body protrusions on the oocyte etc.). Next, the obtained microCT volume is correlated with the fluorescent dataset in 3D to create a map for precise targeting of the ROI during the serial sectioning and ultrastructure image acquisition with EM.

By introducing the reference points in the cytoplasm of the oocyte, we correlated the EM-processed resin-embedded sample with the fluorescent 3D dataset acquired right after the chemical fixation. Thereby, we could rapidly and precisely target the ROI of the oocyte samples (chromosomes during their congression in the early prometaphase).

To introduce the landmarks, before maturation, the oocytes were injected with several oil droplets. Normally, silicone oil is used in the microinjections to prevent mixing of the mRNA, or other injection solutions, with the sea water while submerging the needle into the chamber with the oocytes (see chapter 3.4). As a result of every injection, a small oil droplet remains in the cytoplasm of the oocyte close to the needle entry site. These oil droplets turned out to be visible in the microCT scans of the EM-processed oocytes. To use the oil droplets as landmarks for CLEM, oocytes were injected with several (typically 5, up to 7) small oil droplets aiming to position them close to the nucleus and yet in a scattered manner to uniformly surround the ROI. Well-distributed landmarks increase the robustness and precision of the correlation between the FM and microCT datasets. Generally, oocytes can be injected with volumes of up to 10 % of the cell.

Simultaneously with the oil droplets, the oocytes were injected with fluorescent probes for chromosome labeling, or with tubulin to label the spindle. Matured oocytes, chemically fixed within 5 minutes after NEBD onset, were immediately imaged with the confocal microscope. In addition to visualizing the structures of interest (chromosomes or spindle), fluorescent probes provided background staining of the cytoplasm. Since oil droplets are not penetrable for any water-soluble substances/solutions, and thus did not take up the fluorescent probes, they serve as negatively-stained landmarks mapping the entire oocyte.

Single-point confocal scanning of a whole oocyte in 3D with sufficient resolution in Z axis took approximately 1 minute. During this time, chromosomes can be congressed for a large distance in the cell. Therefore, the oocytes were first chemically fixed, and then imaged immediately. Since glutaraldehyde present in the fixative solution yields strong autofluorescence in the green channel, thereby disabling imaging of any fluorescent probes in the green-range emission wavelength. Therefore, we always used fluorescent probes in the red or far-red channel.

After the complete sample processing for electron microscopy, as described in the *Materials and Methods* chapter, resin-embedded oocytes were subjected to microCT scanning. MicroCT images allowed us to link the fluorescent datasets to the acquisition of the EM images by predicting the position of chromosomes (fig. 6.1.A). The obtained microCT volume was rendered in 3D to display and the resin block, surface of the oocyte and all the oil droplets as reference points. Next, microCT image and 3D fluorescent dataset were superimposed and registered in Amira software to estimate the distance from the surface of the resin block to the chromosomes. Based on these measurements, part of the resin block was trimmed off to reach the ROI. At this position, thin serial sections were produced for TEM imaging (fig. 6.1.B-C). Targeting precision of the correlation reached down to 10 μm precision depending on the quality of the registration between the FM and microCT datasets. Moreover, depending on the number of reference points and their position relative to the ROI, a higher accuracy could be achieved. Ultrastructure images of the chromosomes, obtained by TEM, are shown on fig. 6.2. We were able to detect a kinetochore plate of an individual chromosome. However, no microtubules were visualized on this image. Therefore, remains unknown whether or not this chromosome is captured by a microtubule. In the following, we aim to visualize an oocyte with an assembled spindle, labeled with Cy3-tubulin, to confirm that microtubules are well-preserved through all EM-processing steps. Several more oocytes will be processed and imaged to visualize the ultrastructural details of a chromosome-microtubule capture event.

In conclusion, CLEM workflow based on the X-ray scanning technique is an efficient and rapid approach, which can be potentially transferred to other model systems suitable for microinjections.

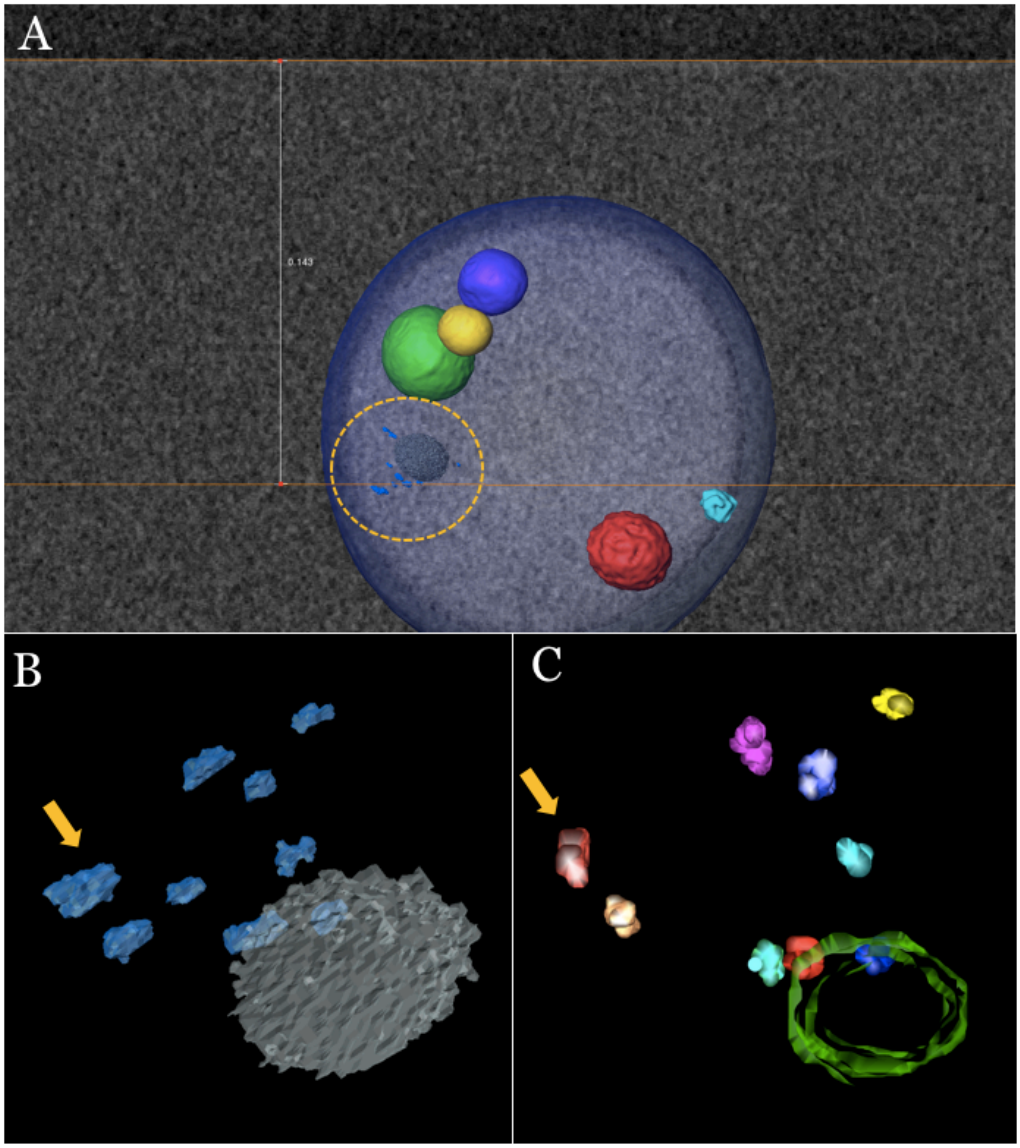

Figure 6.1. CLEM imaging allows to target individual chromosomes in the starfish oocyte. A. 3D rendered correlative map of an entire oocyte, EM-processed and embedded into the resin block. MicroCT and 3D fluorescent dataset are superimposed and registered together. Resin block visualized in gray, outline of the oocyte in light blue. Five different oil droplets, correlated in the two datasets, depicted in different colors each. ROI, marked with yellow dashed circle, contains several chromosomes and a large nucleolus. A single chromosome, nearest to the cell cortex and microtubule asters, was selected for the EM imaging. For that, the upper part of the resin block, as well as part of the oocyte, was trimmed off (represented with a white line ≈ 143 µm from the surface of the block). **B.** Zoom into the ROI on the fluorescence dataset, 3D rendered. Chromosomes shown in blue, nucleolus in gray. **C.** The same dataset in the 3D model for the TEM serial sections. The chromosome, targeted for the ultrastructural imaging is marked with the yellow arrow. 3D model was generated from serial sections imaged with TEM, segmented by Matthia Karreman using Amira software.

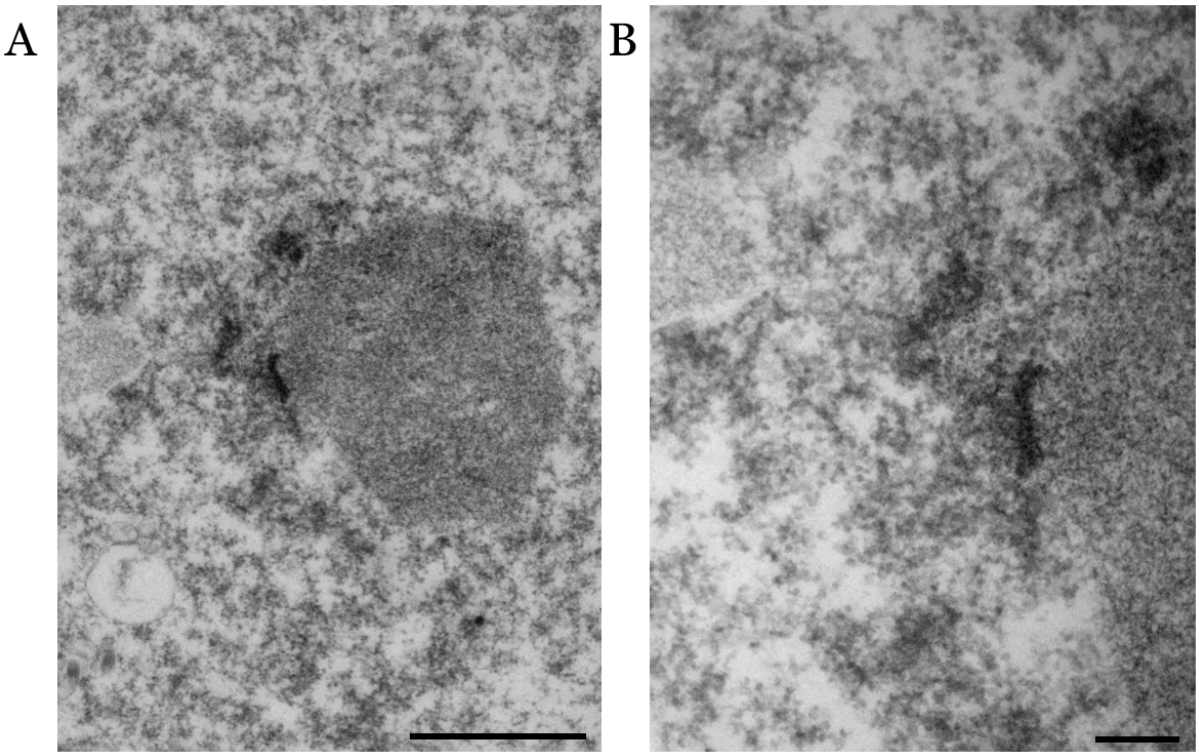

Figure 6.2. Ultrastructure of a chromosome with a kinetochore plate. Oocyte, chemically fixed 5 minutes after NEBD, was processed for CLEM as shown on fig. 1. Electron micrographs were obtained by TEM. Image B is magnified area shown on A. Images were obtained by Matthia Karreman. A: Scale bar 1 μm. B: scale bar 200 nm.

6.2. Microtubule spatial search is quite robust

In starfish oocytes, all chromosomes are captured ultimately by astral microtubules. Actin-dependent chromosome congression greatly, but non-specifically facilitates the microtubule search by bringing the chromosomes into direct proximity to the astral microtubules, from where they are being immediately captured. No chromatin-mediated microtubule nucleation was detected, while other general mechanisms facilitating microtubule search in starfish oocytes remained uncharacterized. I aimed to test the efficiency of the microtubule search *per se* without the actin meshwork in this model system, where the spatial dimensions are exceeding those in somatic cells by several orders of magnitude.

To test the efficiency of the chromosome-microtubule capture in a large geometrical scale, all actin structures were depolymerized with Cytochalasin D and microtubules were additionally stabilized with Paclitaxel (55 nM or 100 nM). Due to the effects of Paclitaxel preventing microtubule depolymerization, asters grow much larger compared to those in the control oocyte (fig. 4.5.A). Surprisingly, long stabilized microtubules were capable of capturing all the chromosomes in the whole volume of the nucleus even when actin-driven chromosome congression is completely abolished. Therefore, microtubule spatial search in large cells seems to be very efficient: all 22 chromosomes were captured by the microtubules in four oocytes. In the two other observed oocytes only one chromosome from the whole set remained lost in the

cytoplasm until the onset of the metaphase. This observation is particularly striking because the volume is increasing to the power of three compared to the radius of the measured spheres. Assuming a microtubule capture range of 35 μm in the untreated control oocyte, and 65 μm in the Paclitaxel-stabilization experiment, the volume of cytoplasm which microtubules span in the chromosome search and capture is increased 6.4 times (according to the formula, where V = 4/3πr^3).

The temporal kinetics of the chromosome capture events have been very similar to control non-treated oocytes: chromosome capture occurs between 5 and 15 minutes in the drug-treated oocyte and at 5 to 10 minutes in the control (see chapter 4.2.1). Moreover, observed chromosome capture events occur in a distance-dependent manner: chromosomes located closer to the asters are captured by microtubules earlier, followed by those located further from the centrosomes. These results agree with the microtubule 'search and capture' model (Kirschner and Mitchison, 1986), as well as predictions of computational modelling (Wollman et al., 2005). According to the hypothesis, time required for the chromosome search is proportional to the distance between the chromosome and the centrosome.

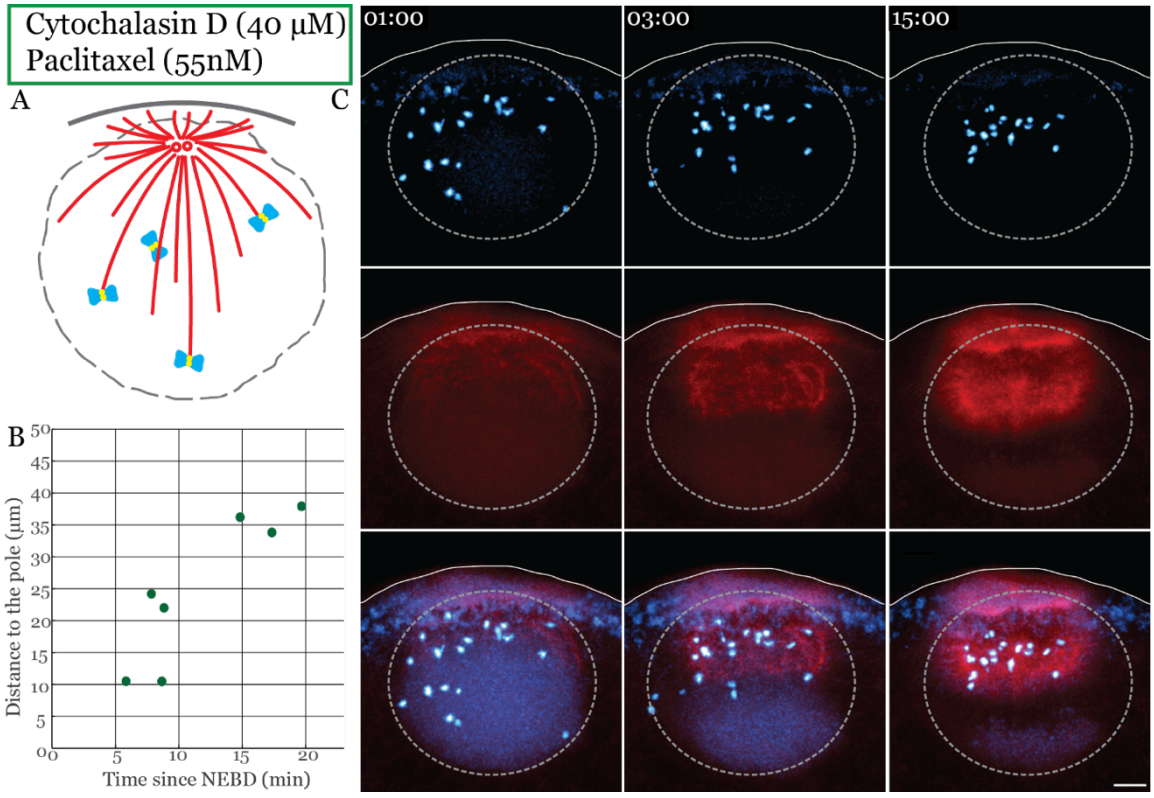

Figure 6.3. Long astral microtubules stabilized with Paclitaxel capture all the chromosomes without actin meshwork. A. Schematic of the experiment. **B.** Chromosome capture distance-time plot. Each dot represents the moment of chromosome capture at certain distance from the pole. Capture event was determined based as the first moment of the fast chromosome motion along the microtubule. **C.** Selected frames from a time series of the nucleus area of an oocyte expressing H2B-GFP (cyan) labeled chromosomes and Cy3-tubulin protein labeling microtubule asters. Time step 10 sec. Z-projection of 60 μm thick confocal slice. Scale bar 10 μm. Time relative to NEBD. Number of oocytes in the experiment: 6.

6.3. *Cytosim* script for the chromosome congression modelling

```
% Chromosome congression in starfish oocyte
% Maria Burdyniuk and Francois Nedelec, September 2015
% Scenario Control 2 - kinetochore binding affinity to the microtubules  =0 in the first
%5 minutes
% Kinetochore binding affinity to the microtubules is gradually increased between 5 and
%8 min after NEBD
set simul capture
{
    time_step = 0.05
    viscosity = 0.1
    steric = 0, 500
    display = (style=1;)
}
set space cell
{
    geometry = ( sphere 35 )
}
set hand glue
{
    binding_rate = 0        % kinetochore binding rate
    binding_range = 0.15    % radius of a single kinetochore
    unbinding = 0, inf      % never unbind
    hold_shrinking_end = 1  % bind to the microtubule tip as well
    activity = move
    stall_force = 1
    max_speed = -1          % dynein motor velocity
}
set single kinetochore
{
    hand = glue
    stiffness = 100
}
set solid chromosome
{
    confine = inside, 100
    steric = 1
    flow_center = 0 33 0    % full congression point for chromosomes by the actin
meshwork at the AP
    flow_time = 750, 900    % All chromosomes congress at 15 min post NEBD, flow is
stopped at 13.5 min
}
set fiber microtubule
{
    rigidity = 22
    segmentation = 3
    confine = inside, 100
    activity         = classic
    growing_speed    = 0.5
    shrinking_speed  = -1
    catastrophe_rate = 0.15
    rescue_rate      = 0
    growing_force    = 1.67
    delete_stub      = 0
    rebirth_rate     = 1
    min_length       = 0.25

    catastrophe_outside = 1
    catastrophe_length = 37;  % microtubule catastrophe is length-dependent, 18 -
average MTs length
}
set hand nucleator
```

```
{
    unbinding = 0, 3
    activity = nucleate
    nucleate = 1, microtubule, ( fiber_length=3; )
    display = { size=5; color=green; }
}
set single complex
{
    hand = nucleator
    activity = fixed
    stiffness = 1000
}
% ----------------- PLACEMENTS ------------------
new space cell
new 22 solid chromosome
{
    point0 = center, 0.8   % radius of a chromosome sphere
    point1 = +0.8 0 0, 0, kinetochore
    point2 = -0.8 0 0, 0, kinetochore
    position = sphere 35    % chromosomes are placed random in the nucleus
}
new 500 single complex     % place the centrosomes
{
    position = sphere 2 at 4 32 0
}
new 500 single complex
{
    position = sphere 2 at -4 32 0
}
% -----------------SIMULATION------------------
run simul *
{
    solve = 1
    nb_steps  = 6000     % for 5 minutes
    nb_frames = 150      % report every 2 sec
}
% ----------------- PLACEMENTS  SIMUL ------------------
change hand glue
{
    binding_rate = 0.4   % kinetochore binding affinity changed
}
run simul *
{
    solve = 1
    nb_steps  = 1200     % for 1 minute
    nb_frames = 30       % report every 2 sec
}
% ----------------- PLACEMENTS  SIMUL ------------------
change hand glue
{
       binding_rate = 0.6   % kinetochore binding affinity changed
}
run simul *
{
       solve = 1
       nb_steps  = 1200     % for 1 minute
       nb_frames = 30       % report every 2 sec
}
% ----------------- PLACEMENTS  SIMUL ------------------
change hand glue
{
       binding_rate = 0.8   % kinetochore binding affinity changed
}
run simul *
```

```
{
       solve = 1
       nb_steps  = 1200     % for 1 minute
       nb_frames = 30       % report every 2 sec
}
% ----------------- PLACEMENTS  SIMUL ------------------
change hand glue
{
       binding_rate = 1     % kinetochore binding affinity changed
}
run simul *
{
       solve = 1
       nb_steps  = 19200    % for 16 minutes
       nb_frames = 480      % report every 2 sec
}
```

6.4. Chromosome capture events for individual oocytes in control, upon actin meshwork disruption or stabilization

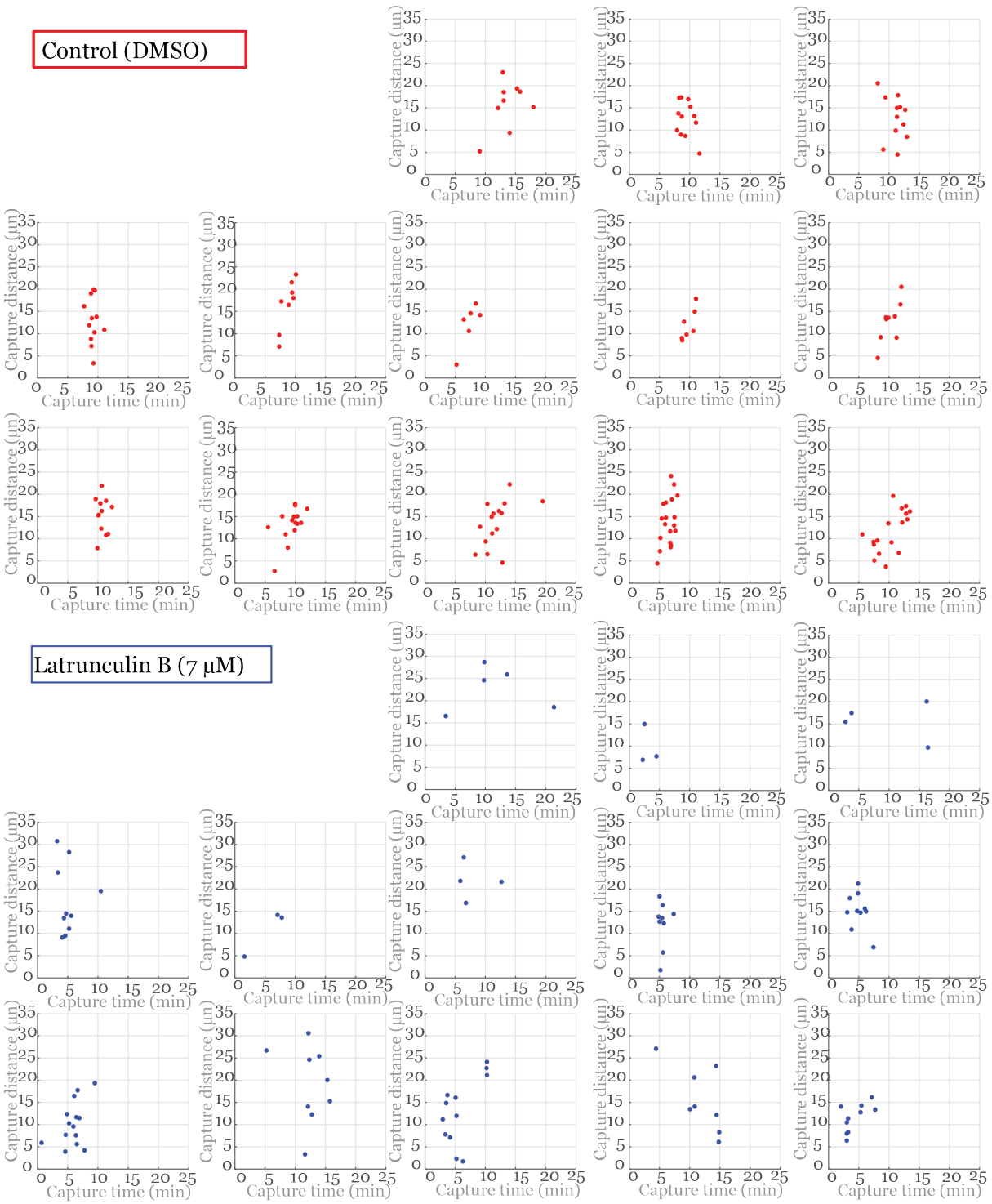

Figure 6.4. Actin synchronizes chromosome capture by microtubules. Data from individual oocytes. Chromosome capture events for individual oocytes in control (above) and threated with 7 µM Latrunculin B.

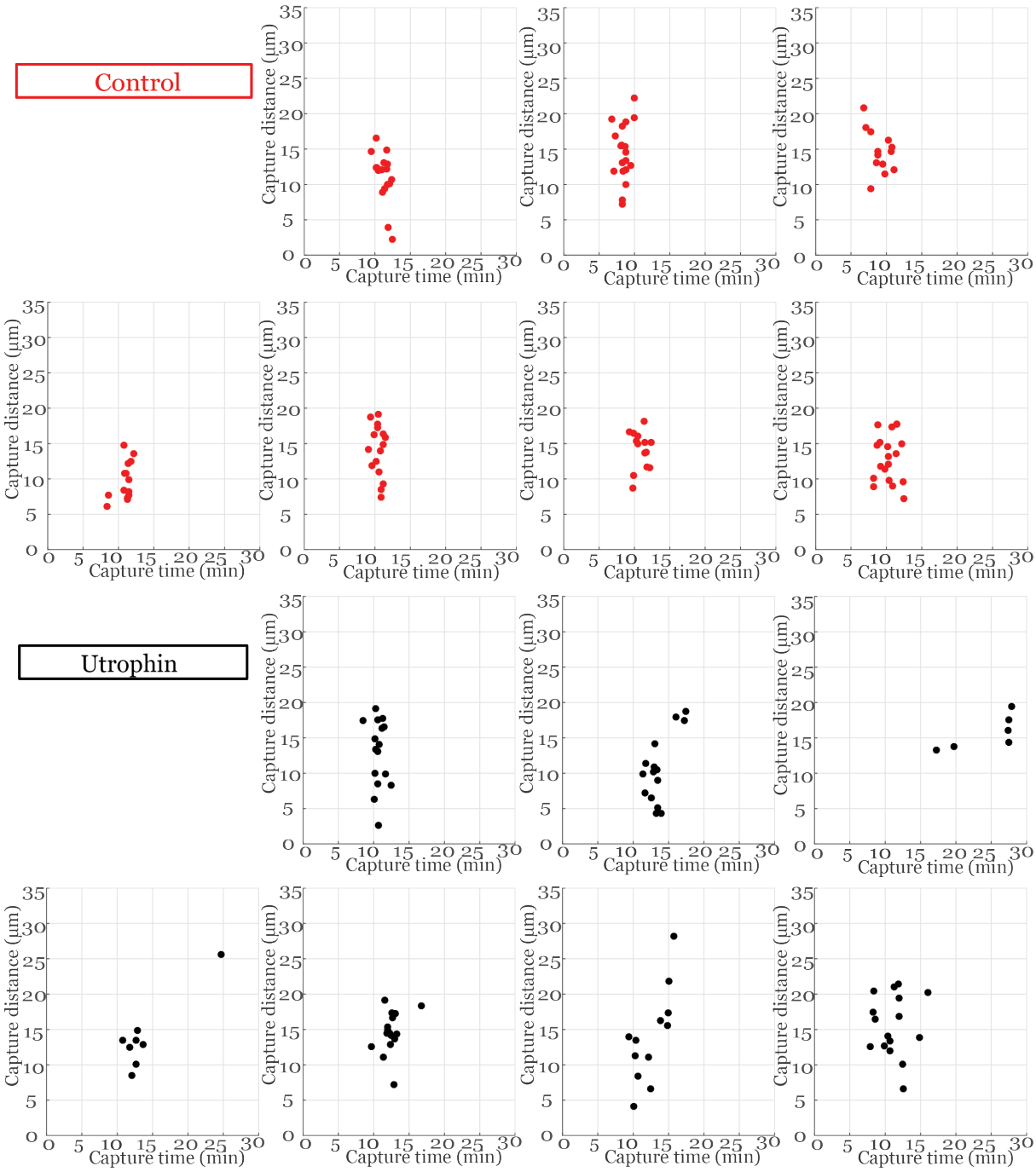

Figure 6.5. Actin meshwork stabilization with the Utrophin-CH protein. Data from individual oocytes. Chromosome capture events for individual oocytes in control (above) and injected with 40 units of Uthophin-CH-A568 protein.

7. References

Abad MA, Zou J, Medina-Pritchard B, Nigg EA, Rappsilber J, Santamaria A, Jeyaprakash AA. Ska3 Ensures Timely Mitotic Progression by Interacting Directly With Microtubules and Ska1Microtubule Binding Domain. Sci Rep. 2016 Sep 26;6:34042.

Akhmanova A, Steinmetz MO. Tracking the ends: a dynamic protein network controls the fate of microtubule tips. Nat Rev Mol Cell Biol. 2008 Apr;9(4):309-22.

Akhshi TK, Wernike D, Piekny A. Microtubules and actin crosstalk in cell migration and division. Cytoskeleton (Hoboken). 2014 Jan;71(1):1-23.

Alberts A, Johnson J, Lewis J, Raff M, Roberts K, Walter P. Molecular Biology of the Cell. 5th Edition. New York, NY: Garland Science; 2007. p. 1036.

Aldrup-Macdonald ME, Sullivan BA. The past, present, and future of human centromere genomics. Genes (Basel). 2014 Jan 24;5(1):33-50.

Alexander SP, Rieder CL. Chromosome motion during attachment to the vertebrate spindle: initial saltatory-like behavior of chromosomes and quantitative analysis of force production by nascent kinetochore fibers. J Cell Biol. 1991 May;113(4):805-15.

Almonacid M, Terret MÉ, Verlhac MH. Actin-based spindle positioning: new insights from female gametes. J Cell Sci. 2014 Feb 1;127(Pt 3):477-83.

Alushin GM, Ramey VH, Pasqualato S, Ball DA, Grigorieff N, Musacchio A, Nogales E. The Ndc80 kinetochore complex forms oligomeric arrays along microtubules. Nature. 2010 Oct 14;467(7317):805-10.

Azoury J, Lee KW, Georget V, Rassinier P, Leader B, Verlhac MH. Spindle positioning in mouse oocytes relies on a dynamic meshwork of actin filaments. Curr Biol. 2008 Oct 14;18(19):1514-9.

Ballestrem C, Wehrle-Haller B, Imhof BA. Actin dynamics in living mammalian cells. J Cell Sci. 1998 Jun;111 (Pt 12):1649-58.

Barak LS, Nothnagel EA, DeMarco EF, Webb WW. Differential staining of actin in metaphase spindles with 7-nitrobenz-2-oxa-1,3-diazole-phallacidin and fluorescent DNase: is actin involved in chromosomal movement? Proc Natl Acad Sci U S A. 1981; 78v:3034–3038.

Barisic M, Aguiar P, Geley S, Maiato H. Kinetochore motors drive congression of peripheral polar chromosomes by overcoming random arm-ejection forces. Nat Cell Biol. 2014 Dec;16(12):1249-56.

Barisic M, Maiato H. Dynein prevents erroneous kinetochore-microtubule attachments in mitosis. Cell Cycle. 2015;14(21):3356-61.

Barisic M, Silva e Sousa R, Tripathy SK, Magiera MM, Zaytsev AV, Pereira AL, Janke C, Grishchuk EL, Maiato H. Mitosis. Microtubule detyrosination guides chromosomes during mitosis. Science. 2015 May 15;348(6236):799-803.

Beaudouin J, Gerlich D, Daigle N, Eils R, Ellenberg J. Nuclear envelope breakdown proceeds by microtubule-induced tearing of the lamina. Cell. 2002 Jan 11;108(1):83-96.

Bennabi I, Terret ME, Verlhac MH. Meiotic spindle assembly and chromosome segregation in oocytes. J Cell Biol. 2016 Dec 5;215(5):611-619. Epub 2016 Nov 22.

Bishop D, Nikić I, Brinkoetter M, Knecht S, Potz S, Kerschensteiner M, Misgeld T. Near-infrared branding efficiently correlates light and electron microscopy. Nat Methods. 2011 Jun 5;8(7):568-70.

Bohnsack MT, Stüven T, Kuhn C, Cordes VC, Görlich D. A selective block of nuclear actin export stabilizes the giant nuclei of Xenopus oocytes. Nat Cell Biol. 2006 Mar;8(3):257-63.

Borrego-Pinto J, Somogyi K, Karreman MA, König J, Müller-Reichert T, Bettencourt-Dias M, Gönczy P, Schwab Y, Lénárt P. Distinct mechanisms eliminate mother and daughter centrioles in meiosis of starfish oocytes. J Cell Biol. 2016 Mar 28;212(7):815-27.

Borrego-Pinto J, Somogyi K, Lénárt P. Live Imaging of Centriole Dynamics by Fluorescently Tagged Proteins in Starfish Oocyte Meiosis. Methods Mol Biol. 2016;1457:145-66.

Brangwynne CP, Mitchison TJ, Hyman AA. Active liquid-like behavior of nucleoli determines their size and shape in Xenopus laevis oocytes. Proc Natl Acad Sci U S A. 2011 Mar 15;108(11):4334-9.

Brugués J, Nuzzo V, Mazur E, Needleman DJ. Nucleation and transport organize microtubules in metaphase spindles. Cell. 2012 Apr 27;149(3):554-64.

Burkel BM, von Dassow G, Bement WM. Versatile fluorescent probes for actin filaments based on the actin-binding domain of utrophin. Cell Motil Cytoskeleton. 2007 Nov;64(11):822-32.

Campellone KG, Welch MD. A nucleator arms race: cellular control of actin assembly. Nat Rev Mol Cell Biol. 2010 Apr;11(4):237-51.

Cane S, Ye AA, Luks-Morgan SJ, Maresca TJ. Elevated polar ejection forces stabilize kinetochore-microtubule attachments. J Cell Biol. 2013 Jan 21;200(2):203-18.

Carazo-Salas RE, Guarguaglini G, Gruss OJ, Segref A, Karsenti E, Mattaj IW. Generation of GTP-bound Ran by RCC1 is required for chromatin-induced mitotic spindle formation. Nature. 1999 Jul 8;400(6740):178-81.

Carlier MF. Role of nucleotide hydrolysis in the polymerization of actin and tubulin. Cell Biophys. 1988 Jan-Jun;12:105-17.

Caudron M, Bunt G, Bastiaens P, Karsenti E. Spatial coordination of spindle assembly by chromosome-mediated signaling gradients. Science. 2005 Aug 26;309(5739):1373-6.

Chaigne A, Campillo C, Gov NS, Voituriez R, Sykes C, Verlhac MH, Terret ME. A narrow window of cortical tension guides asymmetric spindle positioning in the mouse oocyte. Nat Commun. 2015 Jan 19;6:6027.

Cheeseman IM, Chappie JS, Wilson-Kubalek EM, Desai A. The conserved KMN network constitutes the core microtubule-binding site of the kinetochore. Cell. 2006 Dec 1;127(5):983-97.

Cheeseman IM, Desai A. Molecular architecture of the kinetochore-microtubule interface. Nat Rev Mol Cell Biol. 2008 Jan;9(1):33-46.

Cheeseman IM, Niessen S, Anderson S, Hyndman F, Yates JR 3rd, Oegema K, Desai A. A conserved protein network controls assembly of the outer kinetochore and its ability to sustain tension. Genes Dev. 2004 Sep 15;18(18):2255-68.

Cheng L, Zhang J, Ahmad S, Rozier L, Yu H, Deng H, Mao Y. Aurora B regulates formin mDia3 in achieving metaphase chromosome alignment. Dev Cell. 2011 Mar 15;20(3):342-52.

Chmátal L, Yang K, Schultz RM, Lampson MA. Spatial Regulation of Kinetochore Microtubule Attachments by Destabilization at Spindle Poles in Meiosis I. Curr Biol. 2015 Jul 20;25(14):1835-41.

Clarke L, Carbon J. Isolation of a yeast centromere and construction of functional small circular chromosomes. Nature. 1980 Oct 9;287(5782):504-9.

Clift D, Schuh M. Restarting life: fertilization and the transition from meiosis to mitosis. Nat Rev Mol Cell Biol. 2013 Sep;14(9):549-62.

Cojoc G, Florescu AM, Krull A, Klemm AH, Pavin N, Jülicher F, Tolić IM. Paired arrangement of kinetochores together with microtubule pivoting and dynamics drive kinetochore capture in meiosis I. Sci Rep. 2016 May 11;6:25736.

Conde C, Cáceres A. Microtubule assembly, organization and dynamics in axons and dendrites. Nat Rev Neurosci. 2009 May;10(5):319-32.

Czaban BB, Forer A. Rhodamine-labelled phalloidin stains components in the chromosomal spindle fibres of crane-fly spermatocytes and Haemanthus endosperm cells. Biochem Cell Biol. 1992 Aug;70(8):664-76.

Dang I, Gorelik R, Sousa-Blin C, Derivery E, Guérin C, Linkner J, Nemethova M, Dumortier JG, Giger FA, Chipysheva TA, Ermilova VD, Vacher S, Campanacci V, Herrada I, Planson AG, Fetics S, Henriot V, David V, Oguievetskaia K, Lakisic G, Pierre F, Steffen A, Boyreau A, Peyriéras N, Rottner K, Zinn-Justin S, Cherfils J, Bièche I, Alexandrova AY, David NB, Small JV, Faix J, Blanchoin L, Gautreau A. Inhibitory signalling to the Arp2/3 complex steers cell migration. Nature. 2013 Nov 14;503(7475):281-4.

Dasso M. The Ran GTPase: theme and variations. Curr Biol. 2002 Jul 23;12(14):R502-8.

Debec A, Sullivan W, Bettencourt-Dias M. Centrioles: active players or passengers during mitosis? Cell Mol Life Sci. 2010 Jul;67(13):2173-94.

DeLuca JG, Gall WE, Ciferri C, Cimini D, Musacchio A, Salmon ED. Kinetochore microtubule dynamics and attachment stability are regulated by Hec1. Cell. 2006 Dec 1;127(5):969-82.

Dong Y, Vanden Beldt KJ, Meng X, Khodjakov A, McEwen BF. The outer plate in vertebrate kinetochores is a flexible network with multiple microtubule interactions. Nat Cell Biol. 2007 May;9(5):516-22.

Drpic D, Pereira AJ, Barisic M, Maresca TJ, Maiato H. Polar Ejection Forces Promote the Conversion from Lateral to End-on Kinetochore-Microtubule Attachments on Mono-oriented Chromosomes. Cell Rep. 2015 Oct 20;13(3):460-9

Earnshaw WC, Rothfield N. Identification of a family of human centromere proteins using autoimmune sera from patients with scleroderma. Chromosoma. 1985;91(3-4):313-21.

Farina F, Gaillard J, Guérin C, Couté Y, Sillibourne J, Blanchoin L, Théry M. The centrosome is an actin-organizing centre. Nat Cell Biol. 2016 Jan;18(1):65-75.

Feric M, Brangwynne CP. A nuclear F-actin scaffold stabilizes ribonucleoprotein droplets against gravity in large cells. Nat Cell Biol. 2013 Oct;15(10):1253-9.

Field CM, Lénárt P. Bulk cytoplasmic actin and its functions in meiosis and mitosis. Curr Biol. 2011 Oct 11;21(19):R825-30.

Forer A, Jackson WT. Actin in spindles of Haemanthus katherinae endosperm. I. General results using various glycerination methods. J Cell Sci. 1979 Jun;37:323-47.

Forer A, Pickett-Heaps JD. Cytochalasin D and latrunculin affect chromosome behaviour during meiosis in crane-fly spermatocytes. Chromosome Res. 1998 Nov;6(7):533-49.

Forer A, Spurck T, Pickett-Heaps JD. Actin and myosin inhibitors block elongation of kinetochore fibre stubs in metaphase crane-fly spermatocytes. Protoplasma. 2007;232(1-2):79-85. Epub 2007 Dec 19.

Frémont S, Romet-Lemonne G, Houdusse A, Echard A. Emerging roles of MICAL family proteins - from actin oxidation to membrane trafficking during cytokinesis. J Cell Sci. 2017 Apr 3.

Gandhi SR, Gierliński M, Mino A, Tanaka K, Kitamura E, Clayton L, Tanaka TU. Kinetochore-dependent microtubule rescue ensures their efficient and sustained interactions in early mitosis. Dev Cell. 2011 Nov 15;21(5):920-33.

Gard DL, Affleck D, Error BM. Microtubule organization, acetylation, and nucleation in Xenopus laevis oocytes: II. A developmental transition in microtubule organization during early diplotene. Dev Biol. 1995 Mar;168(1):189-201.

Gard DL. Microtubule organization during maturation of Xenopus oocytes: assembly and rotation of the meiotic spindles. Dev Biol. 1992 Jun;151(2):516-30.

Goode BL, Eck MJ. Mechanism and function of formins in the control of actin assembly. Annu Rev Biochem. 2007;76:593-627.

Goshima G, Wollman R, Goodwin SS, Zhang N, Scholey JM, Vale RD, Stuurman N. Genes required for mitotic spindle assembly in Drosophila S2 cells.

Goshima G, Wollman R, Goodwin SS, Zhang N, Scholey JM, Vale RD, Stuurman N. Genes required for mitotic spindle assembly in Drosophila S2 cells. Science. 2007 Apr 20;316(5823):417-21.

Gruss OJ, Vernos I. The mechanism of spindle assembly: functions of Ran and its target TPX2. J Cell Biol. 2004 Sep 27;166(7):949-55.

Gruss OJ, Wittmann M, Yokoyama H, Pepperkok R, Kufer T, Silljé H, Karsenti E, Mattaj IW, Vernos I. Chromosome-induced microtubule assembly mediated by TPX2 is required for spindle formation in HeLa cells. Nat Cell Biol. 2002 Nov;4(11):871-9.

Gundersen GG, Kalnoski MH, Bulinski JC. Distinct populations of microtubules: tyrosinated and nontyrosinated alpha tubulin are distributed differently in vivo. Cell. 1984 Oct;38(3):779-89.

Hauf S, Cole RW, LaTerra S, Zimmer C, Schnapp G, Walter R, Heckel A, van Meel J, Rieder CL, Peters JM. The small molecule Hesperadin reveals a role for Aurora B in correcting kinetochore-microtubule attachment and in maintaining the spindle assembly checkpoint. J Cell Biol. 2003 Apr 28;161(2):281-94.

Hayden JH, Bowser SS, Rieder CL. Kinetochores capture astral microtubules during chromosome attachment to the mitotic spindle: direct visualization in live newt lung cells. J Cell Biol. 1990 Sep;111(3):1039-45.

Heald R, Khodjakov A. Thirty years of search and capture: The complex simplicity of mitotic spindle assembly. J Cell Biol. 2015 Dec 21;211(6):1103-11.

Heald R, Tournebize R, Blank T, Sandaltzopoulos R, Becker P, Hyman A, Karsenti E. Self-organization of microtubules into bipolar spindles around artificial chromosomes in Xenopus egg extracts. Nature. 1996 Aug 1;382(6590):420-5.

Henty-Ridilla JL, Rankova A, Eskin JA, Kenny K, Goode BL. Accelerated actin filament polymerization from microtubule plus ends. Science. 2016 May 20;352(6288):1004-9.

Hetzer M, Gruss OJ, Mattaj IW. The Ran GTPase as a marker of chromosome position in spindle formation and nuclear envelope assembly. Nat Cell Biol. 2002 Jul;4(7):E177-84.

Hoffman DB, Pearson CG, Yen TJ, Howell BJ, Salmon ED. Microtubule-dependent changes in assembly of microtubule motor proteins and mitotic spindlecheckpoint proteins at PtK1 kinetochores. Mol Biol Cell. 2001 Jul;12(7):1995-2009.

Holubcová Z, Blayney M, Elder K, Schuh M. Human oocytes. Error-prone chromosome-mediated spindle assembly favors chromosome segregation defects in human oocytes. Science. 2015 Jun 5;348(6239):1143-7.

Holubcová Z, Howard G, Schuh M. Vesicles modulate an actin network for asymmetric spindle positioning. Nat Cell Biol. 2013 Aug;15(8):937-47.

Ishihara K, Nguyen PA, Groen AC, Field CM, Mitchison TJ. Microtubule nucleation remote from centrosomes may explain how asters span large cells. Proc Natl Acad Sci U S A. 2014 Dec 16;111(50):17715-22.

Itoh G, Yumura S. A novel mitosis-specific dynamic actin structure in Dictyostelium cells. J Cell Sci. 2007 Dec 15;120(Pt 24):4302-9.

Janke C. The tubulin code: molecular components, readout mechanisms, and functions. J Cell Biol. 2014 Aug 18;206(4):461-72.

Jansen LE, Black BE, Foltz DR, Cleveland DW. Propagation of centromeric chromatin requires exit from mitosis. J Cell Biol. 2007 Mar 12;176(6):795-805.

Kalab P, Pralle A, Isacoff EY, Heald R, Weis K. Analysis of a RanGTP-regulated gradient in mitotic somatic cells. Nature. 2006 Mar 30;440(7084):697-701.

Kalab P, Pu RT, Dasso M. The ran GTPase regulates mitotic spindle assembly. Curr Biol. 1999 May 6;9(9):481-4.

Kalab P, Weis K, Heald R. Visualization of a Ran-GTP gradient in interphase and mitotic Xenopus egg extracts. Science. 2002 Mar 29;295(5564):2452-6.

Kalinina I, Nandi A, Delivani P, Chacón MR, Klemm AH, Ramunno-Johnson D, Krull A, Lindner B, Pavin N, Tolić-Nørrelykke IM. Pivoting of microtubules around the spindle pole accelerates kinetochore capture. Nat Cell Biol. 2013 Jan;15(1):82-7.

Kanatani H, Shirai H, Nakanishi K, Kurokawa T. Isolation and indentification on meiosis inducing substance in starfish Asterias amurensis. Nature. 1969 Jan 18;221(5177):273-4.

Karess R. Rod-Zw10-Zwilch: a key player in the spindle checkpoint. Trends Cell Biol. 2005 Jul;15(7):386-92.

Karpen GH, Allshire RC. The case for epigenetic effects on centromere identity and function. Trends Genet. 1997 Dec;13(12):489-96.

Karreman MA, Mercier L, Schieber NL, Solecki G, Allio G, Winkler F, Ruthensteiner B, Goetz JG, Schwab Y. Fast and precise targeting of single tumor cells in vivo by multimodal correlative microscopy. J Cell Sci. 2016 Jan 15;129(2):444-56.

Karsenti E, Newport J, Hubble R, Kirschner M. Interconversion of metaphase and interphase microtubule arrays, as studied by the injection of centrosomes and nuclei into Xenopus eggs. J Cell Biol. 1984 May;98(5):1730-45.

Khodjakov A, Cole RW, Oakley BR, Rieder CL. Centrosome-independent mitotic spindle formation in vertebrates. Curr Biol. 2000 Jan 27;10(2):59-67.

Khodjakov A, Copenagle L, Gordon MB, Compton DA, Kapoor TM. Minus-end capture of preformed kinetochore fibers contributes to spindle morphogenesis. J Cell Biol. 2003 Mar 3;160(5):671-83.

Kim HC, Jo YJ, Kim NH, Namgoong S. Small molecule inhibitor of formin homology 2 domains (SMIFH2) reveals the roles of the formin family of proteins in spindle assembly and asymmetric division in mouse oocytes. PLoS One. 2015 Apr 2;10(4):e0123438.

Kim Y, Heuser JE, Waterman CM, Cleveland DW. CENP-E combines a slow, processive motor and a flexible coiled coil to produce an essential motile kinetochore tether. J Cell Biol. 2008 May 5;181(3):411-9.

King JM, Nicklas RB. Tension on chromosomes increases the number of kinetochore microtubules but only within limits. J Cell Sci. 2000 Nov;113 Pt 21:3815-23.

Kirschner M, Mitchison T. Beyond self-assembly: from microtubules to morphogenesis. Cell. 1986 May 9;45(3):329-42.

Kitajima TS, Ohsugi M, Ellenberg J. Complete kinetochore tracking reveals error-prone homologous chromosome biorientation in mammalian oocytes. Cell. 2011 Aug 19;146(4):568-81.

Kitamura E, Tanaka K, Komoto S, Kitamura Y, Antony C, Tanaka TU. Kinetochores generate microtubules with distal plus ends: their roles and limited lifetime in mitosis. Dev Cell. 2010 Feb 16;18(2):248-59.

Klare K, Weir JR, Basilico F, Zimniak T, Massimiliano L, Ludwigs N, Herzog F, Musacchio A. CENP-C is a blueprint for constitutive centromere-associated network assembly within humankinetochores. J Cell Biol. 2015 Jul 6;210(1):11-22.

Kline SL, Cheeseman IM, Hori T, Fukagawa T, Desai A. The human Mis12 complex is required for kinetochore assembly and proper chromosome segregation. J Cell Biol. 2006 Apr 10;173(1):9-17.

Koestler SA, Rottner K, Lai F, Block J, Vinzenz M, Small JV. F- and G-actin concentrations in lamellipodia of moving cells.PLoS One. 2009;4(3):e4810.

Lampson MA, Grishchuk EL. Mechanisms to Avoid and Correct Erroneous Kinetochore-Microtubule Attachments. Biology (Basel). 2017 Jan 5;6(1).

Landino J, Ohi R. The Timing of Midzone Stabilization during Cytokinesis Depends on Myosin II Activity and an Interaction between INCENP and Actin. Curr Biol. 2016 Mar 7;26(5):698-706.

Lara-Gonzalez P, Westhorpe FG, Taylor SS. The spindle assembly checkpoint. Curr Biol. 2012 Nov 20;22(22):R966-80.

Legal T, Zou J, Sochaj A, Rappsilber J, Welburn JP. Molecular architecture of the Dam1 complex-microtubule interaction. Open Biol. 2016 Mar;6(3).

Lénárt P, Bacher CP, Daigle N, Hand AR, Eils R, Terasaki M, Ellenberg J. A contractile nuclear actin network drives chromosome congression in oocytes. Nature. 2005 Aug 11;436(7052):812-8.

Lin TC, Neuner A, Schiebel E. Targeting of γ-tubulin complexes to microtubule organizing centers: conservation and divergence. Trends Cell Biol. 2015 May;25(5):296-307.

Ma N, Matsunaga S, Morimoto A, Sakashita G, Urano T, Uchiyama S, Fukui K. The nuclear scaffold protein SAF-A is required for kinetochore-microtubule attachment and contributes to the targeting of Aurora-A to mitotic spindles. J Cell Sci. 2011 Feb 1;124(Pt 3):394-404.

Maco B, Holtmaat A, Cantoni M, Kreshuk A, Straehle CN, Hamprecht FA, Knott GW. Correlative in vivo 2 photon and focused ion beam scanning electron microscopy of cortical neurons. PLoS One. 2013;8(2):e57405.

Magidson V, O'Connell CB, Lončarek J, Paul R, Mogilner A, Khodjakov A. The spatial arrangement of chromosomes during prometaphase facilitates spindle assembly. Cell. 2011 Aug 19;146(4):555-67.

Magidson V, Paul R, Yang N, Ault JG, O'Connell CB1, Tikhonenko I, McEwen BF, Mogilner A, Khodjakov A1. Adaptive changes in the kinetochore architecture facilitate proper spindle assembly. Nat Cell Biol. 2015 Sep;17(9):1134-44.

Mahoney NM, Goshima G, Douglass AD, Vale RD. Making microtubules and mitotic spindles in cells without functional centrosomes. Curr Biol. 2006 Mar 21;16(6):564-9.

Maia AF, Feijão T, Vromans MJ, Sunkel CE, Lens SM. Aurora B kinase cooperates with CENP-E to promote timely anaphase onset. Chromosoma. 2010 Aug;119(4):405-13.

Maiato H, DeLuca J, Salmon ED, Earnshaw WC. The dynamic kinetochore-microtubule interface. J Cell Sci. 2004 Nov 1;117(Pt 23):5461-77.

Maiato H, Gomes AM, Sousa F, Barisic M. Mechanisms of Chromosome Congression during Mitosis. Biology (Basel). 2017 Feb 17;6(1).

Maiuri P, Rupprecht JF, Wieser S, Ruprecht V, Bénichou O, Carpi N, Coppey M, De Beco S, Gov N, Heisenberg CP, Lage Crespo C, Lautenschlaeger F, Le Berre M, Lennon-Dumenil AM, Raab M, Thiam HR, Piel M, Sixt M, Voituriez R. Actin flows mediate a universal coupling between cell speed and cell persistence. Cell. 2015 Apr 9;161(2):374-86.

Manandhar G, Schatten H, Sutovsky P. Centrosome reduction during gametogenesis and its significance. Biol Reprod. 2005 Jan;72(1):2-13.

Mandeville EC, Rieder CL. Keratin filaments restrict organelle migration into the forming spindle of newt pneumocytes. Cell Motil Cytoskeleton. 1990;15(2):111-20.

Mao Y. Formin a link between kinetochores and microtubule ends. Trends Cell Biol. 2011 Nov;21(11):625-9.

Martin-Lluesma S, Stucke VM, Nigg EA. Role of Hec1 in spindle checkpoint signaling and kinetochore recruitment of Mad1/Mad2. Science. 2002 Sep 27;297(5590):2267-70.

Matthies HJ, McDonald HB, Goldstein LS, Theurkauf WE. Anastral meiotic spindle morphogenesis: role of the non-claret disjunctional kinesin-like protein. J Cell Biol. 1996 Jul;134(2):455-64.

Maure JF, Komoto S, Oku Y, Mino A, Pasqualato S, Natsume K, Clayton L, Musacchio A, Tanaka TU. The Ndc80 loop region facilitates formation of kinetochore attachment to the dynamic microtubule plus end. Curr Biol. 2011 Feb 8;21(3):207-13.

McEwen BF, Heagle AB, Cassels GO, Buttle KF, Rieder CL. Kinetochore fiber maturation in PtK1 cells and its implications for the mechanisms of chromosome congression and anaphase onset. J Cell Biol. 1997 Jun 30;137(7):1567-80.

McEwen BF, Hsieh CE, Mattheyses AL, Rieder CL. A new look at kinetochore structure in vertebrate somatic cells using high-pressure freezing and freeze substitution. Chromosoma. 1998 Dec;107(6-7):366-75.

McIntosh JR, Grishchuk EL, Morphew MK, Efremov AK, Zhudenkov K, Volkov VA, Cheeseman IM, Desai A, Mastronarde DN, Ataullakhanov FI. Fibrils connect microtubule tips with kinetochores: a mechanism to couple tubulin dynamics to chromosome motion. Cell. 2008 Oct 17;135(2):322-33.

McIntosh JR, Grishchuk EL, West RR. Chromosome-microtubule interactions during mitosis. Annu Rev Cell Dev Biol. 2002; 18:193-219.

Mitchison T, Kirschner M. Dynamic instability of microtubule growth. Nature. 1984 Nov 15-21;312(5991):237-42.

Mitchison TJ. Localization of an exchangeable GTP binding site at the plus end of microtubules. Science. 1993 Aug 20;261(5124):1044-7.

Miyazaki A, Kamitsubo E, Nemoto SI. Premeiotic aster as a device to anchor the germinal vesicle to the cell surface of the presumptiveanimal pole in starfish oocytes. Dev Biol. 2000 Feb 15;218(2):161-71.

Mori M, Monnier N, Daigle N, Bathe M, Ellenberg J, Lénárt P. Intracellular transport by an anchored homogeneously contracting F-actin meshwork. Curr Biol. 2011 Apr 12;21(7):606-11.

Mori M, Somogyi K, Kondo H, Monnier N, Falk HJ, Machado P, Bathe M, Nédélec F, Lénárt P. An Arp2/3 nucleated F-actin shell fragments nuclear membranes at nuclear envelope breakdown in starfish oocytes. Curr Biol. 2014 Jun 16;24(12):1421-8.

Murphy TD, Karpen GH. Centromeres take flight: alpha satellite and the quest for the human centromere. Cell. 1998 May 1;93(3):317-20.

Musacchio A, Desai A. A Molecular View of Kinetochore Assembly and Function. Biology (Basel). 2017 Jan 24;6(1).

Musacchio A, Salmon ED. The spindle-assembly checkpoint in space and time. Nat Rev Mol Cell Biol. 2007 May;8(5):379-93.

Nogales E. An electron microscopy journey in the study of microtubule structure and dynamics. Protein Sci. 2015 Dec;24(12):1912-9.

Paul R, Wollman R, Silkworth WT, Nardi IK, Cimini D, Mogilner A. Computer simulations predict that chromosome movements and rotations accelerate mitotic

spindle assembly without compromising accuracy. Proc Natl Acad Sci U S A. 2009 Sep 15;106(37):15708-13.

Pavin N, Tolić-Nørrelykke IM. Swinging a sword: how microtubules search for their targets. Syst Synth Biol. 2014 Sep;8(3):179-86.

Petry S, Groen AC, Ishihara K, Mitchison TJ, Vale RD. Branching microtubule nucleation in Xenopus egg extracts mediated by augmin and TPX2. Cell. 2013 Feb 14;152(4):768-77.

Petry S, Pugieux C, Nédélec FJ, Vale RD. Augmin promotes meiotic spindle formation and bipolarity in Xenopus egg extracts. Proc Natl Acad Sci U S A. 2011 Aug 30;108(35):14473-8.

Petry S, Vale RD. Microtubule nucleation at the centrosome and beyond. Nat Cell Biol. 2015 Sep;17(9):1089-93.

Pollard TD, Cooper JA. Actin, a central player in cell shape and movement. Science. 2009 Nov 27;326(5957):1208-12.

Preciado López M, Huber F, Grigoriev I, Steinmetz MO, Akhmanova A, Koenderink GH, Dogterom M. Actin-microtubule coordination at growing microtubule ends. Nat Commun. 2014 Aug 27;5:4778.

Ramey VH, Wang HW, Nakajima Y, Wong A, Liu J, Drubin D, Barnes G, Nogales E. The Dam1 ring binds to the E-hook of tubulin and diffuses along the microtubule. Mol Biol Cell. 2011 Feb 15;22(4):457-66.

Rieder CL, Alexander SP. Kinetochores are transported poleward along a single astral microtubule during chromosome attachment to the spindle in newt lung cells. J Cell Biol. 1990 Jan;110(1):81-95.

Rieder CL, Davison EA, Jensen LC, Cassimeris L, Salmon ED. Oscillatory movements of monooriented chromosomes and their position relative to the spindle pole result from the ejection properties of the aster and half-spindle. J Cell Biol. 1986 Aug;103(2):581-91.

Rieder CL, Salmon ED. Motile kinetochores and polar ejection forces dictate chromosome position on the vertebrate mitotic spindle. J Cell Biol. 1994 Feb;124(3):223-33.

Rieder CL. Kinetochore fiber formation in animal somatic cells: dueling mechanisms come to a draw. Chromosoma. 2005 Nov;114(5):310-8.

Riedl J, Crevenna AH, Kessenbrock K, Yu JH, Neukirchen D, Bista M, Bradke F, Jenne D, Holak TA, Werb Z, Sixt M, Wedlich-Soldner R. Lifeact: a versatile marker to visualize F-actin. Nat Methods. 2008 Jul;5(7):605-7.

Rosenblatt J, Cramer LP, Baum B, McGee KM. Myosin II-dependent cortical movement is required for centrosome separation and positioning during mitotic spindle assembly. Cell 2004;117(3):361–72.

Rump A, Scholz T, Thiel C, Hartmann FK, Uta P, Hinrichs MH, Taft MH, Tsiavaliaris G. Myosin-1C associates with microtubules and stabilizes the mitotic spindle during cell division. J Cell Sci. 2011; 124:2521–2528.

Samwer M, Dehne HJ, Spira F, Kollmar M, Gerlich DW, Urlaub H, Görlich D. The nuclear F-actin interactome of Xenopus oocytes reveals an actin-bundling kinesin that is essential for meiotic cytokinesis. EMBO J. 2013 Jul 3;32(13):1886-902.

Sandquist JC, Kita AM, Bement WM. And the dead shall rise: actin and myosin return to the spindle. Dev Cell. 2011 Sep 13;21(3):410-9.

Schuh M, Ellenberg J. A new model for asymmetric spindle positioning in mouse oocytes. Curr Biol. 2008 Dec 23;18(24):1986-92.

Schuh M, Ellenberg J. Self-organization of MTOCs replaces centrosome function during acentrosomal spindle assembly in live mouse oocytes. Cell. 2007 Aug 10;130(3):484-98.

Schuh M, Lehner CF, Heidmann S. Incorporation of Drosophila CID/CENP-A and CENP-C into centromeres during early embryonic anaphase. Curr Biol. 2007 Feb 6;17(3):237-43.

Shrestha RL, Draviam VM. Lateral to end-on conversion of chromosome-microtubule attachment requires kinesins CENP-E and MCAK. Curr Biol. 2013 Aug 19;23(16):1514-26.

Silverman-Gavrila RV, Forer A. Evidence that actin and myosin are involved in the poleward flux of tubulin in metaphase kinetochore microtubules of crane-fly spermatocytes. J Cell Sci. 2000 Feb;113 (Pt 4):597-609.

Skibbens RV, Skeen VP, Salmon ED. Directional instability of kinetochore motility during chromosome congression and segregation in mitotic newt lung cells: a push-pull mechanism. J Cell Biol. 1993 Aug;122(4):859-75.

Small J, Rottner K, Hahne P, Anderson KI. Visualising the actin cytoskeleton. Microsc Res Tech. 1999 Oct 1;47(1):3-17.

Strickland L, von Dassow G, Ellenberg J, Foe V, Lenart P, Burgess D. Light microscopy of echinoderm embryos. Methods Cell Biol. 2004;74:371-409.

Stumpff J, von Dassow G, Wagenbach M, Asbury C, Wordeman L. The kinesin-8 motor Kif18A suppresses kinetochore movements to control mitotic chromosome alignment. Dev Cell. 2008 Feb;14(2):252-62.

Stüven T, Hartmann E, Görlich D. Exportin 6: a novel nuclear export receptor that is specific for profilin.actin complexes. EMBO J. 2003 Nov 3;22(21):5928-40.

Sullivan KF, Hechenberger M, Masri K. Human CENP-A contains a histone H3 related histone fold domain that is required for targeting to the centromere. J Cell Biol. 1994 Nov;127(3):581-92.

Szollosi D, Calarco P, Donahue RP. Absence of centrioles in the first and second meiotic spindles of mouse oocytes. J Cell Sci. 1972 Sep;11(2):521-41.

Tanaka TU, Rachidi N, Janke C, Pereira G, Galova M, Schiebel E, Stark MJ, Nasmyth K. Evidence that the Ipl1-Sli15 (Aurora kinase-INCENP) complex promotes chromosome bi-orientation by altering kinetochore-spindle pole connections. Cell. 2002 Feb 8;108(3):317-29.

Tanaka TU, Stark MJ, Tanaka K. Kinetochore capture and bi-orientation on the mitotic spindle. Nat Rev Mol Cell Biol. 2005 Dec;6(12):929-42.

Tanudji M, Shoemaker J, L'Italien L, Russell L, Chin G, Schebye XM. Gene silencing of CENP-E by small interfering RNA in HeLa cells leads to missegregation of chromosomes after a mitotic delay. Mol Biol Cell. 2004 Aug;15(8):3771-81.

Terasaki M, Campagnola P, Rolls MM, Stein PA, Ellenberg J, Hinkle B, Slepchenko B. A new model for nuclear envelope breakdown. Mol Biol Cell. 2001 Feb;12(2):503-10.

Terasaki M. Quantification of fluorescence in thick specimens, with an application to cyclin B-GFP expression in starfish oocytes. Biol Cell. 2006 Apr;98(4):245-52.

Terasaki M. Redistribution of cytoplasmic components during germinal vesicle breakdown in starfish oocytes. J Cell Sci. 1994 Jul;107 (Pt 7):1797-805.

Thrower DA, Jordan MA, Wilson L. Modulation of CENP-E organization at kinetochores by spindle microtubule attachment. Cell Motil Cytoskeleton. 1996;35(2):121-33.

Traas JA, Doonan JH, Rawlins DJ, Shaw PJ, Watts J, Lloyd CW. An actin network is present in the cytoplasm throughout the cell cycle of carrot cells and associates with the dividing nucleus. J Cell Biol. 1987 Jul;105(1):387-95.

Tsai MY, Wang S, Heidinger JM, Shumaker DK, Adam SA, Goldman RD, Zheng Y. A mitotic lamin B matrix induced by RanGTP required for spindle assembly. Science. 2006 Mar 31;311(5769):1887-93.

Ucar H, Tachibana K, Kishimoto T. The Mos-MAPK pathway regulates Diaphanous-related formin activity to drive cleavage furrow closure during polar body extrusion in starfish oocytes. J Cell Sci. 2013 Nov 15;126(Pt 22):5153-65.

Uehara R, Nozawa RS, Tomioka A, Petry S, Vale RD, Obuse C, Goshima G. The augmin complex plays a critical role in spindle microtubule generation for mitoticprogression and cytokinesis in human cells. Proc Natl Acad Sci U S A. 2009 Apr 28;106(17):6998-7003.

Vanneste D, Ferreira V, Vernos I. Chromokinesins: localization-dependent functions and regulation during cell division. Biochem Soc Trans. 2011 Oct;39(5):1154-60.

Vernos I, Raats J, Hirano T, Heasman J, Karsenti E, Wylie C. Xklp1, a chromosomal Xenopus kinesin-like protein essential for spindle organization and chromosome positioning. Cell. 1995 Apr 7;81(1):117-27.

Walker RA, O'Brien ET, Pryer NK, Soboeiro MF, Voter WA, Erickson HP, Salmon ED. Dynamic instability of individual microtubules analyzed by video light microscopy: rate constants and transition frequencies. J Cell Biol. 1988 Oct;107(4):1437-48.

Wandke C, Barisic M, Sigl R, Rauch V, Wolf F, Amaro AC, Tan CH, Pereira AJ, Kutay U, Maiato H, Meraldi P, Geley S. Human chromokinesins promote chromosome congression and spindle microtubule dynamics during mitosis. J Cell Biol. 2012 Sep 3;198(5):847-63.

Wang SZ, Adler R. Chromokinesin: a DNA-binding, kinesin-like nuclear protein. J Cell Biol. 1995 Mar;128(5):761-8.

Warburton PE, Cooke CA, Bourassa S, Vafa O, Sullivan BA, Stetten G, Gimelli G, Warburton D, Tyler-Smith C, Sullivan KF, Poirier GG, Earnshaw WC. Immunolocalization of CENP-A suggests a distinct nucleosome structure at the inner kinetochoreplate of active centromeres. Curr Biol. 1997 Nov 1;7(11):901-4.

Weber KL, Sokac AM, Berg JS, Cheney RE, Bement WM. A microtubule-binding myosin required for nuclear anchoring and spindle assembly. Nature. 2004 Sep 16;431(7006):325-9.

Webster A, Schuh M. Mechanisms of Aneuploidy in Human Eggs. Trends Cell Biol. 2017 Jan;27(1):55-68.

Weisshart K. The basic principle of Airyscanning. 2014, Technology note. Carl Zeiss Microscopy GmbH.

Wesolowska N, Lénárt P. Nuclear roles for actin. Chromosoma. 2015 Dec;124(4):481-9.

Wilde A, Lizarraga SB, Zhang L, Wiese C, Gliksman NR, Walczak CE, Zheng Y. Ran stimulates spindle assembly by altering microtubule dynamics and the balance of motor activities. Nat Cell Biol. 2001 Mar;3(3):221-7.

Wilde A, Zheng Y. Stimulation of microtubule aster formation and spindle assembly by the small GTPase Ran. Science. 1999 May 21;284(5418):1359-62.

Witt PL, Ris H, Borisy GG. Origin of kinetochore microtubules in Chinese hamster ovary cells. Chromosoma. 1980;81(3):483-505.

Wollman R, Cytrynbaum EN, Jones JT, Meyer T, Scholey JM, Mogilner A. Efficient chromosome capture requires a bias in the 'search-and-capture' process during mitotic-spindle assembly. Curr Biol. 2005 May 10;15(9):828-32.

Woolner S, O'Brien LL, Wiese C, Bement WM. Myosin-10 and actin filaments are essential for mitotic spindle function. J Cell Biol. 2008 Jul 14;182(1):77-88.

Wu JQ, Pollard TD. Counting cytokinesis proteins globally and locally in fission yeast. Science. 2005 Oct 14;310(5746):310-4.

Wynne DJ, Funabiki H. Kinetochore function is controlled by a phospho-dependent coexpansion of inner and outer components. J Cell Biol. 2015 Sep 14;210(6):899-916.

Yajima J, Edamatsu M, Watai-Nishii J, Tokai-Nishizumi N, Yamamoto T, Toyoshima YY. The human chromokinesin Kid is a plus end-directed microtubule-based motor. EMBO J. 2003 Mar 3;22(5):1067-74.

Yasuda H, Kanda K, Koiwa H, Suenaga K, Kidou S, Ejiri S. Localization of actin filaments on mitotic apparatus in tobacco BY-2 cells. Planta. 2005 Sep;222(1):118-29.

Yasuda S, Oceguera-Yanez F, Kato T, Okamoto M, Yonemura S, Terada Y, Ishizaki T, Narumiya S. Cdc42 and mDia3 regulate microtubule attachment to kinetochores. Nature. 2004 Apr 15;428(6984):767-71.

Ye AA, Deretic J, Hoel CM, Hinman AW, Cimini D, Welburn JP, Maresca TJ. Aurora A Kinase Contributes to a Pole-Based Error Correction Pathway. Curr Biol. 2015 Jul 20;25(14):1842-51.